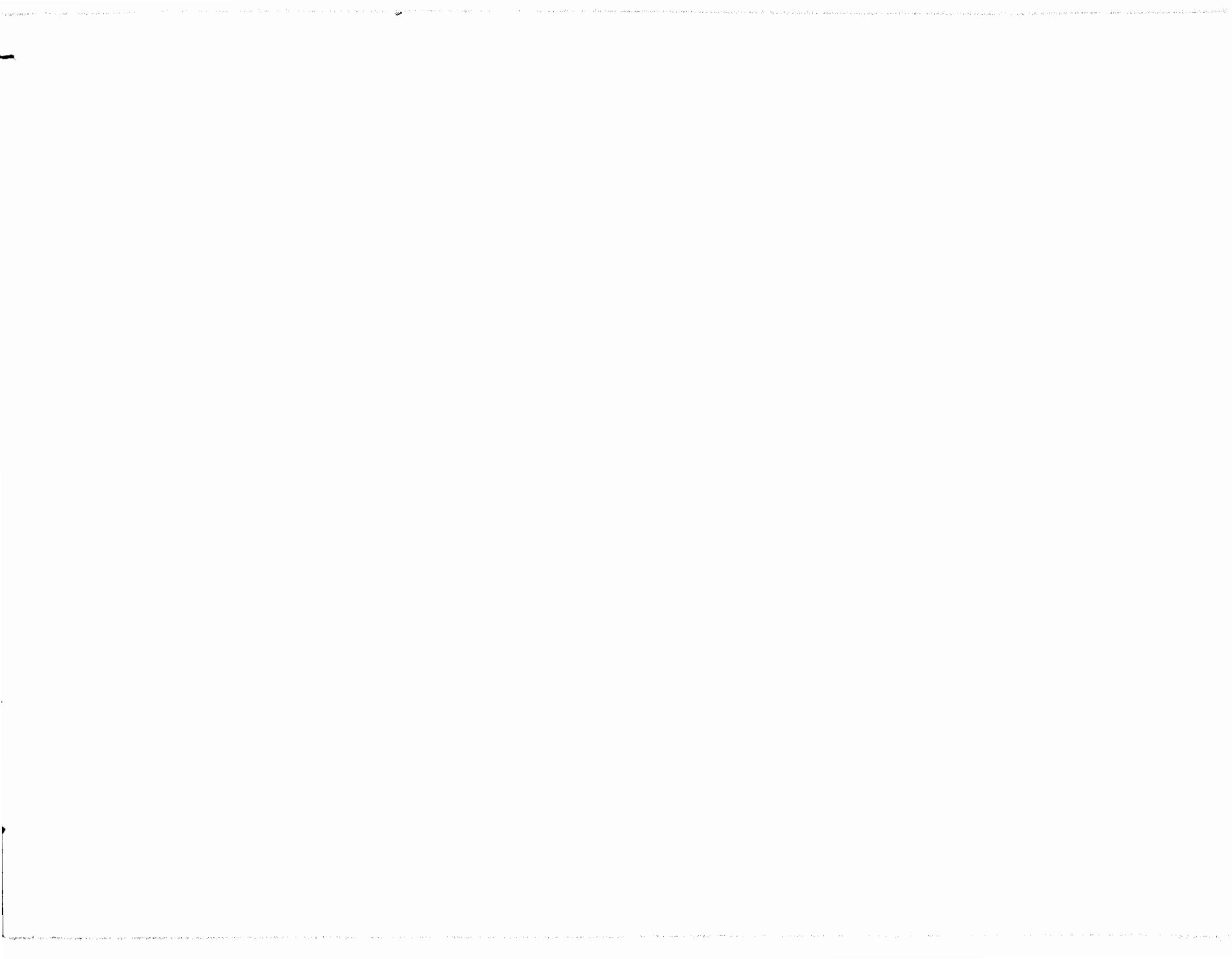


ANALES DE LA DIVISION DE ESTUDIOS DE POSGRADO 1987



FACULTAD DE INGENIERIA DIVISION DE ESTUDIOS DE POSGRADO

UNIVERSIDAD NACIONAL AUTONOMA DE MEXICO

RECTOR

Dr. Jorge Carpizo.

SECRETARIO GENERAL

Dr. José Narro Robles.

SECRETARIO GENERAL ACADEMICO

Dr. Abelardo Villegas.

SECRETARIO GENERAL ADMINISTRATIVO

C.P. José Romo Díaz.

SECRETARIO GENERAL AUXILIAR

Lic. Mario Ruiz Massieu.

ABOGADO GENERAL

Lic. Manuel Barquín Alvarez.

FACULTAD DE INGENIERIA

DIRECTOR

Dr. Daniel Reséndiz Núñez.

SECRETARIO GENERAL

Ing. José Gonzalo Guerrero Zepeda.

COORDINADOR DE SERVICIOS GENERALES

Prof. Francisco Velázquez Pérez.

SECRETARIO ADMINISTRATIVO

Sr. Abel Padilla Fajardo.

DIVISION DE ESTUDIOS DE POSGRADO

JEFE DE LA DIVISION

Dr. Gabriel Echávez Aldape.

SECRETARIO ACADEMICO

M en I. Gabriel Sánchez Guerrero.

DELEGADO ADMINISTRATIVO

Lic. Oscar García Romero.

JEFE DEL DEPARTAMENTO DE

Dr. Gabriel Auvinet Guichard.

INGENIERIA CIVIL

JEFE DEL DEPARTAMENTO DE

Dr. Federico Kuhlmann Rodríguez.

INGENIERIA ELECTROMECANICA

JEFE DEL DEPARTAMENTO DE

Dr. Heber Cinco Ley.

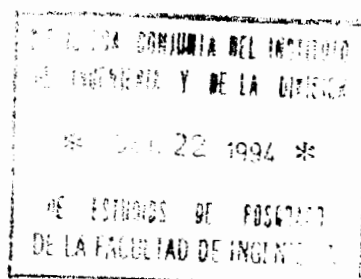
RECURSOS DEL SUBSUELO

JEFE DEL DEPARTAMENTO DE

Dr. Sergio Fuentes Maya.

MATEMATICAS Y COMPUTO

ANALES DE LA DIVISION DE ESTUDIOS DE POSGRADO 1987



**UNIVERSIDAD NACIONAL AUTONOMA DE MEXICO
FACULTAD DE INGENIERIA
MEXICO, 1988**



F-DEPI
MISC
0005
EJ-4

Primera edición: 1988

D.R. C 1988: Universidad Nacional Autónoma de México
Ciudad Universitaria 04510 México, D.F.
DIVISION DE ESTUDIOS DE POSGRADO DE LA
FACULTAD DE INGENIERIA

Impreso y hecho en México.

38078

PRESENTACION

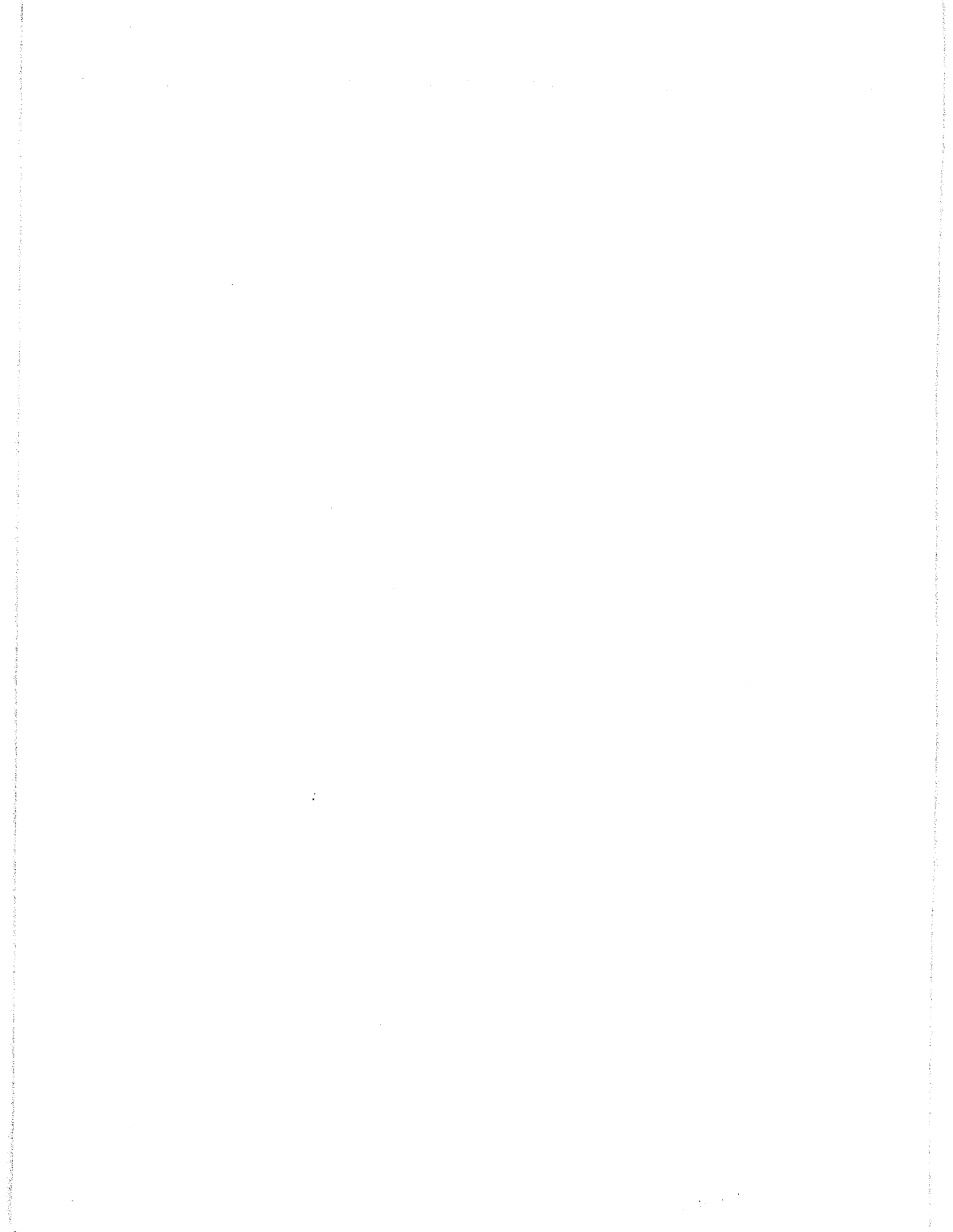
La investigación, búsqueda sistemática de nuevos conceptos, métodos, materiales y maneras de usar el conocimiento científico en la solución de problemas de ingeniería, es uno de los pilares en que debe apoyarse firmemente la Facultad de Ingeniería.

La participación de profesores y alumnos de posgrado en esa labor es de gran valor, pues gracias a ella la ingeniería puede mantener al día su acervo de recursos técnicos.

Los Anales de la División de Estudios de Posgrado, en su edición correspondiente a 1987, reúnen resultados de algunas de nuestras investigaciones. Incluirlos en su totalidad sería excesivo; por ello, sólo se han seleccionado las más representativas en sus diversas áreas.

Estamos seguros de que la publicación de los Anales contribuye no sólo a difundir los resultados de nuestras investigaciones, sino también a reforzar la conciencia interna de la importancia de seguir estimulando esta importante actividad.

DR. DANIEL RESENDIZ NUÑEZ.
Director de la
Facultad de Ingeniería



I N T R O D U C C I O N

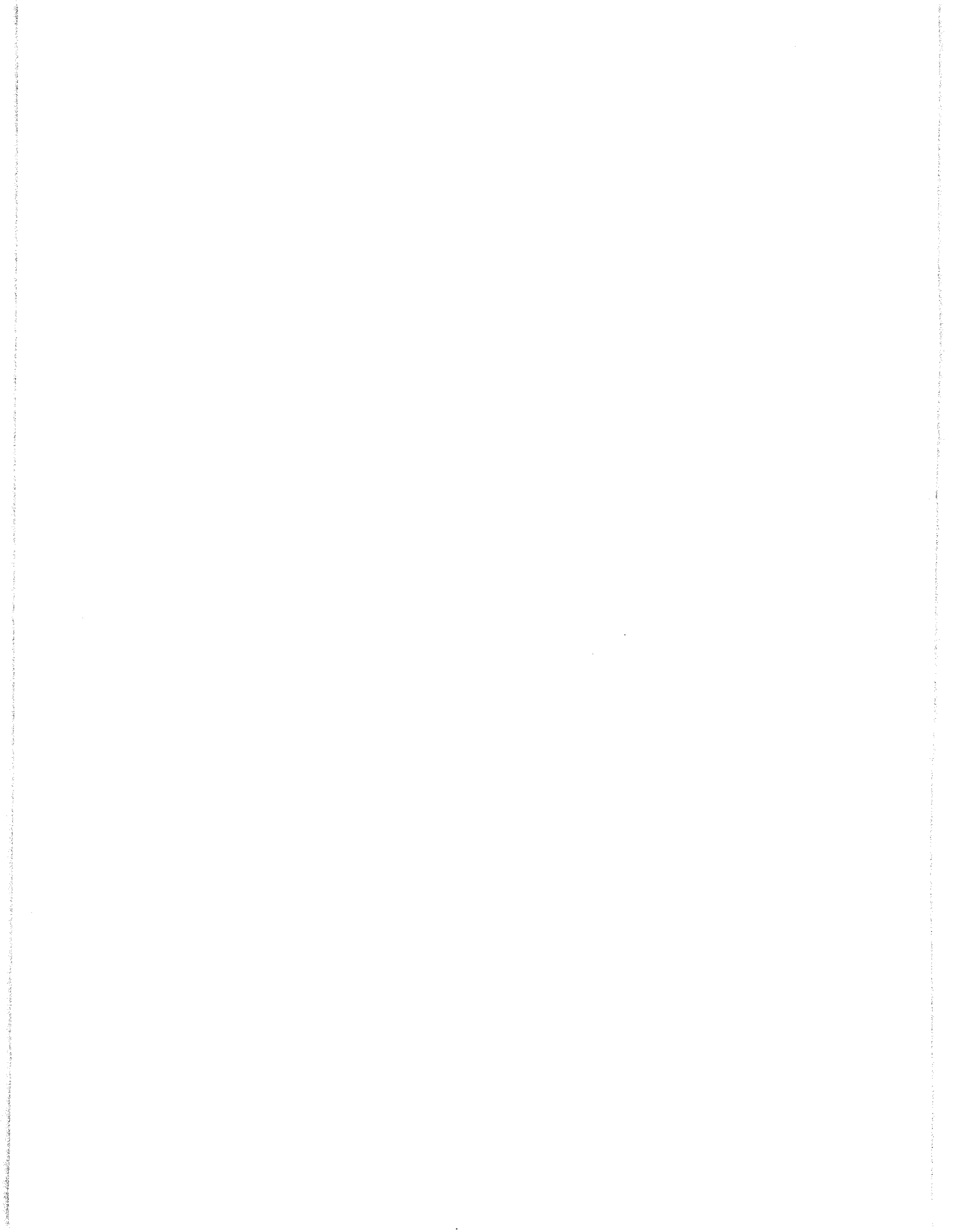
Los avances que se lograron durante 1987, tanto en el campo científico como tecnológico, constituyen una valiosa aportación al desarrollo de la ingeniería en esta Universidad.

Haber celebrado el 30 aniversario del establecimiento de la DEPFI, sirvió para apreciar los esfuerzos que sus profesores e investigadores realizan diariamente en cada una de sus áreas, cuyos resultados han sido fructíferos.

Como muestra de lo anterior, los Anales de esta División contienen algunos de los trabajos más sobresalientes que durante 1987 se realizaron en nuestra institución.

La difusión del presente documento tiene como propósito fundamental, difundir la labor de la División y a la vez fortalecer los conocimientos de los profesionales en las distintas ramas de la ingeniería, así como contribuir a la práctica oportuna de los avances logrados, en favor del progreso.

DR. GABRIEL ECHAVEZ ALDAPE.
Jefe de la División de Posgrado
de la Facultad de Ingeniería.



La División de Estudios de Posgrado de la Facultad de Ingeniería



Personal académico de la DEPFI

Estructura Académica

La estructura académica de la DEPFI, está integrada por cuatro departamentos:

**INGENIERIA CIVIL
INGENIERIA ELECTROMECANICA
INGENIERIA DE RECURSOS DEL SUBSUELO
MATEMATICAS**

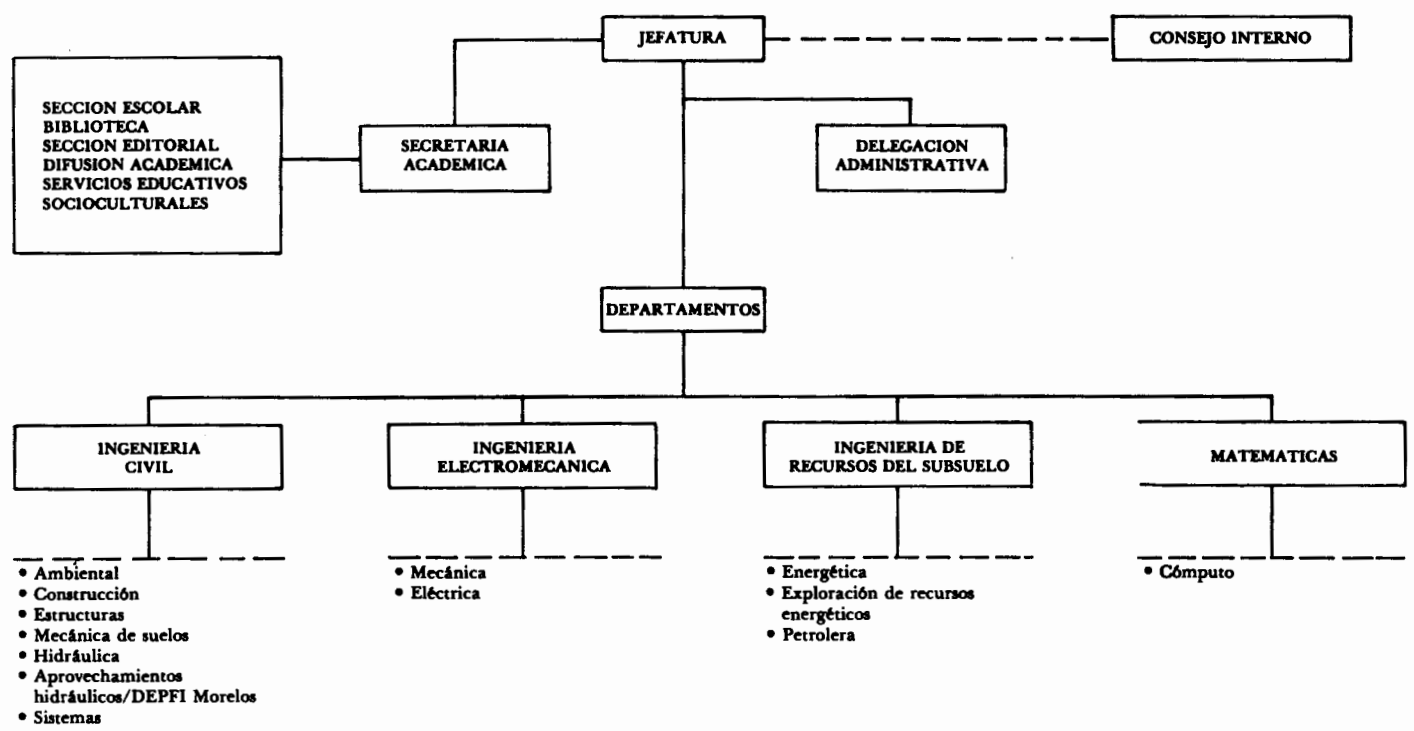
Esta organización que cambia la estructura anterior, no ha sido aprobada de manera oficial, sin embargo funciona operativamente desde el mes de noviembre de 1987 y de acuerdo a ella se ha ordenado la secuencia de esta publicación.

Los primeros tres departamentos se componen de secciones que llevan a cabo los programas académicos y la investigación científica, ambos ajustados a los requerimientos de nuestro país, lo que permite a la investigación especializada practicarse como una disciplina seria que requiere de una metodología completa con estudios profundos.

El departamento de Matemáticas presta apoyo académico a los otros tres.

Entre los proyectos de investigación que se realizan en la División de Posgrado, algunos son patrocinados por instituciones oficiales o privadas que proveen los fondos para su operación y permiten adecuar el conocimiento científico y tecnológico a la realidad actual y a las necesidades nacionales.

ORGANIGRAMA DE LA DIVISION DE ESTUDIOS DE POSGRADO DE LA FACULTAD DE INGENIERIA



Personal

Las personas que prestaron sus servicios en la DEPFI durante 1987 fueron:

Profesores de carrera de tiempo completo	47
Profesores de carrera de medio tiempo	9
Profesores de asignatura	178
Ayudantes de profesor	64
Técnicos académicos	11
Trabajadores de confianza	12
Trabajadores de apoyo administrativo	103

TOTAL 424 personas

Formación Académica

Alumnos de la DEPFI en 1987

Semestre	1er. Ingreso	Reingreso	Total
87-I	132	379	511
87-II	105	418	523

Recibieron diploma de especialización 4 alumnos, se otorgaron 69 grados de maestría y 3 de doctorado.

Superación Académica

CATEDRA ESPECIAL "ENRIQUE RIVERO BORRELL"



En el mes de junio de 1987, fue otorgada la Cátedra Especial "Enrique Rivero Borrell" al Dr. Jorge Abraham Díaz Rodríguez.

El Dr. Díaz Rodríguez es mexicano, actualmente profesor titular en la División de Estudios de Posgrado de la Facultad de Ingeniería en la que fundó el Laboratorio de Dinámica de Suelos.

Creó el grupo Dinámica de Suelos para vincular la docencia a la investigación y coordinó la propuesta de creación de la Maestría en Construcción. Sus principales líneas de investigación han sido: Comportamiento sísmico de suelos granulares finos, compresibilidad dinámica de suelos blandos, resistencia dinámica de suelos blandos y desarrollo de equipo experimental de la dinámica de suelos; sobre estos temas ha publicado artículos y presentado ponencias en eventos nacionales e internacionales.

CATEDRA ESPECIAL "ANTONIO DOVALÍ JAIME"



La cátedra especial "Antonio Dovalí Jaime" fue ocupada por el M en C. Arturo Delgado Rodríguez, de nacionalidad mexicana. El M. en C. Delgado Rodríguez es actualmente profesor de tiempo completo en la DEPFI; de los 38 años que ha entregado a la docencia, 25 los ha dedicado a la Facultad de Ingeniería de la UNAM. Hizo sus estudios profesionales en la Universidad de Yale (1946), la Maestría en Ciencias en la Universidad de Harvard (1948) y la Maestría en Ingeniería en la Universidad de Princeton (1949). Los últimos 20 años se ha dedicado al estudio y a la enseñanza de las matemáticas. Su actual línea de investigación es la de ecuaciones en diferencias.

Departamento de Ingeniería Civil

JEFE
Dr. Gabriel Auvinet Guichard.

COORDINADORES DE SECCION

AMBIENTAL
Dr. Pedro Martínez Pereda.

APROVECHAMIENTOS HIDRAULICOS/DEPFI MORELOS
Dr. José A. Raynal Villaseñor

HIDRAULICA
M. en I. René Autrique Ruiz.

CONSTRUCCION
Dr. Gabriel Auvinet Guichard.

ESTRUCTURAS Y MECANICA DE SUELOS
Ing. Juan José Hanell Campbell.

SISTEMAS
M. en I. Gonzalo Negroe Pérez.

Sección de Ambiental

COORDINADOR
Dr. Pedro Martínez Pereda.

Programas Académicos

ESPECIALIZACION:

Ingeniería Sanitaria

MAESTRIA Y DOCTORADO

Ingeniería Ambiental

Con opciones en:

Ingeniería Sanitaria

Control de calidad del agua

Control de calidad del aire

Control de residuos sólidos

Manejo de sistemas ambientales

Profesores de Carrera y Líneas de Investigación

Tiempo completo

FERNANDEZ VILLAGOMEZ, GEORGINA. Maestra en ingeniería. Universidad Nacional Autónoma de México. Control de calidad del agua.

FUENTES GEA, VICENTE. Maestro en ciencias. Universidad de Texas en Austin, E.U.A. Control de contaminación atmosférica, simulación de procesos.

GARCIA GUTIERREZ, ALFONSO. Doctor en ingeniería. Imperial College, Inglaterra. Procesos biológicos de tratamiento, evaluación de calidad del aire, manejo de residuos sólidos y peligrosos.

MARTINEZ PEREDA, PEDRO. Doctor en ingeniería. Universidad de Wisconsin, Universidad de Michigan, Universidad de Texas en Austin, E.U.A. Caracterización, manejo y disposición de aguas residuales, calidad del agua en ríos, formación de recursos humanos en ingeniería ambiental.

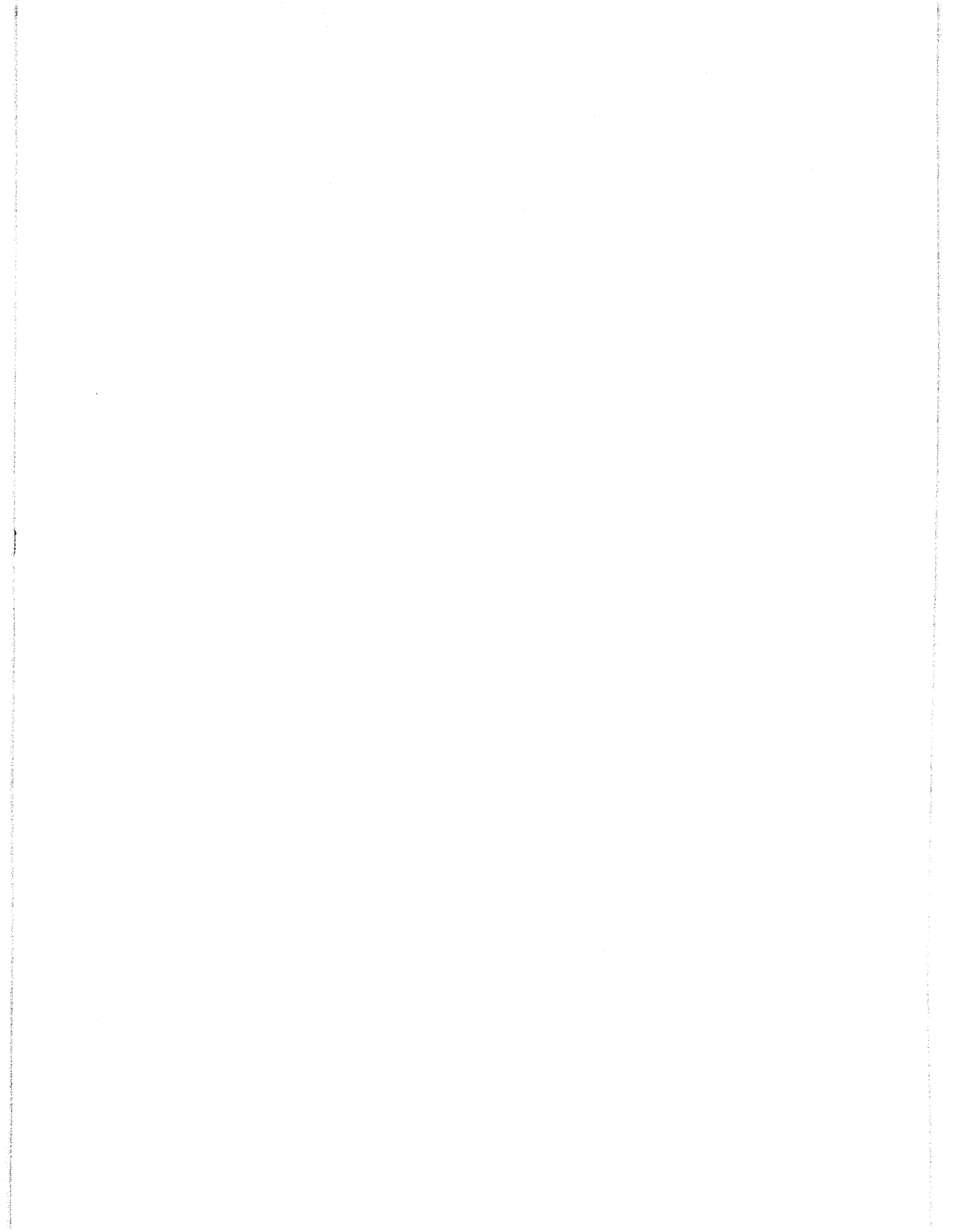
MOELLER CHAVEZ, GABRIELA. Maestra en ingeniería sanitaria. Universidad Nacional Autónoma de México. Microbiología aplicada a los procesos de tratamiento biológico, bioquímica de la digestión anaerobia, biodegradación de desechos.

MONTEJANO URANGA, FRANCISCO. Maestro en ciencias. Universidad de Carolina del Norte, E.U.A. Manejo de aguas residuales.

IZURIETA RUIZ, EDMUNDO. Maestro en ciencias. Universidad de Michigan, E.U.A. Calidad del agua.

Convenios

SARH-CONACYT-UNAM. Fortalecer la docencia e investigación en ingeniería sanitaria.



Sección de Hidráulica

COORDINADORES

APROVECHAMIENTOS HIDRAULICOS
Dr. José A. Raynal Villaseñor.

HIDRAULICA
M. en I. René Autrique Ruiz.

Programas Académicos

ESPECIALIZACION
Obras hidráulicas
Obras marítimas

MAESTRIA Y DOCTORADO
Ingeniería hidráulica
Ingeniería de aprovechamientos hidráulicos

Profesores de Carrera y Líneas de Investigación

Tiempo completo

ARREGUIN CORTES, FELIPE. Doctor en ingeniería. Universidad Nacional Autónoma de México. Obras hidráulicas e hidráulica general.

AUTRIQUE RUIZ, RENE. Maestro en ingeniería. Universidad Nacional Autónoma de México. Hidráulica general y fenómenos transitorios.

ECHAVEZ ALDAPE, GABRIEL. Doctor en ingeniería. Universidad Nacional Autónoma de México. Modelos hidráulicos y mecánica de fluidos.

JAIME ALARID, RODOLFO. Maestro en ciencias. Universidad Estatal de Colorado, E.U.A. Planeación de recursos hidráulicos.

MARTINEZ AUSTRIA, POLIOPTRIO. Doctor en ingeniería. Universidad Nacional Autónoma de México. Métodos numéricos y teoría de la catástrofe.

RAYNAL VILLASEÑOR, JOSE A. Doctor en ingeniería. Universidad Estatal de Colorado, E.U.A. Hidrología determinística y estocástica.

Publicaciones

AUTRIQUE R , *Comments on a new criterion for stability analysis and design of simple and restricted orifice large chambers*, International Simposium on hydraulic structures, Fort Collins, Colorado, E.U.A., agosto.

ECHAVEZ G , ARREGUIN F , *Polyhedric surfaces*, Proceedings of the 1987, National Conference on hydraulic engineering, Williamsburg, Virginia, E.U.A., agosto.

ECHAVEZ G , *Model Study to locate aerators in tunnel spillways*, Proceedings of the 1987, National Conference on hydraulic engineering, Williamsburg, Virginia, E.U.A., agosto.

ECHAVEZ G , FRANCO V , CAGIGAS R , *Estudio en modelo para diseñar los aireadores del P.H. Carlos Ramírez Ulloa*, Informe I.I., diciembre.

LEVI E, RODRIGUEZ N, ECHAVEZ G, *Fluid-structure Interaction, Civil Engineering Practice*, Encyclopedia II Vol., Cheremisinoff P.E. Editors, Technomic Publishing Company, Inc., Lancaster Pennsylvania, E.U.A., diciembre.

RAYNAL J, *Multivariate extreme value distributions in hydrologic analysis*, Proceedings of the International Symposium on water for the future, IASH Publication 164, Roma, Italia, abril.

RAYNAL J , *Remarkable hydrologic works in the aztec empire*, Proceedings of the International Symposium on water for the future, IASH Publication 164, Roma, Italia, abril.

RAYNAL J , *The General extreme value distribution applied to drought frequency analysis*, Engineering Hydrology Symposium, Williamsburg, Virginia, E.U.A., agosto.

RAYNAL J , *La trascendencia de los estudios de posgrado de la DEPFI-UNAM en el aprovechamiento integral del recurso agua*, Simposio Nacional sobre el uso integral del agua, la Paz, B.C., agosto.

RAYNAL J , *Análisis de eficiencia en la estimación de parámetros de la distribución GVE para mínimos*, XIII Congreso de la Academia Nacional de Ingeniería, Guadalajara, septiembre.

RAYNAL J , ECHAVEZ G , *Investigación y desarrollo en hidráulica*, XV Congreso Nacional de Ingeniería Civil, México, diciembre.

Convenios

SARH-CONACYT-UNAM. Fortalecer la docencia e investigación en hidráulica y aprovechamientos hidráulicos.

ESTADO DE MORELOS-SARH-UNAM. Establecer una extensión de la DEPFI en el Edo. de Morelos.

CFE-UNAM. Establecer criterios de optimización en sistemas de bombeo considerando flujo transitorio.

Artículos reproducidos

ECHAVEZ A G , ARREGUIN C.F, *Polyhedral surfaces*, Proceedings of the 1987, National Conference on Hydraulic Engineering, American Society of Civil Engineers, Nueva York, 1987.

RAYNAL V J , DOURIET C J , *The GEV Distribution in Drought Frecuency Analysis*, Proceedings of the Symposium, American Society of Civil Engineers, Nueva York, 1987.

MARTINEZ A P, *Catastrophe model for the forced hydraulic-jump*, Journal of the Hydraulic Research, Vol. 25, No. 3, 1987.

POLYHEDRIC SURFACES

DR. GABRIEL ECHAVEZ*
DR. FELIPE ARREGUIN**

ABSTRACT

A new design for spillways is proposed. The basic idea is to substitute the traditional shape of the continuous vertical bends by polygonal plane surfaces. In this way it is possible to construct spillways with plane surfaces which are easier and cheaper to build.

Aeration system to protect the spillway against cavitation are also easier to construct.

Schwartz-Christoffel transformation is used to analyse the flow on the polyhedric surfaces. The theoretical results agree with the model measurements in the concave curves. For convex curves flow separation precludes its application.

General results that support the new design proposed are shown.

INTRODUCTION

Normally, hydraulic works are designed using criteria derived from model and prototype studies of a few dams. This means that the results obtained from specific situations are adjusted to a particular problem without generally implying its best solution.

A new design criterion that seem to offer possibilities of development as well as a series of advantages over the traditional ones is the polyhedric design of spillways (Refs 1 and 2). This criterion is based on - the idea of changing the traditional vertical curves for polygonal sections (see fig 1). This imply the construction of plane surfaces in spillways, reducing the use of complicated forms, labor, and, in general, of special construction procedures; besides, in high head works it would facilitate the colocation of aeration devices.

THEORETICAL MODEL

To analyze the flow behaviour on polyhedric surfaces with two or three sections, a model based on the Schwartz-Christoffel transformation was developed. The following hypothesis are accepted:

- a) The influence of gravity is negligible on the polyhedric surface.
 - b) The effect of viscosity is negligible
 - c) A uniform velocity distribution upstream the polyhedric surface is assumed.
-

* Dean of the Graduate Engineering School, UNAM. Alborada 412, Parques del Pedregal, Mexico 14010, D.F.

** Head of the Hydraulics Department. Graduate Engineering School, UNAM Alborada 412, Parques del Pedregal, Mexico 14010, D.F.

Polyhedric concave or convex surfaces with two or three sections may be mapped in the upper semiplane, fig 2, by means of the Schwartz-Christoffel transformation.

The value of the complex potential for each case is given by:

Concave surface with two sections

$$P(z) = U \left(\frac{z}{b} \right)^{\frac{\pi}{\alpha}}$$

Convex surface with two sections

$$P(z) = U \left(\frac{z - a}{b - a} \right)^{\frac{\pi}{\alpha}}$$

in which

U is the upstream velocity
 a, b constants
 α deflection angle

In the case of a concave surface with three sections the Schwartz-Christoffel transformation is:

$$\frac{dz}{dw} = A(w + 1)^{\frac{\alpha}{\pi}} - 1$$

in which

A is a constant

From the abovementioned equations the complex velocity and its magnitude are found and, finally, the pressure distribution along the surface is obtained through Bernoulli's theorem.

EXPERIMENTAL SETUP

For the concave curves the hydraulic model, scale 1:50, of the La Angostura dam was used. Pressure measurements were taken with piezometers at the traditional flip bucket and one built with three straight sections with the same exit angle of the original design.

For the two sections concave curve a small lucite spillway model, 0.50m high, was used.

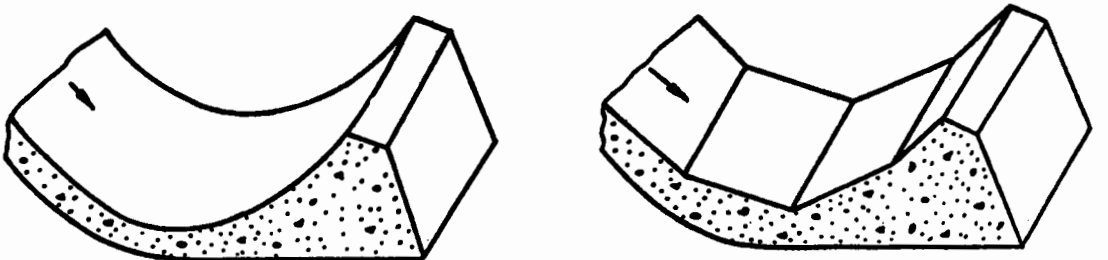
The convex polyhedric surface was studied by means of a channel with - the bottom built of two lucite plane sections, joined with a rubber - hinge, that allowed to change the deflection angle.

Besides the piezometers, limnimeters and calibrated weirs, a quartz - pressure cell, model 603, and an amplifier model 504 both from Kistler Instrument Corporation, a Gould plotter model 222 and a spectrum analyzer model 3852A from Hewlett Packard was used.

EXPERIMENTS

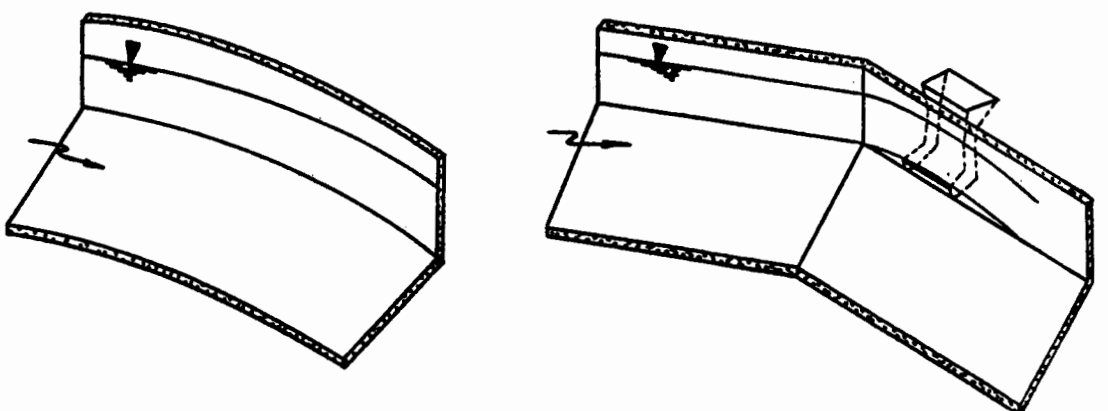
Concave curves:

In the traditional flip bucket and for seven different discharges, between 1400 m³/s and 4000 m³/s, the upstream depths and velocities, the exit velocities and the mean pressure along the model were registered. The polyhedric design was adjusted to the original geometry keeping the



Concave surface

Polyhedral design



Convex surface

Polyhedral design

Fig 1 Comparison between the traditional curve surfaces and the polyhedral surfaces.

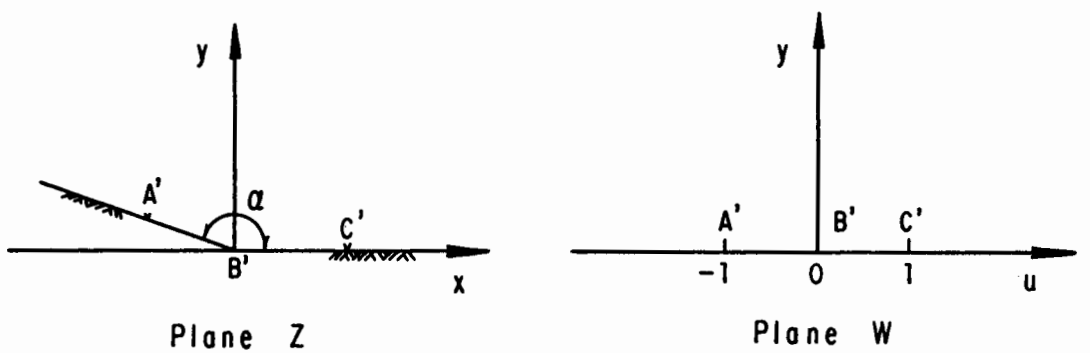


Fig 2 Application of plane Z on plane W. Concave surface

exit angle of 30° , and six piezometers were installed in homologous places to those used in the smooth flip bucket. In fig 3 the pressure distribution for a $4000 \text{ m}^3/\text{s}$ discharge is shown.

To measure pressure fluctuations the quartz cell was installed in five points for both the smooth and the segmented flip buckets, and records were obtained for three discharges 1400 , 2300 and $3300 \text{ m}^3/\text{s}$. For each point the spectra were obtained to see if there is significant differences between the two designs.

In the small spillway model twelve piezometric openings were located - close to the corner of the bend and measurements for five different discharges were registered.

Both convex curve were studied for six discharges, that covered the range above and below a supposedly design discharge, and the velocities - and pressure distribution in a total of 15 piezometers were recorded.

RESULTS

With reference to the results of the flip buckets at La Angostura model, the following was observed:

- 1) The velocities measured at the entrance and exit of the traditional flip bucket differ in up to 28%, with higher values at the entrance.
- 2) The maximum pressures in the traditional bucket take place at its lower point.
- 3) In the polyhedric surfaces there is a normal stress concentration at the corners, especially in the downstream one. Therefore, the final section should be designed so that it can withstand the thrustings it will be subjected to.
- 4) The velocities measured at the entrance and exit of the flip bucket constructed with plane surfaces differ in up to 16%, with greater values upstream.
- 5) There are no considerable differences in pressure fluctuations at - the lower point of the curve and the middle of the polyhedric flip - bucket.
- 6) In the sloped exit section of the polyhedric flip bucket are the -- greatest pressure fluctuations.

The results obtained in the convex curves show that:

- 1) On the polyhedric surfaces there are negative pressures in the upstream section approximately 30% greater with respect to the smooth surfaces.
- 2) For velocities which correspond to discharges of above the 75% of - the design one there are no negative pressures on the upstream reach of the polyhedric surfaces.
- 3) The negative pressures on the polyhedric surfaces are not very sensitive to the angle changes between the two plane sections.
- 4) The polyhedric surfaces present a pressure increment in the downstream reach due to the impact of the water on them.

CONCLUSIONS

The substitution of the traditional smooth vertical curves by polyhedric surfaces was presented.

For concave curves the Potential Theory gives good enough results. There are a concentration of forces at the corners of the segmented curves

that can be considered in the design.

The pressure fluctuations at the surfaces, as shown by their spectra, - are substantially the same for both types of design.

For convex surfaces there are negative pressures that preclude its use without an aeration system.

REFERENCES

1. Echávez G, Arreguín F., "Superficies Poliédricas en Obras de Excedencia", VII Congreso de la Academia Nacional de Ingeniería, Oaxaca, México, Septiembre, 1981.
2. Echávez G, Arreguín F., "Diseño Poliédrico de Obras de Excedencia", X Congreso Latinoamericano de Hidráulica, México, D.F., 1982, pp 270 278.

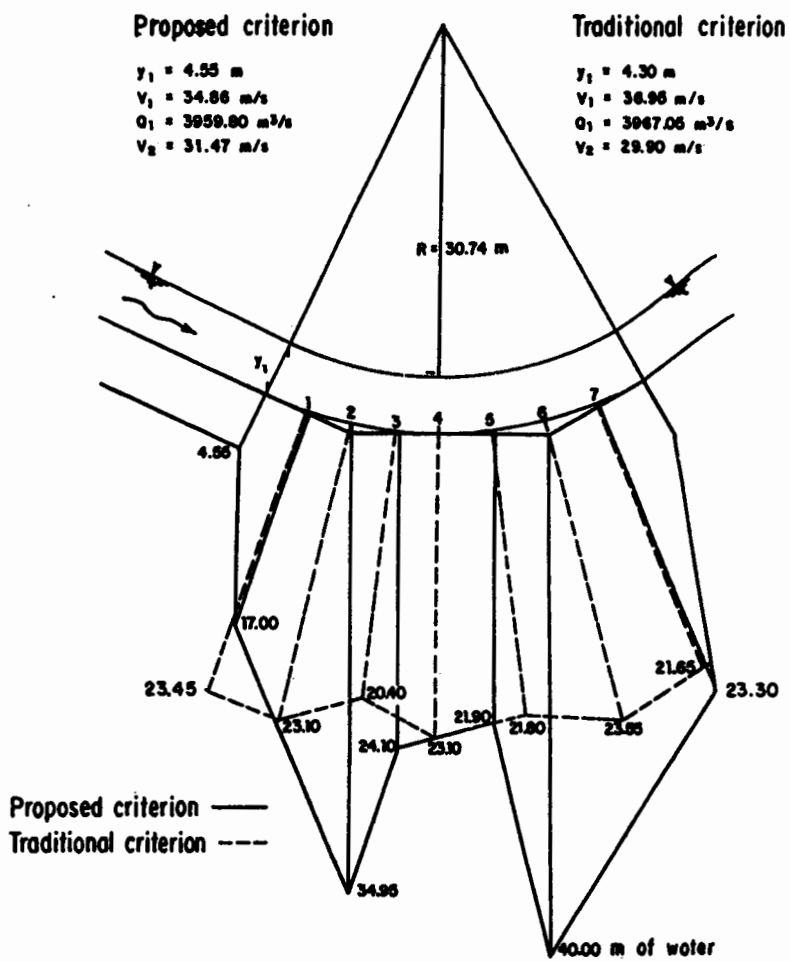


Fig 3 Comparison of pressure distribution between the traditional curve and the polyhedral surface

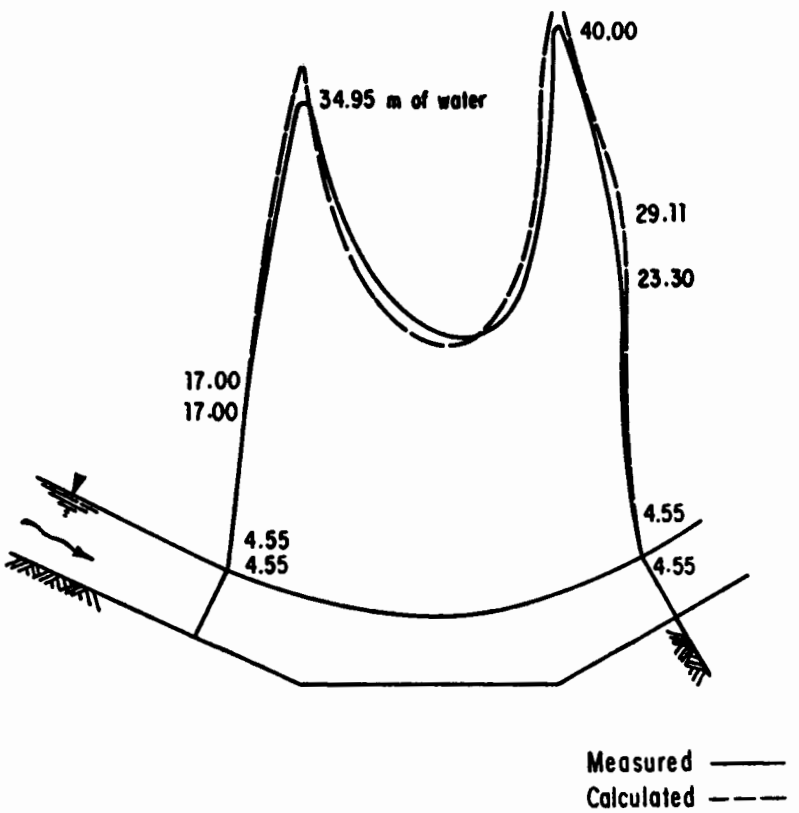


Fig 4 Comparison of pressure distributions measured and calculated

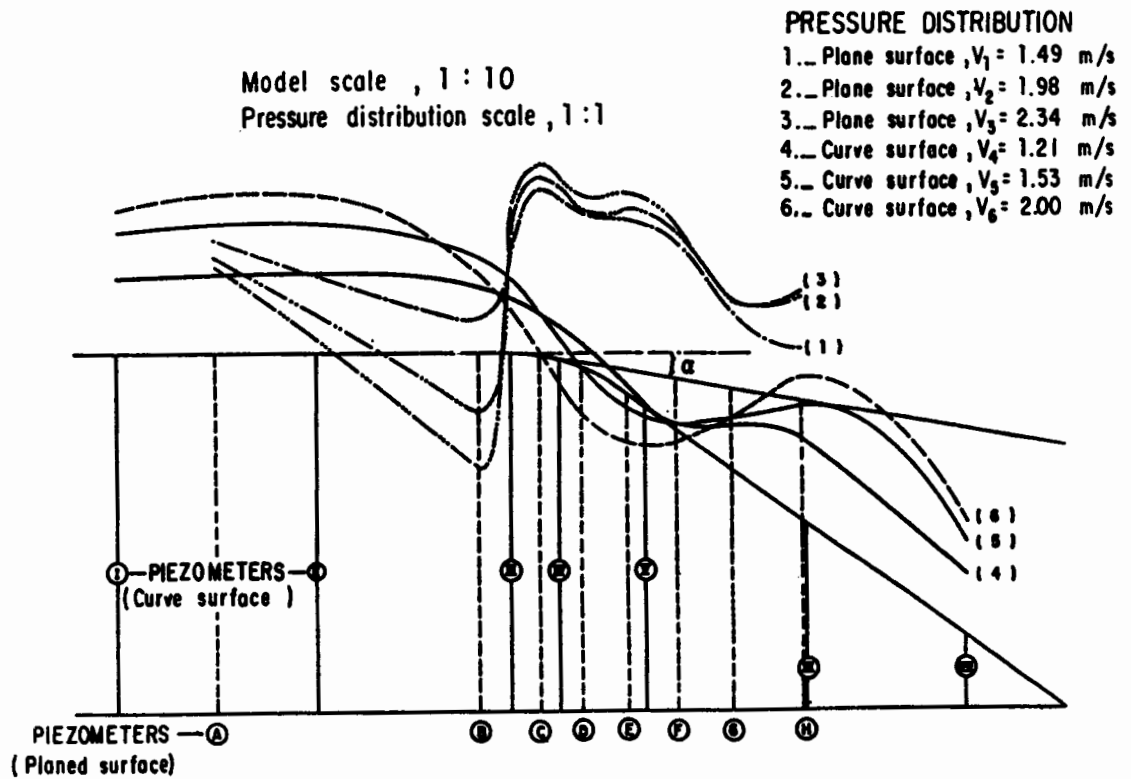


Fig 5 Pressure distributions on the polyhedric and curved surfaces , $\alpha = 9.66^\circ$

The GEV Distribution in Drought Frequency Analysis

Jose A. Raynal-Villaseñor**
M. ASCE
Jose C. Douriet-Cardenas**

Abstract

Three decades have passed since Jenkinson (1955) found the general solution to the Stability Postulate, which is the condition that all the extremes must meet, and after him that solution has been called the general extreme value (GEV) distribution.

The GEV distribution has been widely used in flood frequency analysis, but rarely has been applied to drought frequency analysis. This is the topic of the paper. Furthermore, estimation procedures to obtain its - parameters are included in the text of the paper. The methods depicted are: moments, maximum likelihood and probability weighted moments.. Finally, the results of application of the GEV distribution to a re-gion in Northwestern Mexico are reported, too.

Introduction

Among the most common distributions used to perform drought frequency analysis are: 3 parameter Log-Normal, Gumbel, Extreme Value type III and Pearson types III and V, (Gumbel, 1958 and Matalas, 1963). The - usual methods for parameter estimation of such distributions are the well-known methos of moments and maximum likelihood.

Recently, the so-called GEV distribution has been applied to flood - frequency analysis successfully, estimating its parameters by the me-thods of moments and maximum likelihood, mainly. Due to the property that such distribution can represent extreme value distribution types II and III directly, and as a limiting condition when the shape para-meter goes to zero, extreme value (EV) distribution type I can also be represented, which it makes the distribution a good candidate among - the possible distributions to model extreme values.

The method of probability weighted moments has been proposed in the - literature a few years ago (Greenwood et al, 1979), and due to the -- straightforward expressions that usually are produced for the estima-tors of the parameters of directly invertible probability distribution functions and the unbiased condition of the estimators in this method, constitutes a powerful tool for parameter estimation.

** Water Resources Program, DEPFI, Universidad Nacional Autonoma de Mexico, Cd. Universitaria, 04510 Mexico, D.F., Mexico.

General Extreme Value Distribution for the Minima

The distribution function for the GEV distribution for the maxima is, (NERC, 1975):

$$F(x) = \exp \left[- \frac{(1-(x-x_0)\beta)^{1/\beta}}{\alpha} \right] \quad (1)$$

where x_0 , α and β are the location, scale and shape parameters, respectively. Now, using the symmetry principle, (Gumbel, 1958):

$$F_{\min}(x) = 1 - F_{\max}(-x) \quad (2)$$

the corresponding GEV distribution for the minima can be obtained as:

$$F(x) = 1 - \exp \left[- \frac{(w-x)\beta}{\alpha} \right]^{1/\beta} \quad (3)$$

where w , α and β are the location, scale and shape parameters, respectively. The probability density function of eq. (3) is:

$$f(x) = \frac{1}{\alpha} \exp \left[- \left(1 - \frac{w-x}{\alpha}\beta\right)^{1/\beta} \right] \left(1 - \frac{w-x}{\alpha}\beta\right)^{1/\beta-1} \quad (4)$$

The probability distribution function contained in eq. (3) has two branches:

$$\text{EV type II distribution } \beta < 0; \quad -\infty < x < w - \frac{\alpha}{\beta}$$

$$\text{EV type III distribution } \beta > 0; \quad w - \frac{\alpha}{\beta} \leq x < \infty$$

and taking the limit when β goes to zero, the EV type I distribution is obtained and this distribution is unlimited in both sides.

Estimation Procedures for the Parameters of the GEV distribution for the Minima

Method of Moments

Using the well-known method for moments for the GEV distribution for the minima, the following relationship can be obtained:

$$\gamma = (-1)^i \frac{\Gamma(1+3\beta) - 3\Gamma(1+2\beta) \Gamma(1+\beta) + 2 \Gamma^3(1+\beta)}{[\Gamma(1+2\beta) - \Gamma^2(1+\beta)]^{3/2}} \quad (5)$$

where γ is the skewness coefficient, $i=1$ for $\beta < 0$ and $i=2$ for $\beta > 0$, and $\Gamma(.)$ is the complete gamma function for argument $(.)$.

If eq. (5) is inverted by polynomial regression, the following expressions provide a direct estimation of the shape parameter:

$$\beta > 0; -1.1396 < \hat{\gamma} < 11.35$$

$$\begin{aligned}\hat{\beta} = 0.2794 &+ 0.3335 \hat{\gamma} + 0.0403 \hat{\gamma}^2 - 0.0244 \hat{\gamma}^3 + 0.0037 \hat{\gamma}^4 \\ &- 2.6316 \times 10^{-4} \hat{\gamma}^5 + 7.0135 \times 10^{-6} \hat{\gamma}^6\end{aligned}\quad (6)$$

$$\beta < 0; -19.04 < \hat{\gamma} \leq -1.1396$$

$$\begin{aligned}\hat{\beta} = 0.2466 &+ 0.2866 \hat{\gamma} + 0.0724 \hat{\gamma}^2 + 0.0101 \hat{\gamma}^3 + 0.0008 \hat{\gamma}^4 \\ &+ 3.6385 \times 10^{-5} \hat{\gamma}^5 + 8.6489 \times 10^{-7} \hat{\gamma}^6 + 8.1446 \times 10^{-9} \hat{\gamma}^7\end{aligned}\quad (7)$$

and the location and scale parameters are estimated as follows:

$$\hat{w} = \bar{x} + \frac{\hat{\alpha}}{\hat{\beta}} [1 - \Gamma(1+\hat{\beta})] \quad (8)$$

$$\hat{\alpha} = \frac{\hat{\sigma} \hat{\beta}}{[\Gamma(1+2\hat{\beta}) - \Gamma^2(1+\hat{\beta})]^{1/2}} \quad (9)$$

where \hat{x} and $\hat{\sigma}$ are the estimated mean and standard deviation of the data.

Method of Maximum Likelihood

The likelihood function for the GEV distribution for the minima is:

$$L(x_i; w, \alpha, \beta) = \frac{1}{\alpha^N} \exp \left[- \sum_{i=1}^N \left(1 - \left(\frac{w-x_i}{\alpha} \right) \beta \right)^{1/\beta} \right] \prod_{i=1}^N \left(1 - \left(\frac{w-x_i}{\alpha} \right) \beta \right)^{1/\beta} \quad (10)$$

and the corresponding log-likelihood function is:

$$LL(x_i, w, \alpha, \beta) = -N \ln \alpha - \sum_{i=1}^N \left(1 - \left(\frac{w-x_i}{\alpha} \right) \beta \right)^{1/\beta} + \left(\frac{1}{\beta} - 1 \right) \sum_{i=1}^N \ln \left(1 - \left(\frac{w-x_i}{\alpha} \right) \beta \right) \quad (11)$$

Now, using the approximation to maximum likelihood estimates provided by the method of scoring, the following iterative scheme is used to obtain the maximum likelihood estimates:

$$w_{i+1} = w_i + \delta_w \quad (12)$$

$$\alpha_{i+1} = \alpha_i + \delta_\alpha \quad (13)$$

$$\beta_{i+1} = \beta_i + \delta_\beta \quad (14)$$

where δ_w , δ_α and δ_β are the deviations from the true maximum likelihood estimates at stage i . They are computed as:

$$\delta_w = \frac{\alpha}{N} [bQ - \frac{h}{\beta} (P + Q) - \frac{f}{\beta} (R - \frac{P + Q}{\beta})] \quad (15)$$

$$\delta\alpha = \frac{\alpha}{N} \left(hQ - \frac{a}{\beta} (P + Q) - \frac{g}{\beta} \left(R - \frac{(P + Q)}{\beta} \right) \right) \quad (16)$$

$$\delta\beta = \frac{1}{N} \left[fQ - \frac{g}{\beta} (P + Q) - \frac{a}{\beta} \left(R - \frac{(P + Q)}{\beta} \right) \right] \quad (17)$$

where N is the sample size, a,b,c,f,g,h are teh coefficients of the variance-covariance of the parameters of the GEV distribution for the minima, see table 1.

Table 1. Coefficients of the variance-covariance matrix of the parameters of the GEV distribution for the minima.

	a	b	c	f	g	h
0.10	0.2043	0.5109	-0.7818	0.9519	-0.7132	0.3231
0.20	0.1714	0.7273	-0.3862	0.5063	-0.4679	0.3531
0.30	0.1846	0.8461	-0.1998	0.2667	-0.2944	0.3952
0.40	0.2398	0.9298	-0.1147	0.1425	-0.1638	0.4722
0.50	0.3185	1.0109	-0.0731	0.0628	-0.1034	0.5674
0.60	0.4214	1.1004	-0.0484	0.0085	-0.0798	0.6810
0.70	0.2675	0.5012	-0.0299	0.0310	-0.0317	0.3661
0.80	0.0794	0.1575	-0.0577	-0.0094	-0.0419	0.1118

and P, Q and R are:

$$P = N - \sum_{i=1}^N \bar{e}^{y_i} \quad (18)$$

$$Q = \sum_{i=1}^N e^{(\beta-1)y_i} - (1-\beta) \sum_{i=1}^N e^{\beta y_i} \quad (19)$$

$$R = N - \sum_{i=1}^N y_i + \sum_{i=1}^N y_i \bar{e}^{y_i} \quad (20)$$

where:

$$y_i = -\frac{1}{\beta} \ln \left(1 - \left(\frac{w-X_i}{\alpha} \right) \beta \right) \quad (21)$$

and the convergence criteria are:

$$\left(\frac{\partial LL}{\partial w} \right)_i = \frac{Q}{\alpha} \approx 0 \quad (22)$$

$$\left(\frac{\partial LL}{\partial \alpha} \right)_i = -\left(\frac{P+Q}{\beta} \right) \approx 0 \quad (23)$$

$$\left(\frac{\partial LL}{\partial \beta} \right)_i = -\frac{1}{\beta} \left(R - \left(\frac{P+Q}{\beta} \right) \right) \approx 0 \quad (24)$$

Method of Probability Weighted Moments

The estimators of the parameters for the GEV distribution for the minima are, (Raynal-Villaseñor, 1987):

$$\hat{w} = M_0 - \frac{[1 - \frac{1}{\Gamma(1+\beta)}] [M_0 - 2M_1]^2}{[M_0 + 4M_3 - 4M_1]} \quad (25)$$

$$\hat{\alpha} = \frac{\hat{\beta} [M_0 - 2M_1]^2}{\Gamma(1 + \beta) [M_0 + 4M_3 - 4M_1]} \quad (26)$$

$$\hat{\beta} = \ln \left[\frac{M_0 - 2M_1}{2M_1 - 4M_3} \right] / \ln 2 \quad (27)$$

Examples of Application

The proposed GEV distribution for drought frequency analysis has been applied to the data of the gauging stations contained in table 2, and the computed parameters for the three methods depicted in the article are contained in there.

Table 2. Parameter estimates for the methods of moments, maximum likelihood and probability weighted moments:

Station	Method								
	Moments			Maximum Likelihood			Probability Weighted Mom		
	\hat{w}	$\hat{\alpha}$	$\hat{\beta}$	\hat{w}	$\hat{\alpha}$	$\hat{\beta}$	\hat{w}	$\hat{\alpha}$	$\hat{\beta}$
La Huerta	1.74	0.78	0.42	1.74	0.74	0.40	1.78	0.81	0.49
Ixpalino	1.11	0.70	0.91	1.11	0.64	0.94	1.20	0.79	0.98
Huites	4.08	2.22	1.04	4.10	2.24	1.05	4.12	2.65	1.30

Conclusion

The GEV distribution for the minima has been presented and methods to estimate its parameters have been provided. Due to its flexibility to be adjusted to actual extreme value data its usage is recommended.

Acknowledgement

The authors wish to express their deepest gratitude to the Engineering Graduate Studies Division (DEPFI), Universidad Nacional Autonoma de Mexico, for the support provided in the realization of this paper.

References

- Gumbel, E.J. (1958). "Statistics fo Extremes", Columbia University Press. New York.
- Greenwood, J.A. et al (1979). "Probability weighted moments: definition and relation to parameters of several distributions expressable in inverse form". *J. Wat. Res. Res.*, 15 (5), 1049-1054.
- Jenkinson, A.F. (1955). "The frequency distribution of the annual maximum(minimum) values of meteorological elements". *Quart. J. Roy. Met. - Soc.*, 81, 158-171.
- Natural Environment Research Council (1975). "Flood studies report". Vol. I: Hydrological studies. Whitefriars Press Ltd. London.
- Matalas, N.C. (1963). "Probability distribution of low flows". Statistical studies in hydrology, professional paper 434-A, A1-A27.
- Raynal-Villaseñor, J.A. (1987) "Probability weighted moments estimators for the general extreme value distribution (maxima and minima)". *Hydrological Science and Technology: Short Papers J.* Accepted for publication.

KEYWORDS: droughts, extreme values, frequency analysis, maximum, likelihood, minima, moments, probability density function, probability distribution function, probability weighted moments.

Catastrophe model for the forced hydraulic jump

Modèle de catastrophe pour le ressaut hydraulique forcé

P. M. AUSTRIA

*Associate Professor,
Graduate Division of the Engineering Faculty,
National University of Mexico*



SUMMARY

In open channel flow, when a hydraulic jump is forced, an hysteretic behaviour is observed in a particular range of values of the governing variables. In this paper, the catastrophe theory is applied to the study of this phenomenon. The geometry of the cusp catastrophe is used as a descriptive model and, with this basis a calculation procedure is proposed, in which known hydraulic equations are used. The results are experimentally verified for a simplified study case.

RÉSUMÉ

Dans certaines circonstances, lorsqu'un obstacle perturbe un écoulement supercritique dans un canal ouvert, un ressaut hydraulique apparaît. Dans cet article, le problème est abordé à l'aide de la théorie des catastrophes pour laquelle on utilise la géométrie de la catastrophe fronce comme modèle descriptif; on propose une méthode de calcul basée sur équations bien connues de l'hydraulique. Les résultats sont vérifiés par une expérience faite sur un problème simplifié.

1 Introduction

The existence of an hysteretic behaviour in the transition between subcritical and supercritical flow, upstream of an obstacle, is well known. This problem has been studied by Muskatirovic and Batinic [6] and Abecasis and Quintela [1, 2, 3, 8] among others, who have proposed some calculation methods.

On the other hand, the elementary catastrophe theory, developed by Thom [10], is specially useful for the study of phenomena with a discontinuous and hysteretic behaviour.

In this paper, some concepts of the elementary catastrophe theory are used in the study of the forced hydraulic jump formation. The use of the theory is mainly descriptive.

Some fundamental concepts of the elementary catastrophe theory are presented here, because they are not of a common background. A catastrophe model, of a cusp type, is proposed for the forced hydraulic jump and a computation procedure is proposed, in which the momentum and specific energy equations are used. A simplified case is studied, and the analytical results are experimentally verified in a laboratory flume.

Despite the importance of the forced hydraulic jump itself, another main aim of this paper is to show how the elementary catastrophe theory can be used as a useful descriptive modelling tool in hydraulics.

2 Fundamentals of the catastrophe theory

The catastrophe theory was introduced by Thom in 1973 [10]. Almost immediately, the subject arose great interest. Zeeman has published several papers on the theory and its applications [13]. There are some books on the catastrophe theory and its applications to science and engineering [e.g. 5, 7, and 9].

The catastrophe theory has given rise to contrary opinions, including some amongst mathematicians, above all in relationship with its applications. In a strict mathematical sense, the theory is applied to the study of the gradient systems stability. Nevertheless, the geometries of the catastrophe functions can be very useful as descriptive models of phenomena with hysteresis and discontinuities, among others, grouping them all in one single geometry. This use is justified only when experimental results corroborate the proposed model.

Considering its use as a descriptive modelling tool, in this paper are presented only some fundamental concepts of the catastrophe theory, without any special attention being focused to its mathematical framework.

Let us consider a system whose state can be correctly defined with $X_1, X_2, X_3, \dots, X_n$ variables, that are hence called "state variables". Its value, and with them the system state, will be modified as the values of parameters a_1, a_2, \dots, a_k are changed. These are called "control parameters".

For the majority of the state variables-control parameters combinations, the system state will change continuously, but in some of these combinations a discontinuous behaviour can be observed. With the catastrophe theory, for some type of functions, it is possible to study the system behaviour under any condition.

The catastrophe theory has its main support in the "Thom's classification theorem", which states, in very simplified form, that if there are up to 5 control parameters ($K \leq 5$); and if there are up to 2 state variables ($n \leq 2$), a change of variables exists such that the function can be reduced to a canonical form. These canonical forms are called "elementary catastrophe functions" or, simply, "catastrophe functions", and are presented in Table 1.

Table 1. Elementary catastrophe functions
Catastrophes élémentaires

n	K	catastrophe function		name
		germen	perturbation	
1	1	X^3	$a_1 X$	fold
1	2	$\pm X^4$	$a_1 X + a_2 X^2$	cusp
1	3	X^5	$a_1 X + a_2 X^2 + a_3 X^3$	swallowtail
1	4	$\pm X^6$	$a_1 X + a_2 X^2 + a_3 X^3 + a_4 X^4$	butterfly
1	5	X^7	$a_1 X + a_2 X^2 + a_3 X^3 + a_4 X^4 + a_5 X^5$	
2	3	$X^2 y - y^3$	$a_1 X + a_2 y + a_3 y^2$	elliptic umbilic
2	3	$X^2 y + y^3$	$a_1 X + a_2 y + a_3 y^2$	hyperbolic umbilic
2	4	$X^2 y + y^4$	$a_1 X + a_2 y + a_3 y^2 + a_4 X^2$	parabolic umbilic
2	5	$X^2 y - y^5$	$a_1 X + a_2 y + a_3 X^2 + a_4 y^2 + a_5 y^3$	
2	5	$X^2 y + y^5$	$a_1 X + a_2 y + a_3 X^2 + a_4 y^2 + a_5 y^3$	
2	5	$X^3 \pm y^4$	$a_1 X + a_2 y + a_3 X y + a_4 y^2 + a_5 X y^2$	

In many cases it is very difficult to find this change of variables, because the governing equation is complicated; it is a differential equation with unknown solution or, in the worst case, the governing equation itself is unknown. Under these circumstances it is possible to suspect the existence of a catastrophe if the phenomenon exhibit certain characteristics, known as "catastrophe flags".

So, when one or more catastrophe flags have been identified, then one may proceed to propose a catastrophe geometry or model, of qualitative nature, which will be corroborated directly by experimental results. When a catastrophe model is proposed thus, that is, taking directly into consideration the phenomenon behaviour; in fact the catastrophe theory applicability itself is an hypothesis, because the theory application range has only been demonstrated for gradient systems, and hence the model can be only verified experimentally.

The main catastrophe flags can be observed in the cusp catastrophe geometry, which has proven specially useful for engineering applications [e.g. 7, 12].

The cusp catastrophe equation can be written as:

$$f(X; a_1, a_2) = \frac{1}{4}X^4 + \frac{1}{2}a_1 X^2 + a_2 X \quad (1)$$

The geometry of this function will be modified as the parameters a_1, a_2 change. For the majority of the values of a_1, a_2 the function has only one critical point (that is, a point where the derivative is zero), a minimum, but for some a_1, a_2 combinations the function has three critical points, two of them minima. We must consider that, between all the values of the function for any, a_1, a_2 combination, the system can only remain in one of those minima. Hence the minima of the catastrophe function defines the state of the system.

Then, the state surface of a catastrophe function is defined by the equation:

$$\nabla f(X_i; a_j) = 0 \quad \begin{matrix} 1 \leq i \leq 2 \\ 1 \leq j \leq 5 \end{matrix} \quad (2)$$

For the cusp catastrophe, the state surface equation is obtained by deriving Equation (1):

$$X^3 + a_1 X + a_2 = 0 \quad (3)$$

The geometry defined by this equation is shown in Fig. 1. The region where multiple solutions exist is known as "singularity subset", and its projection over the control surface, that is, the plane formed by the control parameter axis, is known as "bifurcation set".

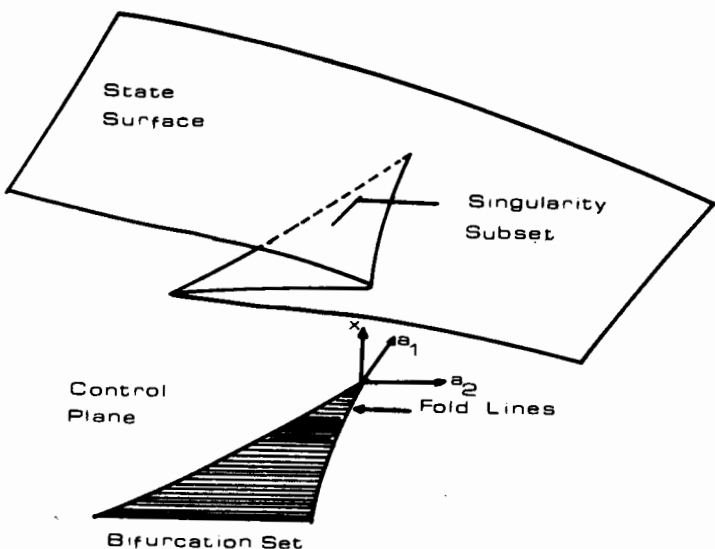


Fig. 1. Geometry of the cusp catastrophe.
Géometrie de la catastrophe fronce.

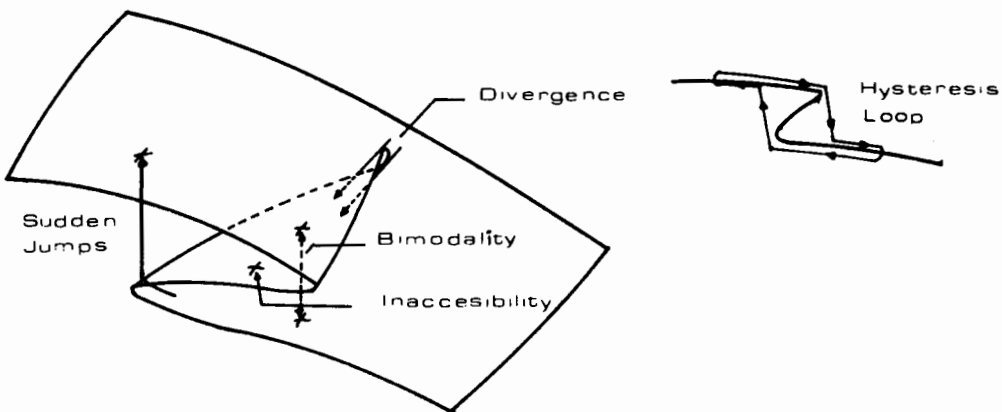


Fig. 2. Catastrophe flags in the cusp catastrophe.
Signes de catastrophe dans la catastrophe fronce.

The catastrophe flags observed in the cusp catastrophe geometry are shown in Fig. 2. They are:
Sudden jumps: In the singularity subset limits, a small change in the control parameters can cause a significant modification in the system state.

Inaccessibility: The surface which joins the inferior and superior sheets is unreachable.

Bimodality: In the singularity subset, the system can have two different states.

Divergence: A small modification in the initial state can give rise to a very different final state.

Hysteresis: In the singularity subset the system state is not only defined by one particular combination of control parameters, but also by the phenomenon's history, which determines in which sheet, superior or inferior, of the catastrophe surface, the system remain.

When in a phenomenon some one of these catastrophe flags are identified, it is possible to proceed with the search of others that could be present, and define thus a catastrophe geometry.

3 Catastrophe model for the forced hydraulic jump

When an obstacle is opposed to a supercritical open channel flow, under certain circumstances, a forced hydraulic jump is produced. Let us consider, for the sake of simplicity, the installation shown in Fig. 3, provided with a vertical sluice gate and a sudden step, placed in a rectangular cross-section flume. According to flow rate (Q) and step height (ΔZ), an hydraulic jump will be formed between the step and the gate.

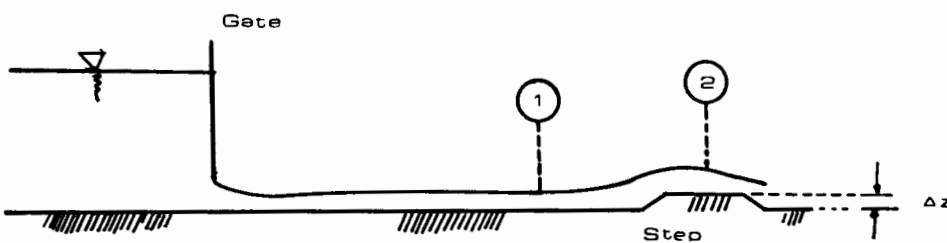


Fig. 3. Geometry for the forced hydraulic jump analysis.
Géometrie pour l'étude du ressaut hydraulique forcé.

In case that the flow is supercritical in any cross-section, condition that can be called "super-critical configuration", the depth, and hence the specific energy in Section 1, upstream of the step, will be defined by an upstream control section, the gate in Fig. 3; while the depth in the Section 2, over the step, can be calculated simply by applying the specific energy equation between both Sections, 1 and 2. For a rectangular cross-section it results:

$$y_2^3 - y_2^2(E_1 - \Delta Z) + \frac{q^2}{2g} = 0 \quad (4)$$

Where E_i and y_i are the specific energy in cross-section i , ΔZ the step height and q the volumetric flow rate for channel unit width.

The depth in Section 1 is a function of the flow rate, and can be calculated with relative easiness from the upstream control section, for instance, if the depth in the contraction, downstream of the gate, is known, and then the water surface profile until Section 1 is determined. Hence it is possible, to write a relationship between the flow rate and the depth in this section:

$$y_1 = f_1(q) \quad (5)$$

and also between flow rate and specific energy:

$$E_1 = f_2(q) \quad (6)$$

In this form, Equation (4) can be written as:

$$y_2^3 - y_2^2(f_2(q) - \Delta Z) + \frac{q^2}{2g} = 0 \quad (7)$$

This equation is valid, for a particular value of ΔZ , for high values of the volumetric rate q , such that it is possible that supercritical flow over the step occurs. It can be viewed, with a change of variables, that a bifurcation point beyond which the equation has not physically possible solutions, exists.

With the well-known change of variables [e.g. 5, page 155].

$$w = y - \frac{1}{3}(f_2(q) - \Delta Z) \quad (8)$$

Equation (7) is transformed into a reduced equation of third degree:

$$w^3 + \frac{1}{3}(f_2(q) - \Delta Z)^2 w - \frac{2}{27}(f_2(q) - \Delta Z)^3 + \frac{q^2}{2g} = 0 \quad (9)$$

The advantage of this presentation is that it is simpler to determine the range in which three or less real solutions exist. This can be done by considering the discriminant:

$$D = 0.04[-(f_2(q) - \Delta Z)]^3 \frac{q}{2g} + 0.25 \left(\frac{q^2}{2g}\right)^2 \quad (10)$$

If $D > 0$, there is only one negative solution, without physical signification.

If $D < 0$, there are three real solutions, two of them positive. The point $D = 0$ is a bifurcation point. In Fig. 4, the qualitative form of Equation (9) is presented. The point beyond which no positive solution exists defines the limit where the equation governs the phenomenon, and physically corresponds to the condition when, due to a continuous decreasing of discharge, the depth over the step becomes critical.

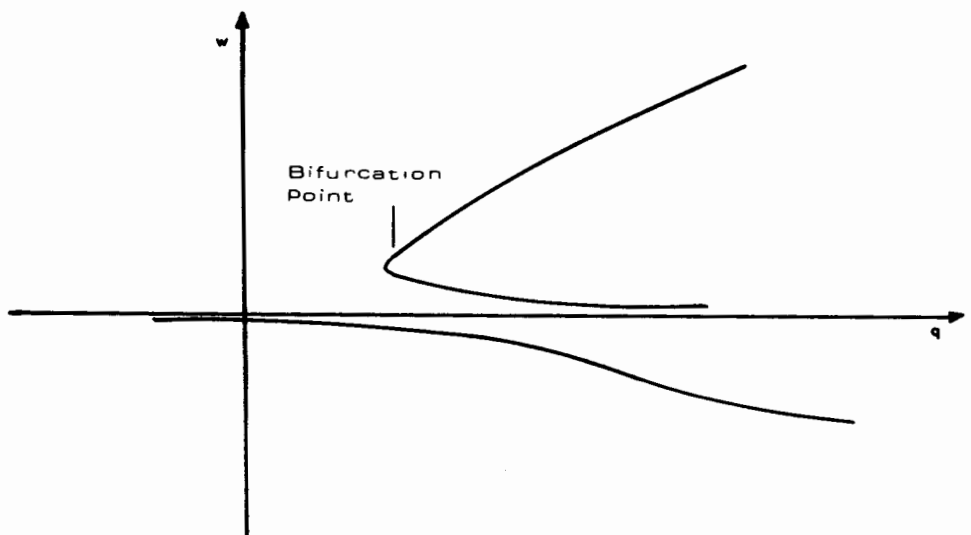


Fig. 4. Qualitative representation of Equation (9) solutions.
Représentation qualitative des solutions de l'équation (9).

In this condition, any additional decrease will cause the occurrence of an hydraulic jump upstream of the step. This flow configuration can be called "subcritical configuration", and at the sudden transition between flows, "subcritical catastrophe".

If after a subcritical catastrophe desirable to return to the supercritical configuration, a small flow rate increase is not enough. Due to the energy dissipation in the hydraulic jump, a significant increase in the system energy, and then in the volumetric flow rate, is needed. This increase in the energy only can be performed by increasing the volumetrical rate.

Hence, there exists a range of discharges at which both flow configurations, supercritical and subcritical, are possible, that is bimodality and there is hysteresis and sudden jumps too; all of which are catastrophe flags observed in the cusp catastrophe.

The change from subcritical to supercritical configuration, that is when the hydraulic jump is forced to cross the step and disappear downstream, can be called "supercritical catastrophe".

In subcritical configuration, the step section is a control section, and hence here the depth is critical, and the specific energy the minimum:

$$y_2 = y_c = \sqrt[3]{\frac{q^2}{g}} \quad (11)$$

$$E_2 = E_{\min} = \frac{3}{2} \sqrt[3]{\frac{q^2}{g}} \quad (12)$$

The upstream depth, in Section 1, will be determined by applying the specific energy equation between both Sections, 1 and 2. It results:

$$y_1^3 - y_1^2(E_2 + \Delta Z) + \frac{q^2}{2g} = 0 \quad (13)$$

and from the Equation (12):

$$y_1^3 - y_1^2 \left(\frac{3}{2} \sqrt[3]{\frac{q^2}{g}} + \Delta Z \right) + \frac{q^2}{2g} = 0 \quad (14)$$

The discharge corresponding to subcritical catastrophe can be calculated both by solving Equation (10) with $D=0$ or looking for the point where the depth, calculated with Equation (7), is equal to the critical depth.

For determining the discharge corresponding to supercritical catastrophe, due to the discontinuity in energy because of the hydraulic jump is not possible to analyse Equation (14) as we did with Equation (7). The supercritical catastrophe takes place when the conjugate of the depth obtained from Equation (5) is the same as the depth calculated with Equation (14).

In Figs. 5 and 6 the relationships between q and y , for the sections over the step and upstream of it, are presented. In Fig. 7 the relations y_1/y_2 vs q is presented. Both Figs. 6 and 7, can be viewed as cross-sections of a cusp catastrophe surface.

Introducing the usual nomenclature in catastrophe theory applications, the existence of stable and metastable supercritical and subcritical flows can be established, as well as hysteretic ranges and catastrophe regions, among others, as shown in Fig. 7.

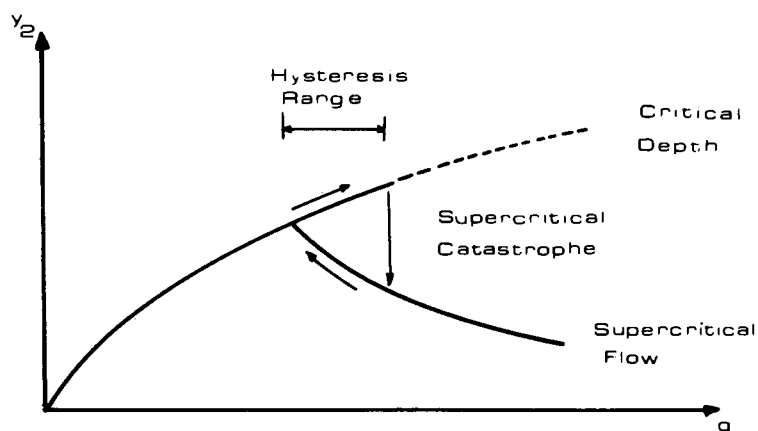


Fig. 5. Depth variation over step.
Variation du hauteur sur l'échelon.

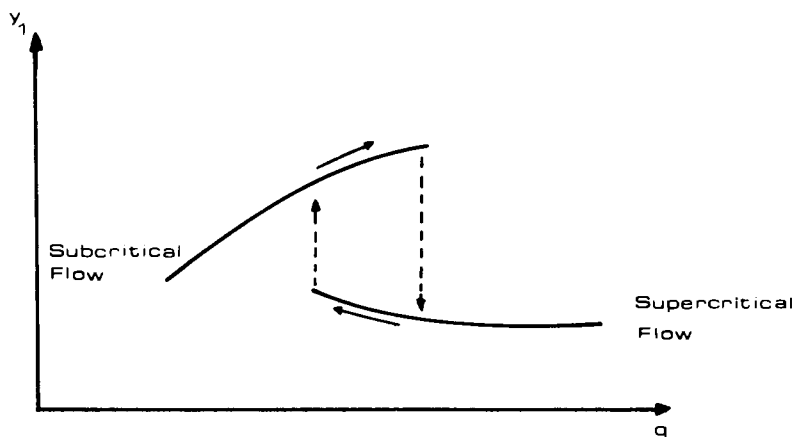


Fig. 6. Depth variation upstream of the step.
Variation du hauteur en amont de l'échelon.

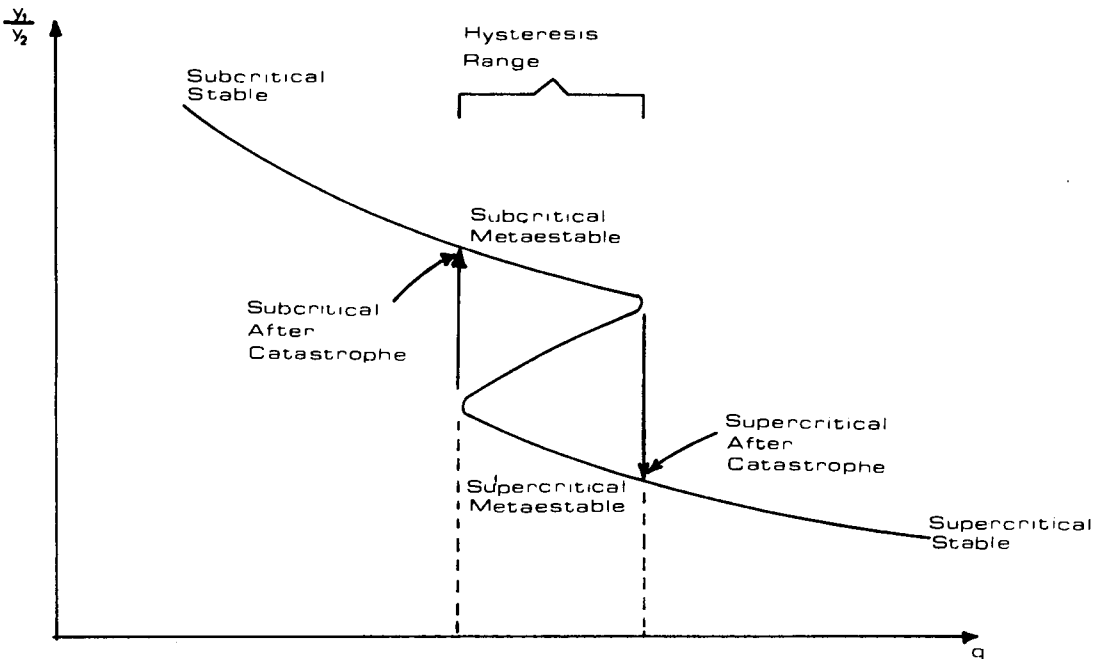


Fig. 7. Catastrophe nomenclature for the forced hydraulic jump.
Nomenclature de catastrophe pour le ressaut hydraulique forcé.

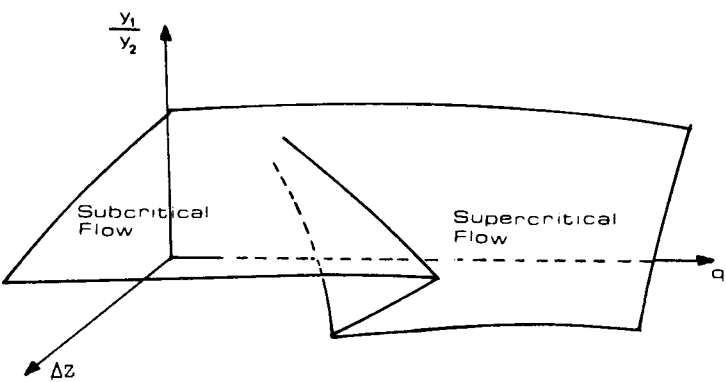


Fig. 8. Catastrophe model for the forced hydraulic jump.
Modèle de catastrophe pour le ressaut hydraulique forcé.

As the Figs. 6 and 7 show, the flow rate is a control parameter, and in both Equations (7) and (14), it is possible to see that the other is the height of the step, and hence the catastrophe geometry is as it is presented qualitatively in Fig. 8.

The computation procedure, as proposed herein, is easily programmable in a microcomputer, which can trace cross-sections of the catastrophe surface, for different ΔZ values, and for each gate opening.

4 Experimental verification

In order to corroborate the proposed catastrophe model, several experiments have been made in a laboratory flume, in the Hydraulics Laboratory of the Graduate Division in the Engineering Faculty, National University of Mexico.

The flume cross-section is rectangular of 0.30 m width. The volumetric rate is measured with a flowmeter in the supply pipe.

A device as shown in Fig. 3 has been mounted in the flume. Experiments with several gate openings and step heights were made, finding in all cases consistency with theoretical results. As an example, in Figs. 9 and 10 the results obtained for a 4 cm gate opening and $\Delta Z = 4.4$ cm are presented.

In Fig. 9 the y_2 vs Q and y_1 vs Q relationships are presented and in Fig. 10 y_1/y_2 vs q . In all cases the continuous line represents the analytically obtained results.

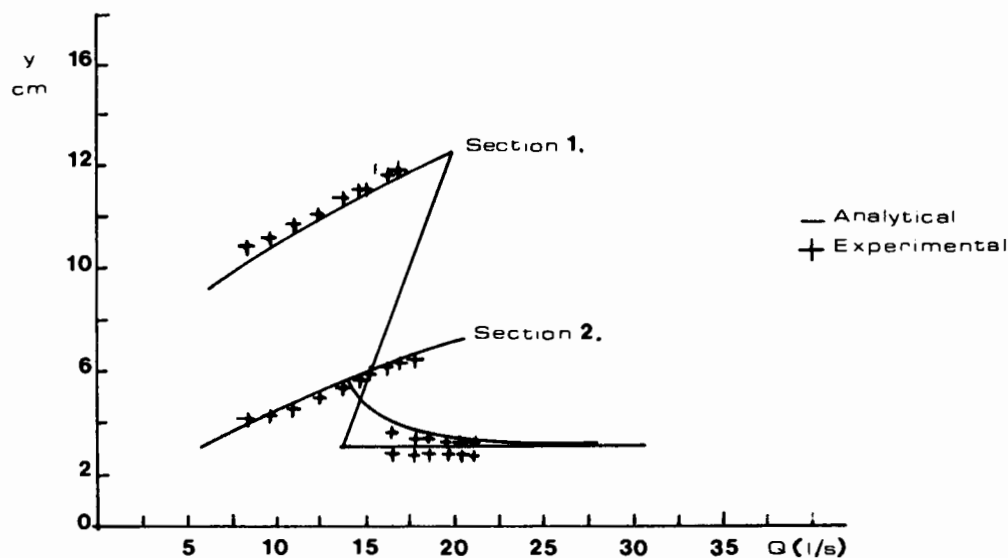


Fig. 9. Analytical and experimental results.
Résultats experimentels et analytiques.

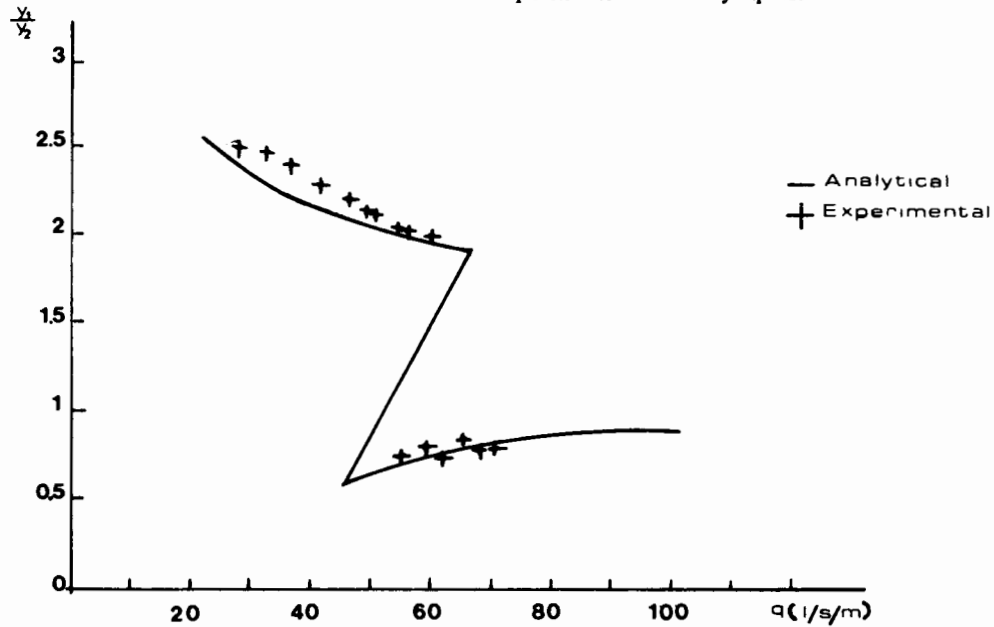


Fig. 10. Analytical and experimental results y_1/y_2 vs q relationship.
Résultats experimentels et analytiques y_1/y_2 vs q .

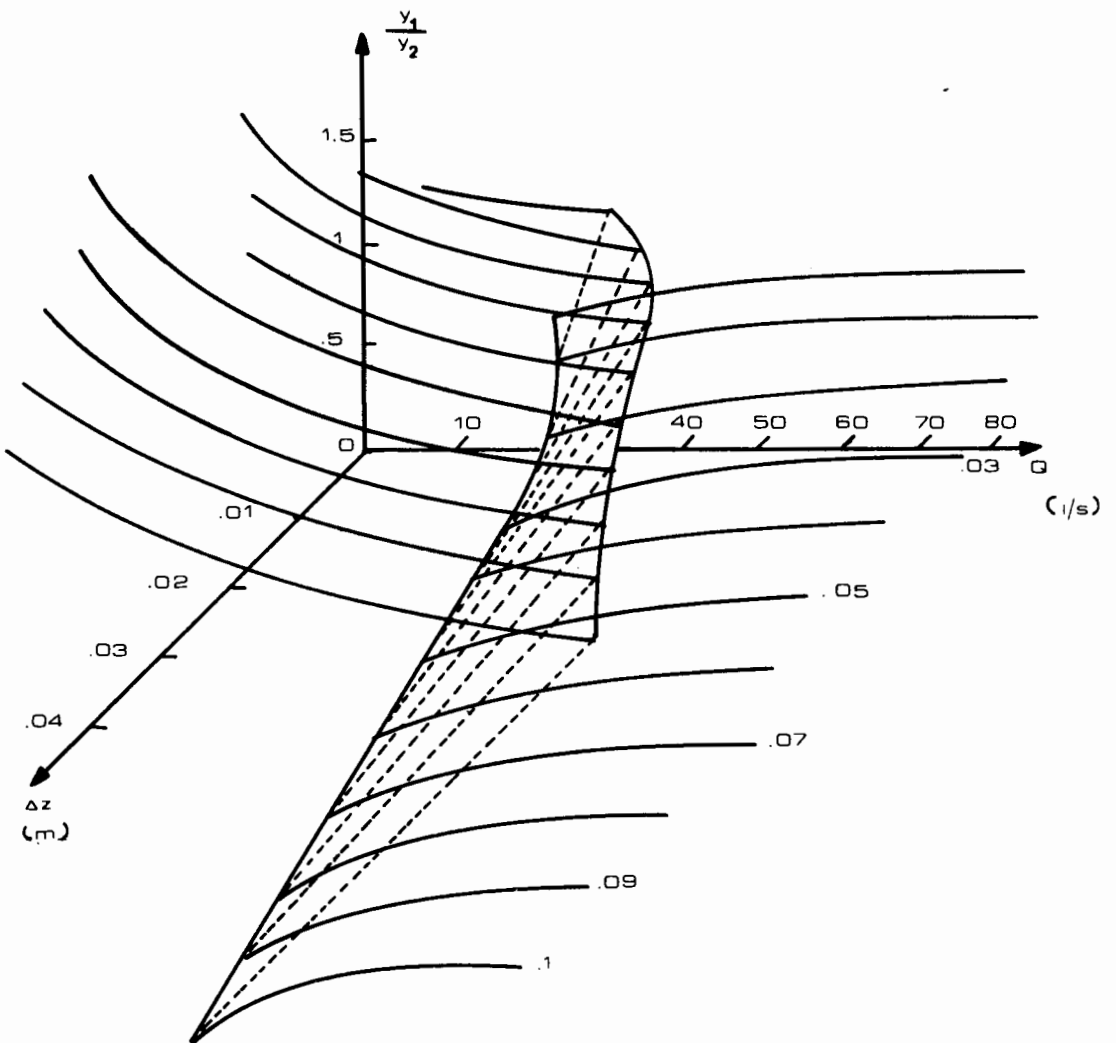


Fig. 11. Catastrophe geometry for the example. Gate opening 4 cm.
Géométrie de catastrophe pour l'exemple. Ouverture de vanne 4 cm.

The difficulty of attaining in the experiments the theoretical volumetric flow rates of catastrophe must be emphasized, which is due to the fact that in its proximity, small perturbations can easily produce the transition between supercritical and subcritical flow.

The whole catastrophe geometry, analytically obtained, for a 4 cm gate opening, computed with the procedure before sketched, is shown in Fig. 11.

Due to the fact that the system behaviour is hardly dependent of the depth-flow rate relationship in the upstream control section, it is not possible to obtain a general catastrophe surface for all cases.

5 Conclusions

In this paper an application of the elementary catastrophe theory concepts to the forced hydraulic jump has been made.

The cusp catastrophe geometry is used as a descriptive model, with which it is possible to gather certain behaviour peculiarities in the phenomenon, such as hysteresis, sudden jumps, bimodality and divergence. In addition, a nomenclature in accordance with the usual one in catastrophe theory has been introduced.

The cusp catastrophe geometry has been used mainly as a descriptive model, the quantitative solution procedure consists essentially in applying well-known equations such as the specific energy equation, with the aid of the qualitative model, and considering the control parameter variation.

6 Acknowledgements

This study is based on part of the work conducted by the writer in partial fulfilment of the requirements for the Doctoral degree in the Graduate Division of the Engineering Faculty of the National University of Mexico. Guidance and assistance provided by his advisor, Gabriel Echavez, is gratefully acknowledged. The writer wishes to express too his gratitude to Enzo Levi, for giving useful comments during the preparation of the manuscript.

Notations

X_i	state variable $i = 1, 2, \dots, n$
a_j	control parameter $j = 1, 2, \dots, K$
ΔZ	step height
Q	volumetric flow rate
q	volumetric flow rate for channel unit width
y_i	depth in i -cross-section
E_i	specific energy in i -cross-section
g	gravity acceleration
y_c	critical depth
E_{\min}	minimum specific energy

References / Bibliographie

1. ABECASIS, F. and QUINTELA, A., Problems of hydraulic hysteresis on steady free surface flow, 9th General Meeting, International Association for Hydraulic Research, Dubrovnik (1961).
2. ABECASIS, F. and QUINTELA, A., Problemas de histeresis hidráulica nos escoamentos permanentes em superficie livre, Technical report 316, National Laboratory of Civil Engineering, Lisbon (1961).
3. ABECASIS, F. and QUINTELA, A., Hysteresis in Steady Free-surface flow, Water Power, April (1964), pp. 147-157.
4. BRONSHTEIN, I. and SEMENDIAEV, K., Manual de matemáticas, 3rd. edition in Spanish, MIR, Moscú, (1977).
5. GILMORE, R., Catastrophe theory for scientist and engineers, Wiley, New York (1981).
6. MUSKATIROVIC, D. and BATINIC, B., The influence of abrupt change of channel geometry on hydraulic regime characteristics. 17th General Meeting International Association for Hydraulic Research, Baden-Baden (1977), Vol. 2, pp. 397-404.
7. POSTON, T. and STEWART, I., Catastrophe theory and its applications, Pitman, London, (1978).
8. QUINTELA, A. and ABECASIS, F., Hysteresis in the transition from supercritical to subcritical flow, Technical report 523, National Laboratory of Civil Engineering, Lisbon (1979).
9. SAUNDERS, P. T., An introduction to catastrophe theory, Cambridge University Press, Cambridge (1980).
10. THOM, R., Structural stability and morphogenesis, Addison Wesley, New York (1975). Translated from French, Stabilité structurelle et morphogénèse (1972).
11. ZEEMAN, C., Catastrophe model for the stability of ships, III Escola Latinoamericana de Matemática, IMPA, Rio de Janeiro, Brasil, (1976).
12. ZEEMAN, C., Euler Buckling, Symposium on Structural Stability, the theory of catastrophes and applications in the sciences, Lectures notes in mathematics 525. Springer-Verlag, Berlin and New York, (1976).
13. ZEEMAN, C., Catastrophe theory. Selected papers 1972-1977, Addison-Wesley, London (1978).

Sección de Construcción Estructuras Mecánica de Suelos

COORDINADORES

CONSTRUCCION
Dr. Gabriel Auvinet Guichard.

ESTRUCTURAS Y MECANICA DE SUELOS
Ing. Juan José Hanell Campbell

Programas Académicos

ESPECIALIZACION
Construcción

MAESTRIA
Construcción
Estructuras
Mecánica de suelos

DOCTORADO
Estructuras
Mecánica de suelos

Profesores de Carrera y Líneas de Investigación

Tiempo completo

AUVINET GUICHARD, GABRIEL. Doctor en ingeniería. Universidad Nacional Autónoma de México. Influencia de la estructura de los medios granulares sobre sus propiedades mecánicas, aplicación del enfoque probabilista en geotecnia.

DIAZ RODRIGUEZ, ABRAHAM. Doctor en ingeniería. Universidad Nacional Autónoma de México. Compresibilidad dinámica de suelos cohesivos, características esfuerzo-deformación, resistencia dinámica de suelos cohesivos, comportamiento sísmico de depósitos de suelos granulares finos, diseño de equipo de dinámica de suelos.

JUAREZ BADILLO, EULALIO. Doctor en ingeniería. Harvard University-UNAM. Relaciones esfuerzo-deformación de geomateriales, resistencia al esfuerzo cortante, consolidación de los suelos, ecuaciones constitutivas de geomateriales.

DEL VALLE CALDERON, ENRIQUE. Maestro en ciencias. Universidad de Illinois, E.U.A. Estructuras e ingeniería sísmica.

Medio tiempo

RODRIGUEZ CUEVAS, NEFTALI. Ingeniero. Universidad Nacional Autónoma de México. Problema de viento, interacción suelo-estructura, inestabilidad estructural, problemas de silos.

ZEEVAERT WIECHERS, LEONARDO. Doctor en ingeniería. Universidad Urbana de Illinois, E.U.A. Comportamiento sismogeodinámico de la superficie del suelo en la ciudad de México.

Publicaciones Construcción, Estructuras, Mecánica de Suelos

ALBERRO A J , RODRIGUEZ C N , MARTINEZ J M , *Almacenamiento de petróleo en domos salinos*, Series del Instituto de Ingeniería, UNAM, México, julio.

AUVINET G G , ESQUIVEL D R , *Impermeabilización de lagunas artificiales*. Publicación de la Sociedad Mexicana de Mecánica de Suelos y LIMUSA, México, febrero.

AUVINET G G , *Comportement de trois barrages en terre lors des séismes du Mexique de Septembre 1985*, Journées d'étude sur le Calcul Dynamique des Barrages, Electricité de France, Aix-les-Bains, Francia, junio.

AUVINET G G , *Low porosity granular soils mixtures*, Proceedings, VIII Panamerican Conference on Soil Mechanics and Foundations Engineering, Vol. III, Cartagena, Colombia, agosto.

AUVINET G G , *Foundations design and construction in Mexico City after the September 1985 earthquake*, International Conference on Design Construction and Repair of Building Structures in Earthquake Zones, Dubrovnik, Yugoslavia, septiembre.

AUVINET G G , CAMBOU B , *Contribution a l'étude de la structure des milieux granulaires formés de grains non sphériques*, Colloque Franco-Polonais de Mécanique des Soils, Grenoble, Francia, noviembre.

AUVINET G G , MENDOZA M , *Consideraciones respecto al diseño de cimentaciones sobre pilotes de fricción en zonas sísmicas*, Memoria del VII Congreso Nacional de Ingeniería Sísmica, Querétaro, México, noviembre.

DEL VALLE C E , *Preliminary study of the collapse of the Pino Suárez building, report on Michoacan earthquake 1985*, National Academy of Sciences and Earthquake Engineering Research Institute.

DIAZ R J A , *Strength of Mexico City clay subjected to cyclic loading*, VIII C.P.M. Congreso Internacional de Mecánica de Suelos, Cartagena, Colombia.

GONZALEZ A R , RODRIGUEZ C N , *Correlación entre características dinámicas observadas y calculadas, de un edificio*. Proyecto 7703, Instituto de Ingeniería, UNAM, México, julio.

JUAREZ B E , *Mechanical characterization of Mexico City clay*, Sociedad Mexicana de Mecánica de Suelos, Ed. Manuel J. Mendoza y Luis Montañez, México, agosto.

RODRIGUEZ C N , *Análisis experimental de vibraciones de edificios*, Informe final, proyecto 6702, Instituto de Ingeniería, UNAM, México, enero.

RODRIGUEZ C N , *Curso Víctor Hardy 87. Capítulo 3, Proyecto, Asociación Mexicana de Ingeniería de túneles y obras subterráneas, A.C., México, julio.*

RODRIGUEZ C N , *Interacción suelo-estructura, Curso internacional de Ingeniería Sismica, División de Educación Continua, UNAM., México, agosto.*

RODRIGUEZ C N , *2nd. U.S. México workshop on 1985 México earthquake research slender structure with unstable behavior, Earthquake Engineering Research Institute, México, noviembre.*

ZEEVAERT W L , *Liquefaction Induced in the Sea Bed Sediments Due to Wave Action ,* 20th International Conference on Coastal Engineering, Taiwan, Republic of China, noviembre.

ZEEVAERT W L , *Estudio del comportamiento Sismo-Dinámico de la superficie del suelo de la ciudad de México ,* III Coloquio Anual de Profesores de la DEPFI, Facultad de Ingeniería, UNAM, México, diciembre.

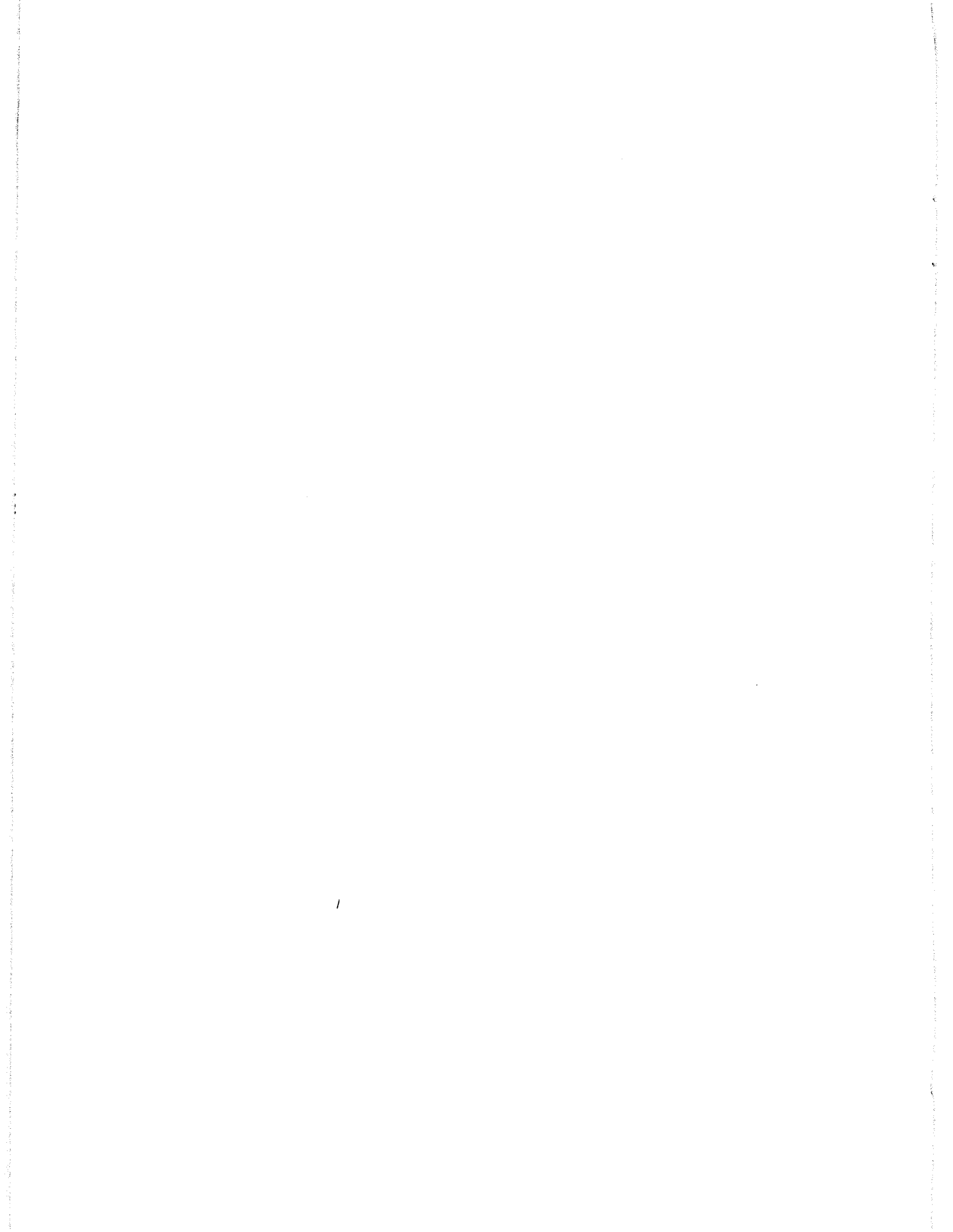
ZEEVAERT W L , *Soil-Structure Interaction of Deep Foundation in Tall Buildings Panamerican Conference, International Society for Soil Mechanics and Foundations Engineering. Cartagena 87, Colombia, agosto.*

ZEEVAERT W L , *Design and Response of Structural Steel Building in the September 1985 Strong Earthquake in Mexico City, Twentieth Annual Meetings and Conference, International Iron and Steel Institute, Río de Janeiro, Brasil, octubre.*

ZEEVAERT W L , *Seismo-Soil Dynamics Response of the Ground Surface and Building Foundations in Mexico City Earthquake, September 19, 1985. TERZAGHI LECTURE, OCTOBER 27, 1987 American Society of Civil Engineers Convention, Anaheim, Cal., E.U.A., octubre.*

Convenios

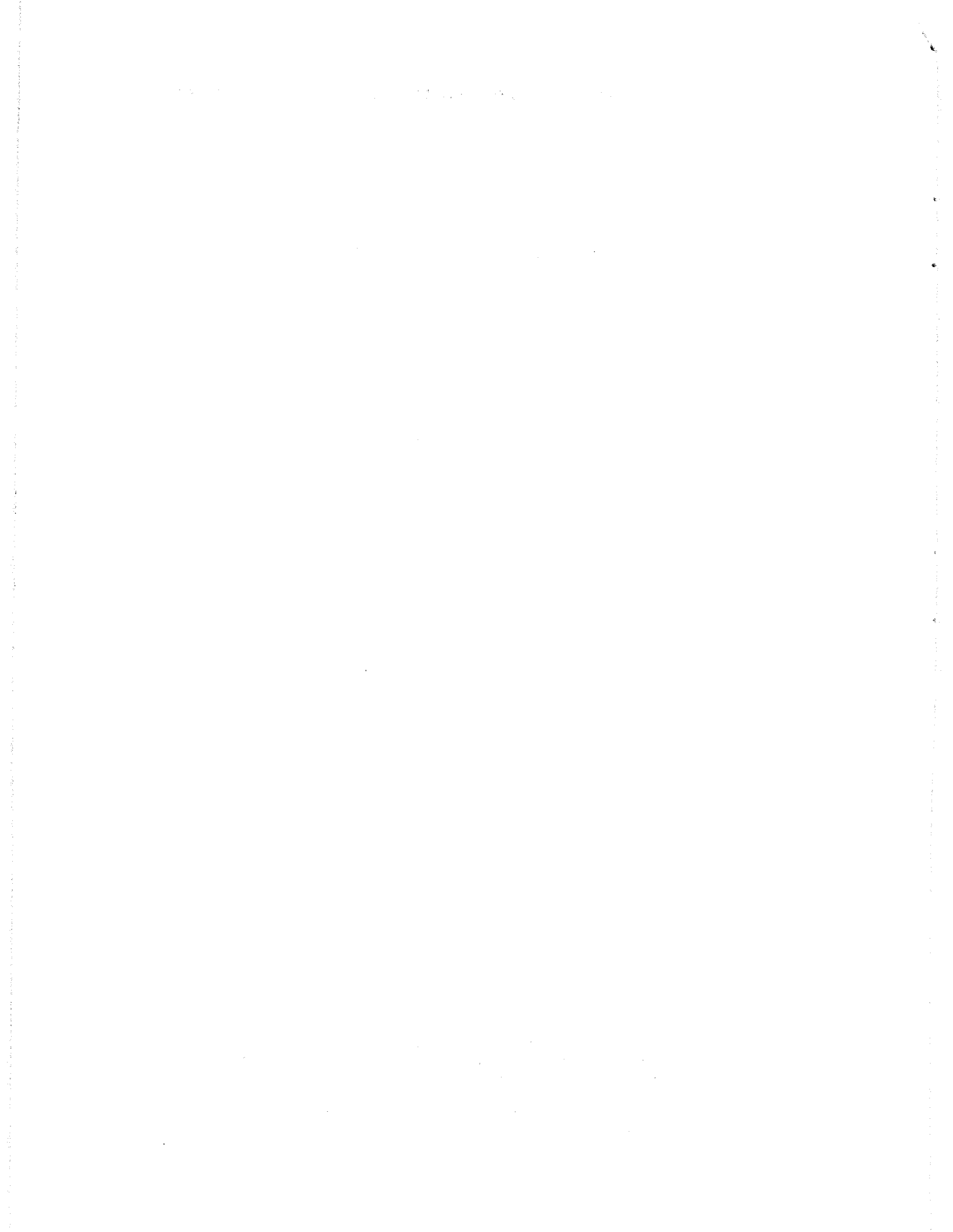
DEPFI-CONACYT. Investigación sobre hundimientos regionales y grietas en la Delegación Iztapalapa. Sección de Construcción.



Artículos reproducidos

DEL VALLE C E. *Preliminary study of the collapse of the Pino Suárez building*, Report on Michoacán earthquake 1985, National Academy of Sciences and Earthquake Engineering Research Institute. (en prensa).

ZEEVAERT W L. *Soil-Structure Interaction of Deep Foundation in Tall Buildings* Panamerican Conference, International Society for Soil Mechanics and Foundations Engineering. Cartagena 87, Colombia, agosto.



PRELIMINARY STUDY OF THE COLLAPSE OF
THE PINO SUAREZ BUILDING

*E. DEL VALLE

INTRODUCTION

On top of the Pino Suarez station of the Mexico City, line 2, "Metro, and in order to have enough load on it to avoid emergence of the station due to overcompensation caused by the deep excavation in soft clay, five buildings were constructed; two of them, oriented in the North-South direction, located at the ends of the station, and 14 stories high, and three located on the central part of the station, oriented East-West, 21 stories high, fig 1. All of them had rigid frame steel structures with diagonal bracings and lightweight concrete slabs. Facade walls and interior partitions were "non structural" and there were gaps between them and the structure to allow for motion of the buildings due to lateral wind or earthquake loads.

One of the taller buildings collapsed during the September 19, 1985 earthquake that affected Mexico city, and while collapsing swept away one of the smaller buildings, figs. 2,3. The other two taller buildings were seriously damaged, the smaller was less affected. This problem has attracted the interest of many engineers, due to the importance of the buildings involved.

DESCRIPTION OF THE BUILDINGS

The taller buildings were 12m wide, 28m. long and 73.25m. tall, with two bays in the short direction and four in the long one. Diagonal braces were used in three of the bays to reduce lateral deflections caused by earthquake or wind forces, see fig. 4, however, the layout of the braced bay in the longitudinal

*Professor of Earthquake Engineering, UNAM. Consulting Engineer

direction produced important eccentricities in plan.

All columns had 60 x 50cm box sections formed by welding four plates, the thicknesses varied from 32mm to 19mm at the bottom floors to 8mm at the top floors. Beams were 70cm deep, with open web sections, formed by angles and cover plates; in the longitudinal direction they had two webs, in the transverse direction only one web. Diagonal bracing members were 20 x 20 cm wide flange sections, see fig 5.

The structures were designed using the 1966 version of Mexico City's code, with seismic coefficient of 6% gravity and allowable stresses for the combination of vertical and horizontal loads 50% greater than those required for gravity loads alone. Design eccentricities for the calculation of torsional effects were computed increasing 50% static eccentricities, to take into account dynamic amplification, and adding or subtracting an accidental eccentricity of 5% of the dimension of the plan perpendicular to the direction of analysis. The design spectrum specified by the code to make modal dynamic analysis had maximum ordinate of 6% g for periods between 1 and 2.5 sec.

PREVIOUS BEHAVIOR OF THE BUILDINGS

The steel structures were completed in 1969 but the whole construction was finished until 1972. An earthquake that occurred in 1973 produced slight cracking in partition walls of the tall building located at the center of the station: the problem was attributed to flexibility of the structure as well as to amplification of motion due to interaction with the station, that was the common foundation of the five buildings. Periods of vibration of all the buildings were measured by the author with a portable seismometer under ambient conditions, to see if there was any difference between similar buildings and for further reference, see fig. 6. There were no significant differences in the periods of the different tall or shorter buildings, see table 1.

Another earthquake that occurred on March 14, 1979 (ref 1) stronger than the 1973 shock, produced cracking of partition walls and gypsum ceilings of the five buildings and damage in expansion joints between the buildings in the lower levels where they were connected by simple supported spans.

A thorough inspection of the buildings, uncovering several connections and column bases for inspection was made. It was not found any structural damage, but it was recommended to the owner to check the original computations and to study the convenience of an increase in stiffness in order to reduce deformations; it is ignored if this study was made. A new measurement of the periods of vibration with the same instrument gave values very similar to the ones obtained in 1973, see fig 7 and table 1, from which it was confirmed that there was not structural damage. It can be observed in table 1 that measured periods were fairly similar to those computed, showing small collaboration of non-structural elements to the stiffness, for small displacements.

Due to differential movements of the station the buildings were out of plumb. In 1979, the building that collapsed had an inclination of 20cm to the South and 3cm to the West, values which were near the tolerance specified in the Code for buildings of this height in the North-South direction; it was estimated that the inclination reduced the capacity of the building to resist earthquake forces on the order of 10%, and it was recommended to correct the problem.

PRELIMINARY STUDIES OF THE COLLAPSE

A check on the strength of the buildings after the collapse revealed that they satisfied the Code, although the eccentricity caused by the braced frame of the longitudinal direction

was on the order of 20% of the dimension of the plan of the buildings in the transverse direction, because the stiffness of that frame was nearly three times larger than that of the parallel unbraced frames. Accidental eccentricity specified by the 1966 Code was modified by a factor of two in the 1976 Code, in an effort to improve the consideration of torsional effects. The emergency rules after the 1985 earthquake limit the maximum static computed eccentricity to 20% of the plan dimension perpendicular to the direction of analysis.

It is considered that the collapse of the buildings was caused by a summation of different effects; probably the main cause was resonance, as the dominant period of the soft soil motion is on the order of 2 seconds, very close to the periods measured in 1973 and 1979 as shown in figures 6 and 7. Figure 8 shows the response spectrum obtained from the record of SCT for 5% damping, where the large amplification for structures whose periods are near two seconds can be clearly seen with maximum values on the order of 1g. If it is taken into account that 5% damping is a value relatively large for welded steel structures, the maximum amplification increases even more; therefore, there is no doubt that the forces induced by the earthquake on the building were much larger than those used to design it. It should also be taken into account the probability of larger accelerations in the Pino Suarez area, as the destruction and number of collapses in its vicinity were larger than around SCT. Another possible causes are overloads in several floors, out of plumb effects, possible defects in the structure or hidden damage due to previous earthquakes. Interaction with the station and the surrounding soil might have also contributed to the collapse.

Several observations can be made in the two similar buildings that did not collapse, but were very seriously damaged, figs 9, 10. The first one is that almost all of the columns of the

braced frame in the longitudinal direction had buckling problems see figs 11 and 12. This might have happened because that frame attracted nearly 60% of the east-west forces of the earthquake (this was the strongest component in the SCT record).

Outriggering action (ref 2) of the braced bays in the transverse direction may have increased the stiffness of the longitudinal braced frame, developing very high axial forces in the columns due to overturning effects. It can be seen in figure 11 that buckling of the columns occurred at different levels, this will have to be studied in future investigations of this buildings. Very high stresses developed in the diagonal bracings, with local buckling in some instances.

Diagonal members of the webs of the beams had also buckling problems, reducing the ductility of the frames. Emergency regulations reduce the global ductility that can be used in the case of open web beams to a maximum of 3, unless special precautions to avoid buckling are taken, in which case a value of 4 can be used.

In the longitudinal frame of the unbraced facade, it was found some interaction between the beams and the "non-structural" walls. The L-shaped walls occupied the central part of the span and were independent of the beams, but due to the very large displacements that occurred, due to torsional effects and forces larger than those used for design, some contact, that reduced the span of the beam and produced buckling of the web diagonals in the zone of the extremes of the wall occurred, producing also torsion of the two webbed beams with separation of it from the slab, fig 13.

CONCLUSIONS

Several conclusions can be obtained from this preliminary analysis, as follows:

1. It is very difficult to obtain reliable seismic design coefficients, because the information to predict the strongest earthquake that might occur is scarce, and even when there is some information about past strong earthquakes, their impact on modern structures is difficult to assess; strong earthquakes than have occurred in Mexico City in the past have shaken very different "cities", with other types of structures that have other dynamic properties and therefore were not affected in the same way, as modern buildings. Due to this reason, satisfaction of the Code is not enough, as design accelerations may be exceeded, and the structures should develop very large ductilities to survive.
2. A building that has periods of vibration close to the dominant periods of vibration of the soil on which it is constructed, will respond in a violent way to relatively small earthquakes, producing at least damage to "non-structural" elements. I consider that the building is "sending messages for help" that should be clearly understood, and something has to be done to modify their dynamic characteristics. Stiffening of the structure, elimination of unnecessary weights or addition of external dampers might be necessary.
3. Torsional effects due to static eccentricities in plan are not well taken into account assuming elastic behavior of the structure; additional studies have to be made in order to take into account, in a practical way, the inelastic behavior which may lead to drastic changes in the position of the shear center. By the moment, the best recommendation is to try to avoid static eccentricities, using symmetric layouts, especially in tall buildings.
4. Out of plumb should be avoided in tall buildings, because they may reduce the strength to resist lateral forces, due to asymmetric hysteresis loops.

5. Open web beams should be carefully designed to avoid local buckling of the diagonal elements, that may reduce ductility.

REFERENCES

1. Del Valle E. "Some lessons from the March 14, 1979 earthquake in Mexico City". Proceedings VII WCEE, Istanbul Turkey, 1980.
2. Bertero, et al . "Earthquake simulator tests and associated experimental, analytical and correlation studies of one-fifth scale model", ACI, SP 84.

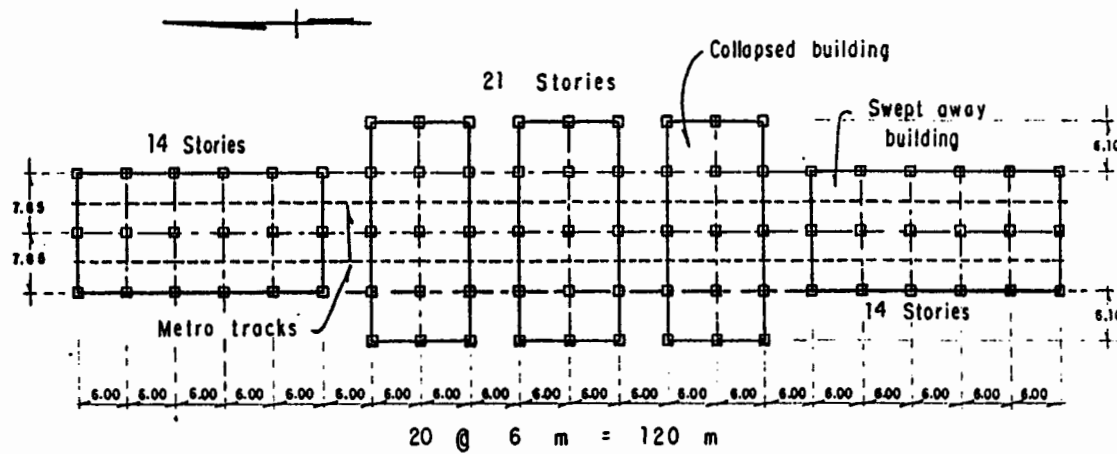


Fig 1 Location of buildings

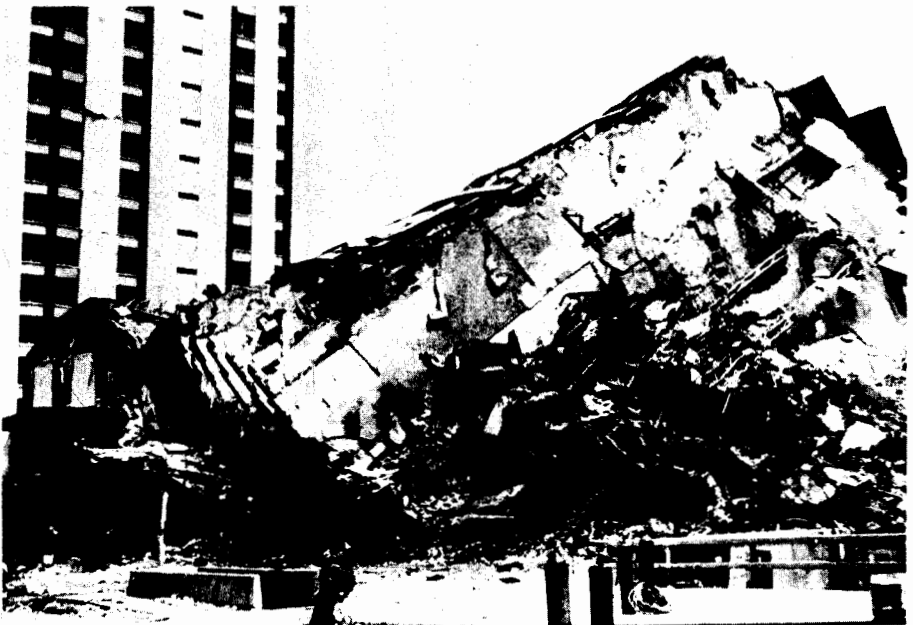


Fig 2

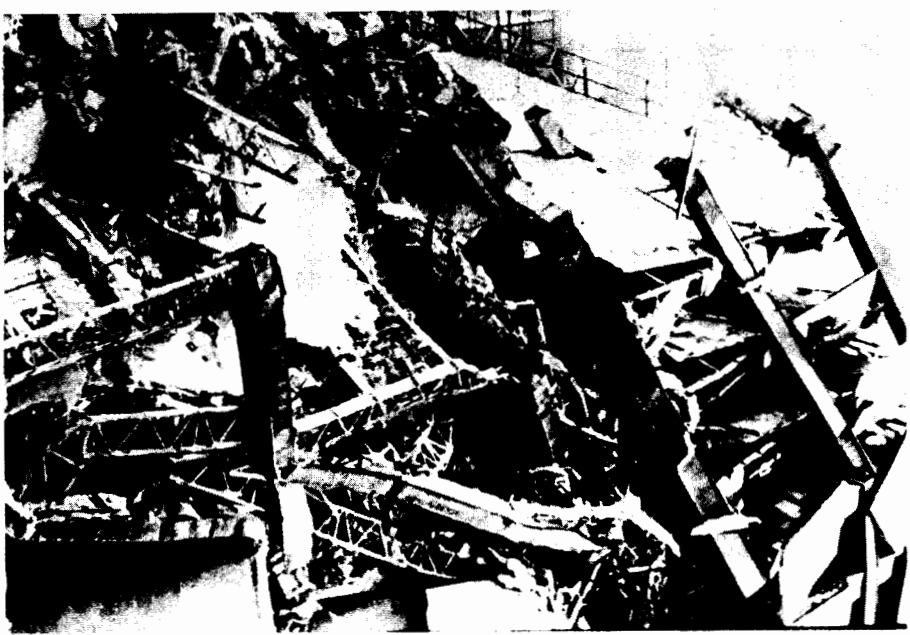


Fig 3

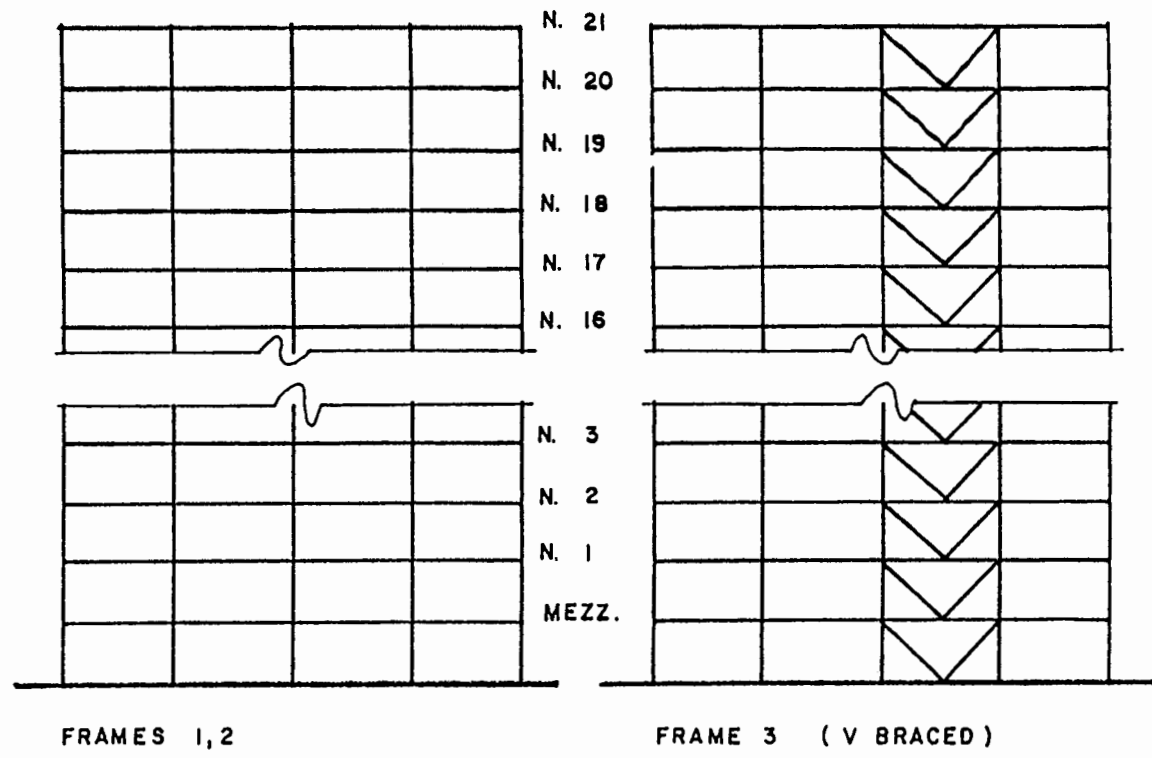
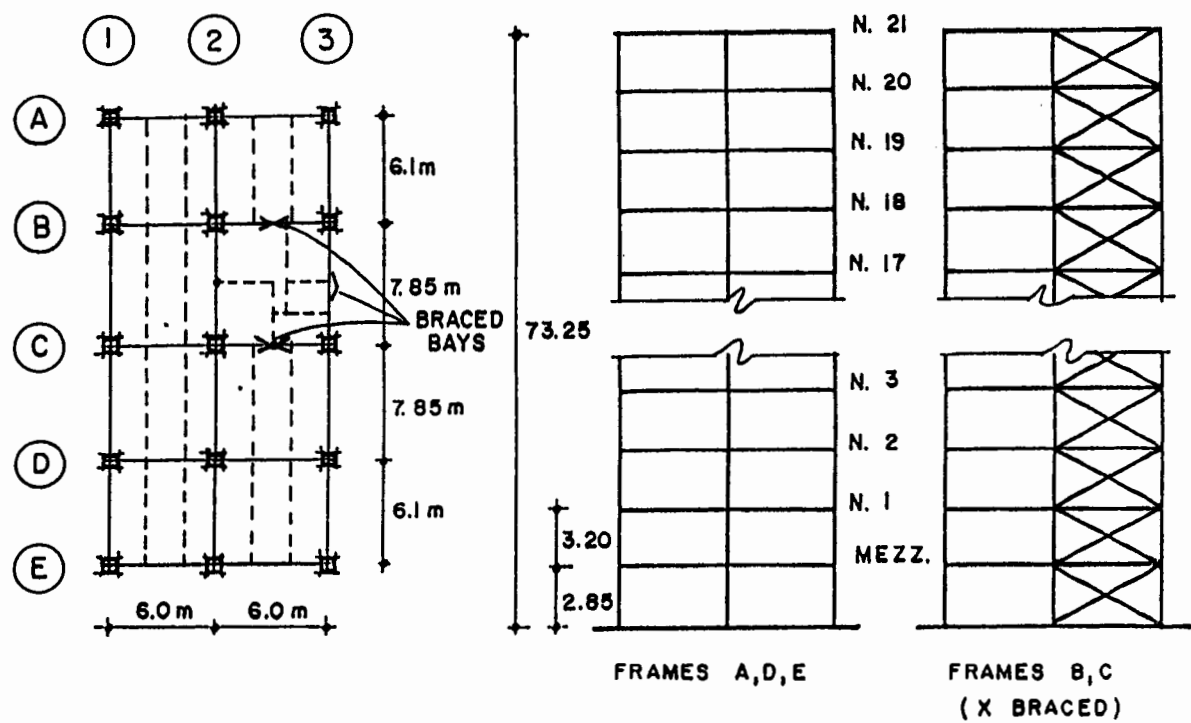
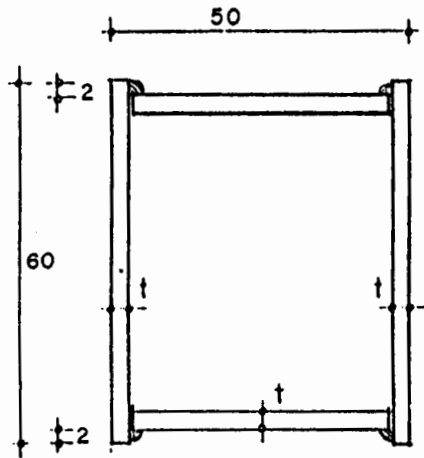
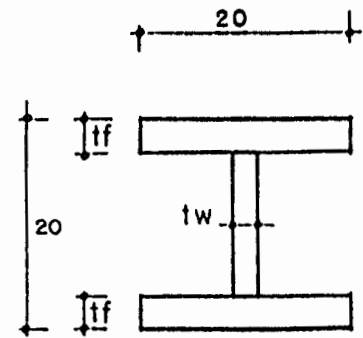


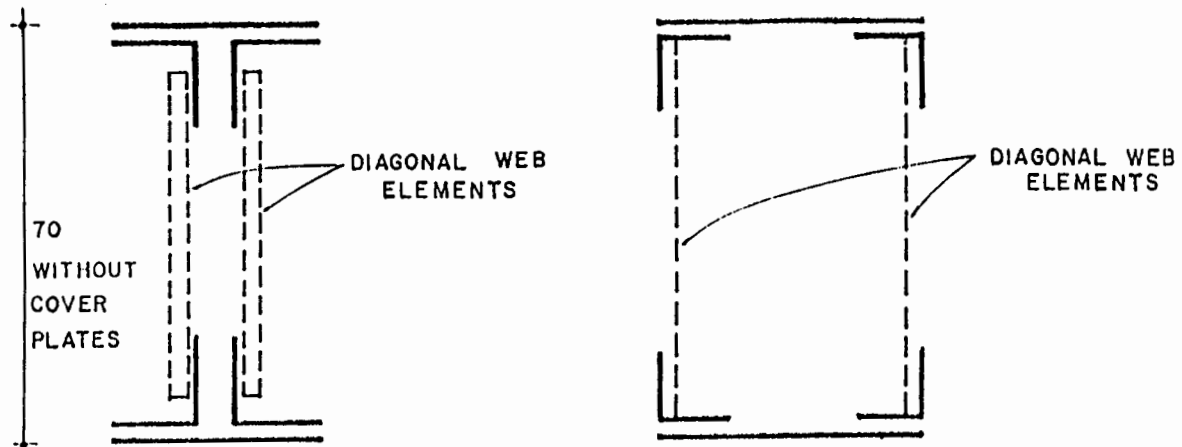
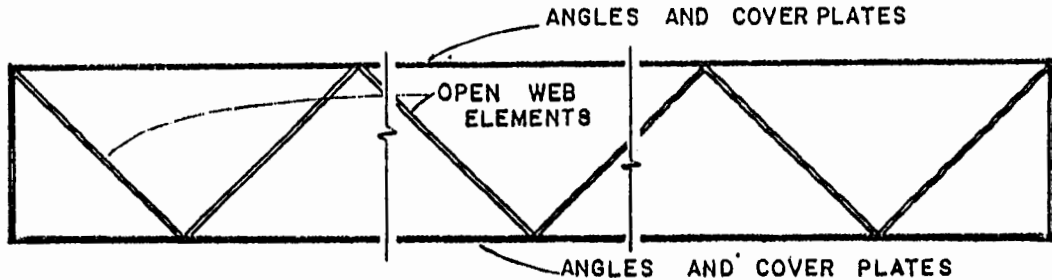
Fig 4



TYPICAL SECTION OF COLUMNS



TYPICAL BRACE MEMBERS



TYPICAL BEAM SECTIONS

Fig 5

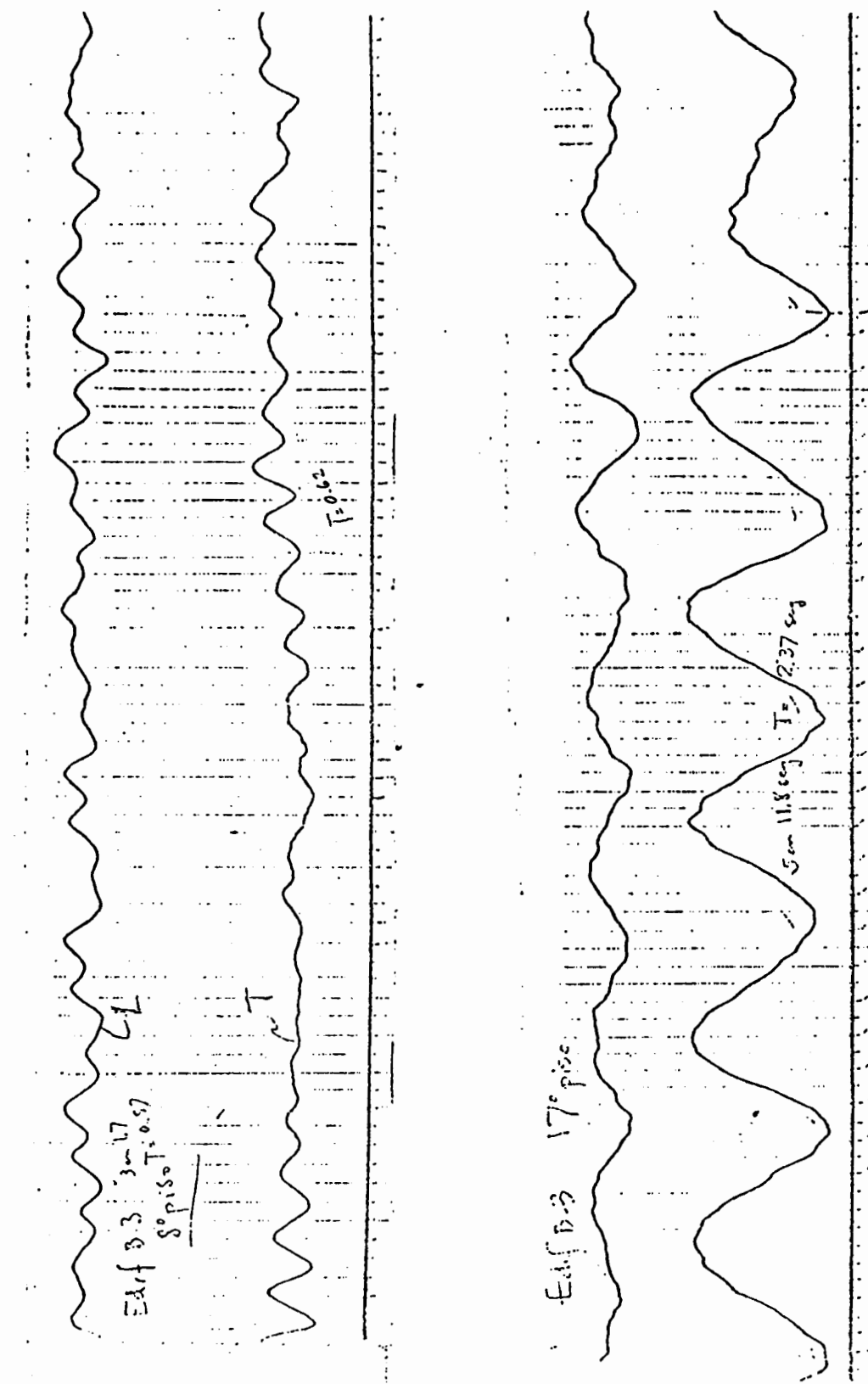


Fig 6 Vibration records obtained in 1973

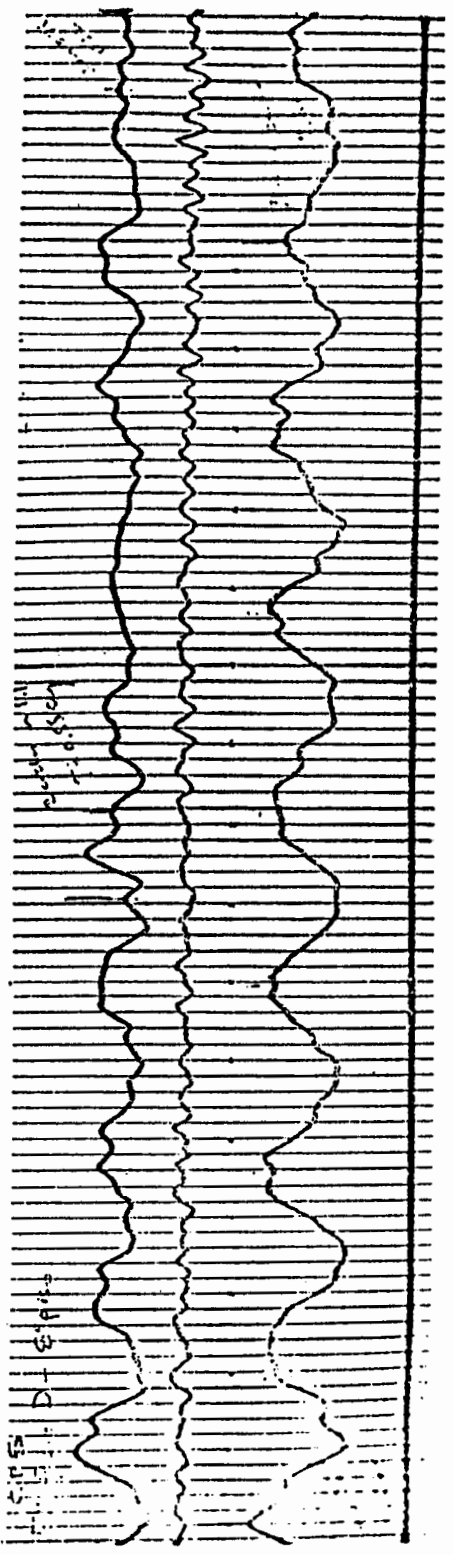
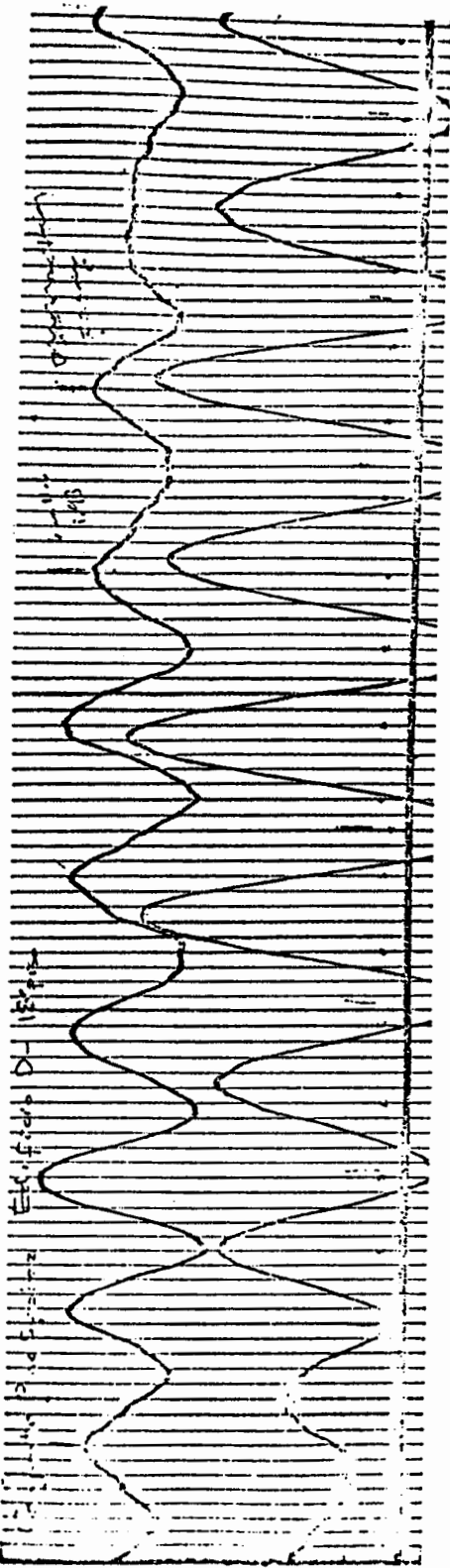


Fig. 7. Vibration records obtained in 1979

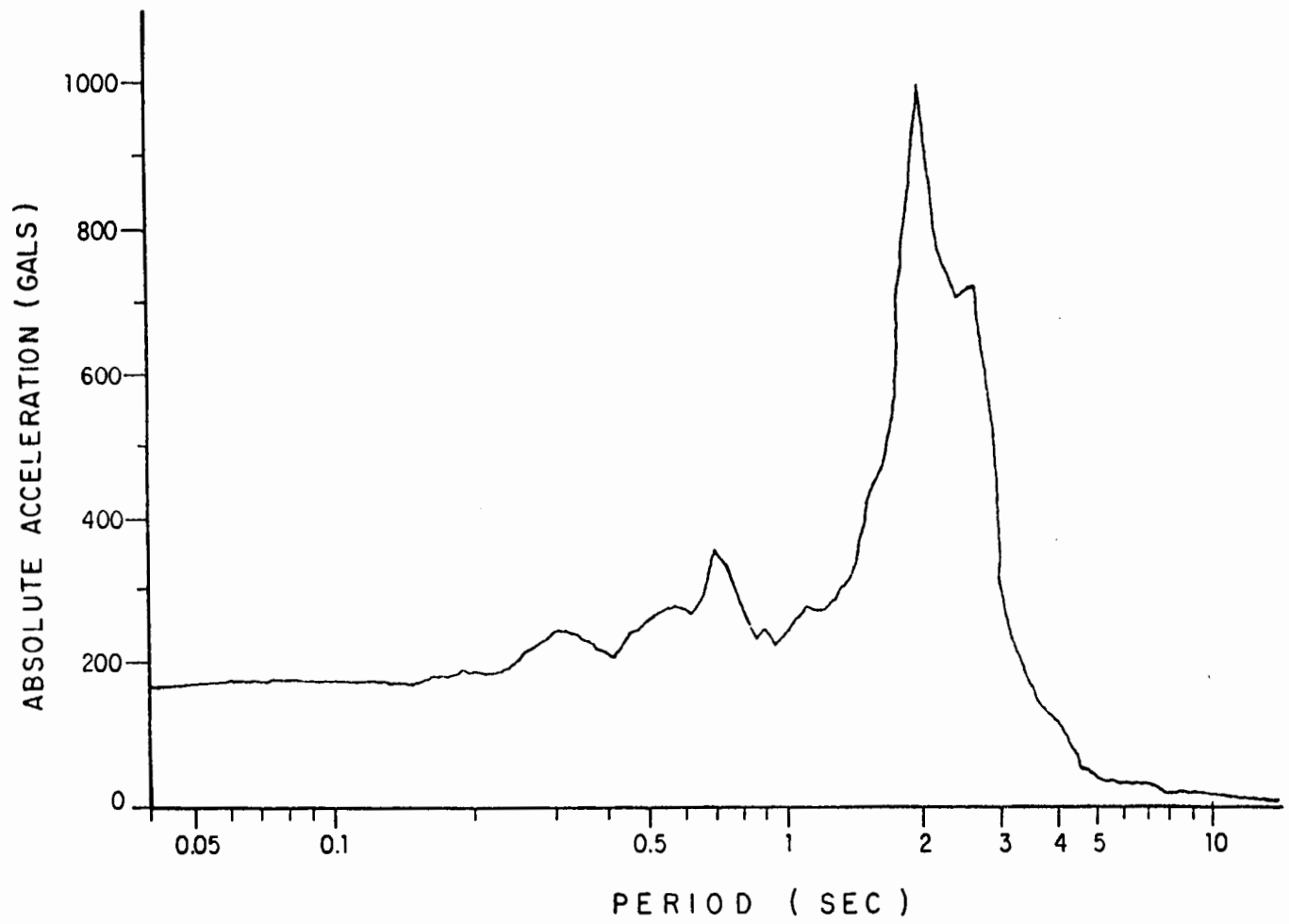


FIG 8. ELASTIC RESPONSE SPECTRUM FOR THE E-W COMPONENT OF
THE GROUND MOTION RECORDED AT SCT, FOR 5 % DAMPING



Fig 9



Fig 10



Fig 11



Fig 12

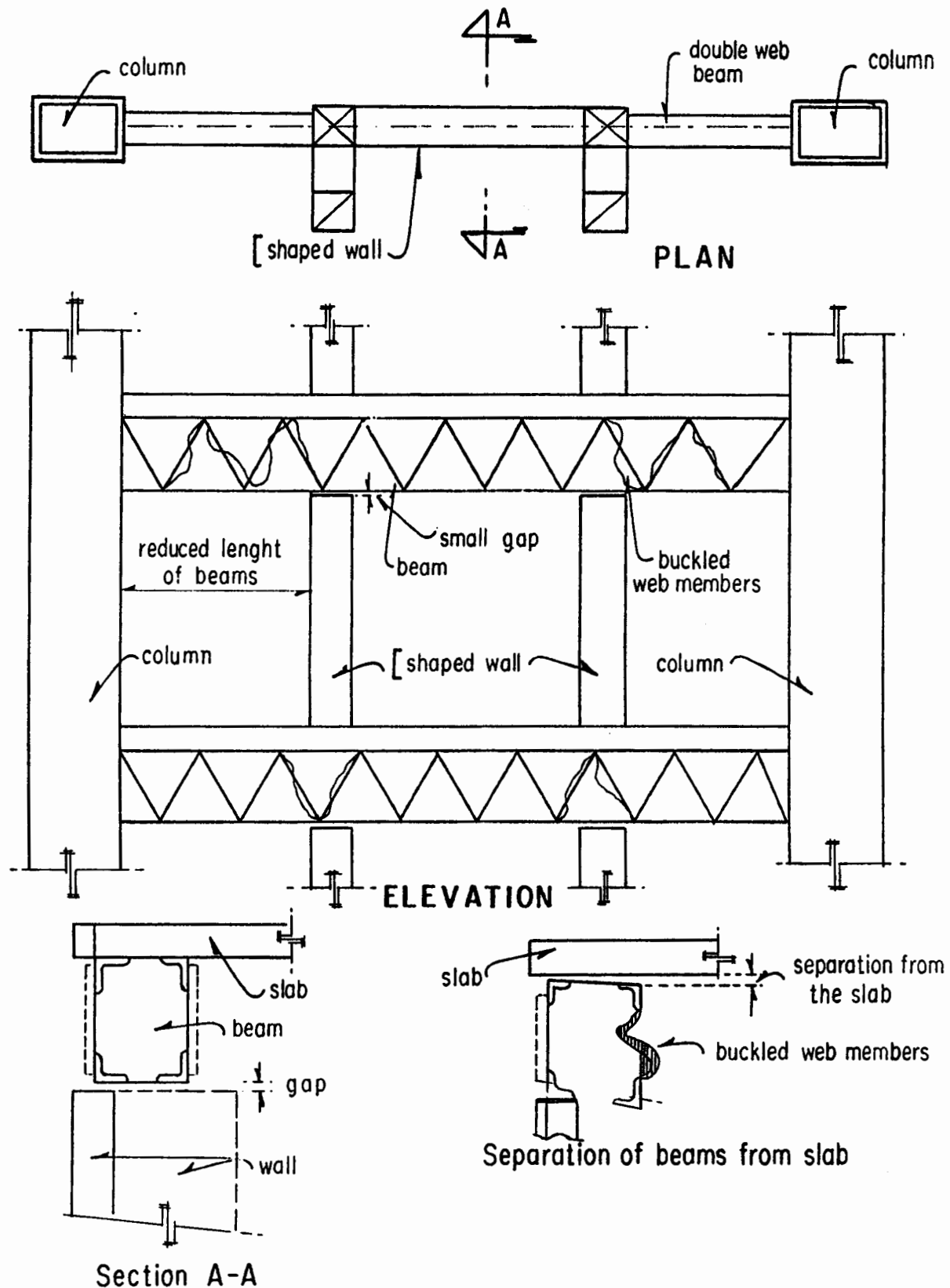


Fig 13 Interaction between beams and non-structural facade walls .

MEASURED PERIODS*, SECONDS
(1979)

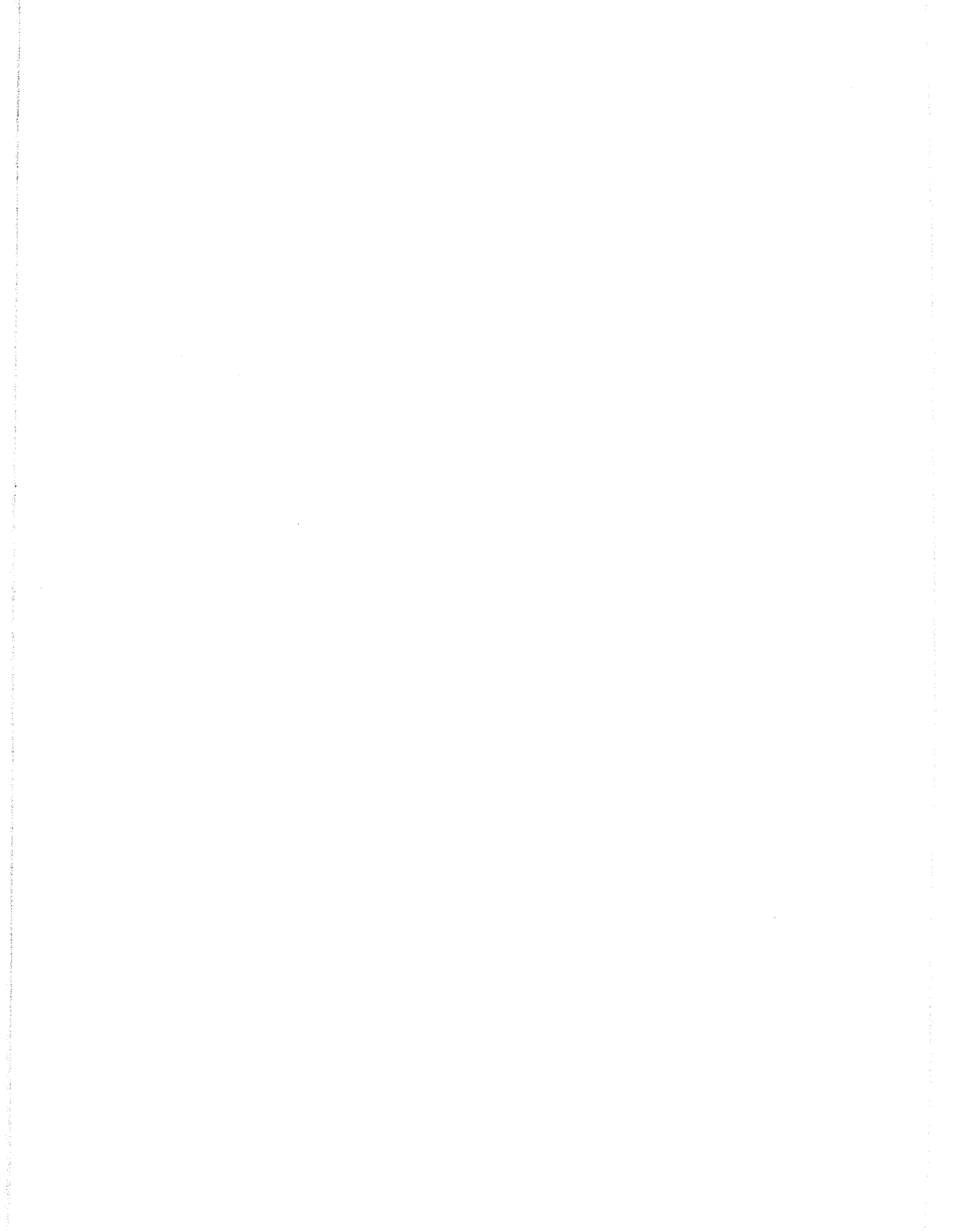
BUILDING	Transverse direction			Longitudinal direction		
	T1	T2	T3	T1	T2	T3
A	1.48 (1.46)	0.45 (0.44)	-	1.32 (1.27)	0.50 (0.42)	-
B	2.0 (2.28-2.35)	0.60-0.63 (0.65)	- (0.27)	1.9 (1.94)	0.59 (0.59)	-
C	2.38-2.50 (2.45-2.47)	0.65-0.68 (0.66-0.68)	(0.30)	1.95-2.07 (2.0)	0.64 (0.67)	0.33 (0.35)
D	2.30 (2.37)	0.62 (0.62-0.64)	0.35 -	1.93 (1.88)	0.55 (0.57-0.60)	0.32 -
E	1.39-1.45 (1.40)	0.40-0.42 (0.45)	-	1.32 (1.33)	0.40 (0.42)	

* Values indicated in parenthesis are those measured in 1973

Computed values, for the first mode are:

Buildings A and E, T transv.= 1.465 sec, T long.= 1.452 sec.

Buildings B, C, D, T transv.= 2.393 sec, T long.= 2.026 sec.



INTERACCION SUELO ESTRUCTURA DE CIMENTACIONES PROFUNDAS EN EDIFICIOS ALTOS
SOIL-STRUCTURE INTERACTION OF DEEP FOUNDATIONS IN TALL BUILDINGS

L., Zeevaert

Profesor Emérito. División de Estudios de Posgrado, Facultad de Ingeniería,
Universidad Nacional Autónoma de México. Cartagena, Colombia. Agosto 18, 1987.

SINOPSIS

En regiones sísmicas y sujetas a hundimiento regional de la superficie del suelo, se presenta la necesidad de soportar el peso de las construcciones sobre pilotes o pilas, apoyados en estratos profundos. Para justificar la acción de estos elementos que trabajan a la flexocompresión, es necesario llevar a cabo cálculos de interacción suelo-pilote como los que se indican en esta disertación. Sin embargo, la sismo-dinámica de cimentaciones se encuentra aún en embrión por lo que hay necesidad de ejercer mayor apoyo en el futuro a la investigación básica, así también en el campo por medio de la instrumentación y obtención de muestras inalteradas y finalmente perfeccionar en el laboratorio el equipo y la técnica de los ensayos con que se cuenta en la actualidad.

I INTRODUCCION

El autor ha tenido la oportunidad de observar en varias cimentaciones piloteadas el daño motivado por las fuerzas sísmicas en estos elementos. La fotografía (1) muestra el desplazamiento de la junta en un pilote, debido al refuerzo defectuoso en ésta. La fotografía (2) muestra un pilote de concreto reforzado, el cual falló debido a altos esfuerzos de cortante y flexión. La fotografía (3) muestra un pilote reforzado solamente al centro de la sección, que fué dañado por altos esfuerzos cíclicos de flexión en la cabeza del pilote los cuales originan la rotura que se muestra en ambos lados de la sección del pilote. Finalmente, en la fotografía (4) se muestra un pilote, cuya parte superior falló al extremo de que el concreto podía retirarse de ese lugar a mano sin dificultad.

SYNOPSIS

In seismic regions subjected to ground surface subsidence there is the necessity to support the weight of constructions on piles or piers bearing on deep firm strata. To justify the action of these elements working under flexo-compression, it is necessary to perform calculations of soil-pile interaction as those indicated in this paper. Nevertheless, the seismo-dynamic of the foundations may be found in a early stage, therefore, the need to give more support in the future to the basic investigation, also in the field by means of instrumentation, the obtention on undisturbed samples, and finally to improve the testing methods used today.

I INTRODUCTION

The author has had the opportunity to observe in several pile foundations the damage motivated in this elements because of the seismic forces. The photograph 1 shows the sliding of a pile joint, because of defective reinforcement at this section. Photograph 2 shows tension and diagonal tension cracks in a reinforced concrete pile, that failed because high flexion and shear stresses. Photograph 3 shows a pile reinforced at the center of its section damaged because of high flexional cyclic stresses induced by moment at the head of the pile, which created the failure of the concrete at both sides of the pile section. Finally, photograph 4 shows a pile that failed in its upper part to the extent that one could withdraw the concrete by hand without difficulty.

El método de construcción de pilotes o pilas coladas en el lugar puede cambiar en cierto grado los parámetros de diseño. La experiencia de parte del contratista en la construcción de estos elementos es necesaria para prever desde un punto de vista estratigráfico, hidráulico y de las propiedades del suelo la forma más económica, segura y expedita del método de construcción que permita conservar las propiedades mecánicas del suelo utilizadas en el diseño de estos elementos, y en algunas ocasiones inclusive, tratar de mejorar para obtener su mejor comportamiento. El profesor Lymon C. Reese en su trabajo titulado "Construcción de Cimientos Profundos Colados en Sitio"⁽¹⁾, ha discutido ampliamente varios procedimientos convenientes que pueden usarse en diferentes condiciones estratigráficas, algunos de ellos pueden aplicarse al problema de pilas o pilotes de gran diámetro que atraviesan sedimentos blandos bajo el nivel del agua superficial.

En Rusia se han utilizado fundas de bentonita para disminuir la fricción lateral de fricción negativa en la construcción de grandes pilas⁽²⁾. La inyección de cemento a alta presión ha sido utilizada con éxito en Argentina para mejorar la capacidad de carga en la base de pilas profundas⁽²⁾. En otros países, como en Colombia, las pilas o pilotes colados en el lugar se ejecutan satisfactoriamente por la combinación de equipo mecánico y excavación a mano cuando el problema del agua no es muy crítico. Cuando el estrato soportante es arena fina bajo el nivel del agua, puede presentarse el fenómeno de licuación, este problema podrá resolverse bombeando de pozos profundos para crear un flujo descendente del agua bajo la base de la pila. En el caso de usar el método de desplazamiento bentonítico para la construcción de pilas bajo el agua, sería necesario inyectar a presión morteros de cemento para asegurar buen contacto entre la base de la pila y el estrato soportante^{(2),(3)}.

El ingeniero de cimentaciones debe de prever el método de construcción y modificar convenientemente los parámetros del suelo para efectuar el diseño de las pilas o pilotes. Los parámetros deben considerarse a largo plazo después de que la cimentación ha sido construida y de acuerdo con las condiciones ambientales. Por ejemplo, en caso de fricción negativa en pilas profundas, la reducción de los niveles piezométricos del agua con el tiempo aumentan considerablemente esta fuerza. Este fenómeno no puede omitirse en el diseño de estos elementos de cimentación profunda. Así pues, las fuerzas ambientales no pueden estimarse de reglas

The method of construction of piles or piers cast in place may change to certain degree the design parameters. The experience of the contractor in the construction of these elements is necessary to foresee, from a stratigraphical point of view, hydraulic and soil properties, the most economical, safe and speedy method of construction preserving the mechanical properties of the subsoil used in the design of these elements, and in occasions trying to improve them to obtain a better behavior. Professor Lymon C. Reese in his paper "Construction of Drilled Shafts"⁽¹⁾ discusses with length the various convenient procedures to use in different stratigraphical conditions, some of them may be applied to the problem of piers or piles of large diameter going through soft sediments under the surface water table.

In Russia bentonite has been used applied at the pile shaft to reduce the lateral friction or negative friction on the shaft of heavy piers⁽²⁾. The injection of cement at high pressure has been used with success in Argentina to improve the base bearing capacity of very deep piers⁽²⁾. In other places, like in Colombia, the piles and piers cast in place are constructed very satisfactorily with the combination of mechanical equipment and hand excavation when the water problem is not very critical. When the supporting stratum is fine sand under the water table the phenomenon of liquefaction may be present. This problem may be solved by means of deep wells pumping water to create a downward water flow under the base of the pier. In case the method of bentonitic displacement is used for the construction of piers underwater, it is necessary to inject under pressure cement mortars to assure a good contact between the base of the pier and the bearing stratum^{(2),(3)}.

The foundation engineer has to foresee the construction method and modify conveniently the soil parameters to achieve the design of the piers or piles. The parameters used should be considered to be those on a long term basis after the foundation has been constructed in accordance with the environmental conditions. In case of negative friction of deep seated piles or piers, the reduction of the water piezometric levels with time increases this force considerably. This action can not be omitted in the design of these elements in deep foundations. Therefore, the environmental forces can not be estimated by means of

prácticas obtenidas de la estadística de otros lugares. La acción de estas fuerzas en cimentaciones profundas dependen en gran parte de las condiciones estratigráficas e hidráulicas locales del sitio en cuestión y de las propiedades geotécnicas de los sedimentos del suelo a través de la profundidad. El método para la construcción de cada uno de estos elementos cuando son colados en sitio juega un papel muy importante en el comportamiento futuro de la cimentación. Más aún, un edificio queda soportado generalmente sobre varias pilas o pilotes cuyas cabezas quedan sujetas en alguna forma con la estructura de cimentación. Cuando se presentan fuerzas de arrastre lateral como las que aquí se discuten, siempre deben unirse estos elementos para que la cimentación trabaje como una unidad.

La cimentación con pilas es un método milenario de cimentación usado en todo el mundo y ha demostrado ser bueno cuando se aplica correctamente. En la actualidad la mecánica de suelos proporciona una poderosa herramienta para la interpretación, del comportamiento y construcción de estos elementos. Por tanto, los ingenieros están tratando de entender cada vez mejor el comportamiento de las cimentaciones con pilas y los métodos de construcción más seguros y económicos en diferentes condiciones del subsuelo. Los métodos de construcción se están desarrollando rápidamente en todo el mundo, así también los medios para verificar la teoría con las observaciones, dejando siempre un amplio margen al ingeniero estudiioso para futuras investigaciones e interpretaciones del comportamiento de las cimentaciones donde se usan pilas o pilotes.

Una pila es una columna de concreto armado o de acero generalmente de diámetro importante si se compara con un pilote hincado de diámetro pequeño. Por tanto, el perímetro y la rigidez que proporciona la sección transversal y el módulo de elasticidad del material usado, son factores importantes en la magnitud de las fuerzas de arrastre originadas en estas cimentaciones.

Los elementos mecánicos a los cuales queda sujetada una pila se muestran en la Fig. 1. En la cabeza queda aplicada una fuerza axial Q_0 que representa el peso de la estructura o edificio incluyendo cualquier incremento ocasionado por momentos de volteo producidos ya sea por viento o fuerzas sísmicas en la superestructura. La fuerza cortante V_0 y el momento M_0 representan las fuerzas que accionen en la cabeza de la pila que en conjunto con Q_0 mantienen a la estructura de la cimentación en equilibrio. Las fuerzas Q_b , V_b y

practical rules obtained from statistics of other locations. The action of these forces in deep foundations is an important function of the stratigraphical and hydraulic conditions locally found at the site in question, and also of the geotechnical properties of the soil sediments with depth. The construction method for each case of these elements when they are cast in place plays a very important role in the future behavior of the foundations. Furthermore, a building will be supported generally on several piers or piles where the heads of these elements may be connected in certain way with the structure of the foundation. When horizontal seismic drift forces are present as the ones discussed here, these elements should be tied together to achieve a unit action of the foundation structure.

The foundation method with piers is a milenary method of foundation used throughout the world that has demonstrated to be a good method when it is applied properly. Today soil mechanics gives a powerful tool for the interpretation of the behavior and construction of these elements. Therefore, the engineers are trying to understand better the behavior of these foundations, and by the same token, the most safe and economical construction for different subsoil conditions. The methods of construction are developing very fast around the world, also the means to verify the theory with observations. However, there is always and ample margin for the studious engineer in future investigations and interpretations of the behavior of pile or piers foundations.

A pier is a column of reinforced concrete or steel generally of an important diameter if it is compared with driven piles of small diameter. Therefore, the perimeter and the rigidity given by the cross section of the pier and the modulus of elasticity used, are important factors in the magnitude of the drifting forces originated in these foundations.

The mechanical elements to which the pier is subjected are shown in Fig. 1. At the head an axial force Q_0 is applied representing the weight of the structure of the building including any increment created by an overturning moment produced, either by wind or seismic forces in the super-structure. The shear force V_0 and the moment M_0 are representing the forces acting at the head of the pile that in conjunction with Q_0 maintain the foundation structure in equilibrium. The forces Q_b , V_b and the moment M_b at the base of the pier

momento M_b en la base de la pila son representativas de las condiciones de apoyo de la pila sujeta a las fuerzas de arrastre y cargas del edificio. Su valor es función de los siguientes factores: el número de pilas, del peso y geometría de la superestructura, rigidez de la cimentación, de la forma en que la pila se fije a la estructura de cimentación, de la sección transversal de la pila, de la profundidad al suelo firme, y finalmente, de las propiedades geotécnicas del suelo alrededor del vástago de la pila.

represent the support conditions of the pier subjected to the drifting forces and building loads. Their value is a function of the following factors: the number of piers, the weight and geometry of the foundations structure, the rigidity of the foundation, of the form the pier is fixed to the foundation structure, the rigidity of the foundation structure, of the cross section of the pier, of the depth of the firm soil and finally of the geotechnical subsoil properties around the shaft of the pier.

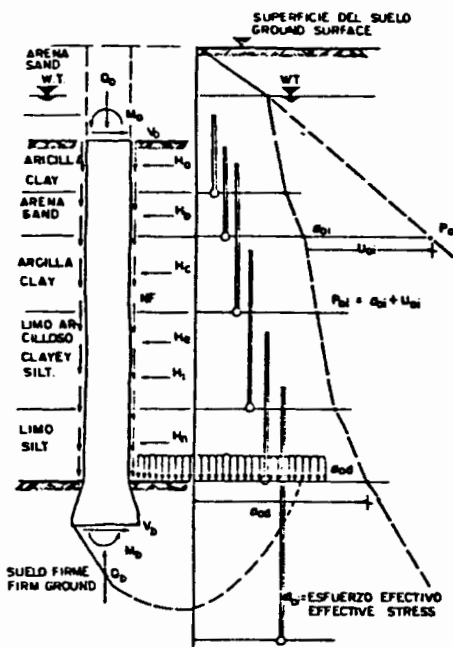


FIG. 1r FUERZAS SOBRE UNA PILA.
FORCES ON A PIER

Las fuerzas de arrastre debidas a la fricción negativa y movimientos sísmicos fuertes deberán analizarse separadamente para investigar sus efectos máximos sobre el vástago de la pila y el apoyo sobre el suelo firme. Debe reconocerse, sin embargo, que la capacidad de carga de una pila cuando estas fuerzas ambientales se presentan depende de la resistencia al esfuerzo cortante y de la deformabilidad del suelo bajo la base de la pila, esto es, de las propiedades mecánicas, estáticas y dinámicas, del suelo y de su preservación durante la construcción.

En ambientes sísmicos y con hundimiento regional donde se encuentran suelos superficiales de baja resistencia y alta compresibilidad se hace necesario cimentar usando pilotes o pilas. Generalmente, las pilas se diseñan a manera de columnas para tomar grandes cargas, por tanto, su apoyo deberá efectuarse en estratos resistentes de muy baja compresibilidad. Los pilotes de

The drifting forces because of negative friction and seismic strong motions should be analyzed separately to investigate their maximum effects on the shaft of the pile and its support on the firm soil. We have to recognize, however, that the load capacity of a pier when these environmental forces are present is a function of the shear strength and the deformability of the soil under the base of the pier, that is to say, of the mechanical properties of the soil and of their preservation during construction.

In seismic environments with regional ground surface subsidence and where the upper subsoil is of low strength and high compressibility, it is necessary to use foundations supported on piers or piles. Generally the piers are designed as columns to take large loads, therefore their base bearing should be made on strata of high strength and very low compressibility. The

gran diámetro siendo más rígidos que el subsuelo que atravesan, oponen resistencia al desplazamiento horizontal de la masa del suelo, haciéndolos trabajar a la flexocompresión y fuerza cortante, adicionada de la fuerza de arrastre vertical generada por la fricción negativa, y el peso del edificio. Finalmente, la respuesta sismica de la cimentación depende también en forma importante del momento de volteo sismico el cual puede aumentar en forma considerable la carga axial sobre los elementos extremos de la cimentación.

II FRICCIÓN NEGATIVA

Los pilotes o pilas son usadas para soportar cargas puestas sobre suelos firmes a través de sedimentos suaves del subsuelo. Las fuerzas de arrastre son aquellas relacionadas con las condiciones ambientales del lugar en cuestión. La acción puede analizarse por separado para cada condición ambiental, y después estudiar la acción de los diferentes fenómenos para encontrar la respuesta máxima.

El procedimiento de construcción es importante para asignar los parámetros de resistencia al esfuerzo cortante a lo largo del vástago de la pila, cohesión y ángulo de fricción interna. Cuando se coloca concreto en una perforación no ademáda la resistencia al esfuerzo cortante aumenta en la interfase del vástago de la pila con el suelo por la inclusión de lechada de cemento en el suelo circundante. Cuando se origina el movimiento relativo entre pila y suelo debido a la consolidación de los sedimentos alrededor del vástago de la pila, la superficie potencial de deslizamiento puede quedar localizada a cierta distancia del vástago de la pila hasta una superficie vertical no afectada por la lechada de cemento del concreto utilizado. Esta distancia de la pila depende de la permeabilidad del suelo alrededor de la pila. Por otro lado en el caso de pilotes hincados desde la superficie del suelo, el vástago queda rodeado de un anillo de suelo amasado por el desplazamiento del suelo al hincar el pilote⁽⁴⁾

Cuando los estratos del subsuelo se encuentran en estado de consolidación sobre el suelo firme donde se apoyan los pilotes, se desarrolla la fricción negativa debido al movimiento relativo entre suelo y pilotes, Fig. 2. Esta fuerza friccionante es función de los parámetros de esfuerzo cortante a largo plazo representativos de los sedimentos a diferentes profundidades y de los esfuerzos horizontales que actúan sobre el vástago de la pila⁽⁴⁾. Sin embargo, el esfuerzo

large diameter piles or piers being more rigid than the subsoil, they opposed resistance to the horizontal displacements of the soil mass. Therefore these elements are forced to work under flexo-compression and shear, added by the vertical drift force created by negative friction and the building load. Finally, the seismic response of the foundation is an important function of the overturning moment that increases very considerably the axial load on these elements at the edges of the foundation.

II NEGATIVE FRICTION

Piles or piers are used to support heavy loads bearing on firm ground, through soft soil sediments. The drift forces are those related with the environmental conditions at the site in question. The action can be analyzed separately for each environmental conditions, and to study separately the action of the different phenomena to find the maximum response.

The construction methods are important to assign the shear strength parameters along the pier shaft; cohesion and angle of internal friction. When concrete is placed in an unprotected shaft excavation, the shear strength increases at the interphase of the pier shaft and soil because of the inclusion of cement slurry in the surrounding soil. When the relative movement between pile and soil takes place because of the consolidation of the sediments around the pile shaft, the potential surface of sliding may be localized at certain distance from the pile shaft to a vertical surface not affected by the cement of the concrete used. This distance from the pile is related with the permeability of the soil around the pier. On the other hand, in case of piles driven from the ground surface, the shaft of the pile is surrounded by a ring of impervious remolded soil, this is originated during pile driving because of the soil displacement.

When the soft soil strata above the firm ground where the piles are bearing is encountered in a state of consolidation, then negative friction is created because of the relative movement between piles and soil, Fig. 2. The friction force is a function of the shear strength parameters based on a long term basis, representative of the sediments with depth, and of the horizontal stresses acting on the pile shaft⁽⁴⁾. Nevertheless, the horizontal stresses may take

horizontal inmediatamente después de la construcción puede tomar valores imprevisibles que pueden ser en parte función del procedimiento de construcción. Sin embargo, a largo plazo y debido al relajamiento de las deformaciones horizontales durante el movimiento relativo entre suelo y pilotes, se puede estimar con seguridad el esfuerzo horizontal cerca del vástago en función del esfuerzo vertical, según la siguiente ecuación

unforeseen values immediately after construction related with the method of construction. However, on a long time because of consolidation and relaxation of the horizontal strains during the relative movement between soil and pile, we can estimate safely the horizontal stresses close to the pile shaft as a function of the vertical stresses, according to the equation

$$\sigma_h = \frac{1 - \operatorname{sen}^2 \phi_r}{1 + \operatorname{sen}^2 \phi_r} \sigma_z \quad (1)$$

llamando

calling

$$\bar{N}_\phi = \frac{1 + \operatorname{sen}^2 \phi_r}{1 - \operatorname{sen}^2 \phi_r} \quad (2)$$

el esfuerzo horizontal que se ejerce sobre el vástago de la pila es

the horizontal stress acting on the pile shaft is

$$\sigma_h = \frac{1}{\bar{N}_\phi r} \sigma_z \quad (3)$$

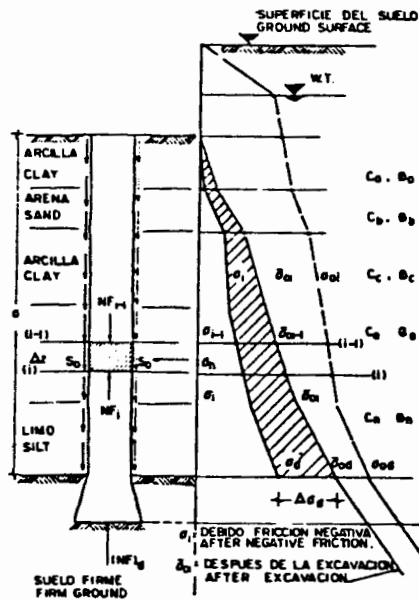


FIG-2- FRICCIÓN NEGATIVA SOBRE UNA PILA.
NEGATIVE FRICTION ON A PIER.

Donde σ_z es el esfuerzo vertical efectivo que actua en un plano horizontal cerca del vástago de la pila a una profundidad z , durante la acción del fenómeno de la fricción negativa.

La integración de la resistencia al esfuerzo cortante totalmente movilizada a lo largo de la superficie potencial de deslizamiento dará la medida total de la

in which σ_z is the effective vertical stress acting on a horizontal plane close to the pile shaft at a depth z , during the action of the negative friction phenomenon.

The integration of the totally mobilized shear strength along the potential surface of sliding gives the total measure of the negative friction transferred to the base

fricción negativa transmitida a la base del pilote o pila.

of the pile or pier.

$$(NF)_d = \bar{w} \sum_1^n (c_i + \sigma_i \frac{\tan \phi_i}{N_{\phi_i}}) \Delta z_i \quad (4)$$

en donde

in which

- \bar{w} perímetro de la superficie potencial de deslizamiento.
- c_i, ϕ_i parámetros medios de resistencia al esfuerzo cortante del suelo, representativos del estrato de espesor Δz_i , a la profundidad media z_i .
- σ_i esfuerzo efectivo vertical residual cercano al vástago de la pila, obtenido por la transferencia del esfuerzo inicial $\bar{\sigma}_{oi}$ sobre la pila, Fig. 2.

\bar{w} perimeter of the potential surface of sliding.

c_i, ϕ_i parameters of shear strength representative of the soil for the stratum of thickness Δz_i , at middle depth z_i .

σ_i residual vertical effective stress close to the pile shaft, obtained because of the transfer of the initial vertical stress $\bar{\sigma}_{oi}$ on the pier, Fig. 2.

La fuerza total $(NF)_d$ de arrastre vertical o fricción negativa sobre el vástago de la pila a la profundidad d está dada por la ecuación (4), la que representa la transferencia de esfuerzos de la masa del suelo al vástago de la pila durante el hundimiento del suelo circundante⁽⁴⁾.

The vertical drift force or negative friction $(NF)_d$ on the pile shaft at depth d is given by equation (4) representing the transfer of the subsoil vertical stresses on the pile shaft during the ground surface subsidence.

Supongamos Fig. 2, un elemento de pila cortado por dos planos horizontales a las profundidades $(i-1)$ e i , respectivamente. Debido a la transferencia del peso del suelo al vástago de la pila, el esfuerzo vertical efectivo inicial $\bar{\sigma}_{oi-1}$ sobre el plano $(i-1)$ se reduce a (σ_{i-1}) y en el plano horizontal i se reduce de $\bar{\sigma}_{oi}$ a σ_i , respectivamente. Por consiguiente, la resistencia media última por unidad de longitud es

Assume Fig. 2, a pier element cut by two horizontal planes at depths $(i-1)$ and i , respectively. Due to the transfer on the soil weight to the pile shaft, the vertical initial effective stress $\bar{\sigma}_{oi-1}$ on plane $(i-1)$ is reduced to (σ_{i-1}) , and in the horizontal plane i is reduced from $\bar{\sigma}_{oi}$ to σ_i , respectively. Therefore, the average ultimate shear strength per unit of length is

$$s_{oi} = \bar{w} \{c_i + 1/2(\sigma_i + \sigma_{i-1}) \frac{\tan \phi_i}{N_{\phi_i}}\} \quad (5)$$

o bien

or

$$s_{oi} = c_i \bar{w}_i + m_i \sigma_i + m_i \sigma_{i-1} \quad (6)$$

donde

in which

$$m_i = \frac{\bar{w}_i \tan \phi_i}{2 N_{\phi_i}} \quad (7)$$

El equilibrio de un segmento de pila en términos de la fricción negativa y resistencia al esfuerzo cortante del suelo cercano al vástago de la pila, Fig. 3, se lee como sigue:

The equilibrium of a pier segment in terms of negative friction and the shear strength of the soil close to the pier shaft, Fig. 3, may be written as follows:



$$(NF)_i - (NF)_{i-1} = s_{oi} \Delta z_i \quad (8)$$

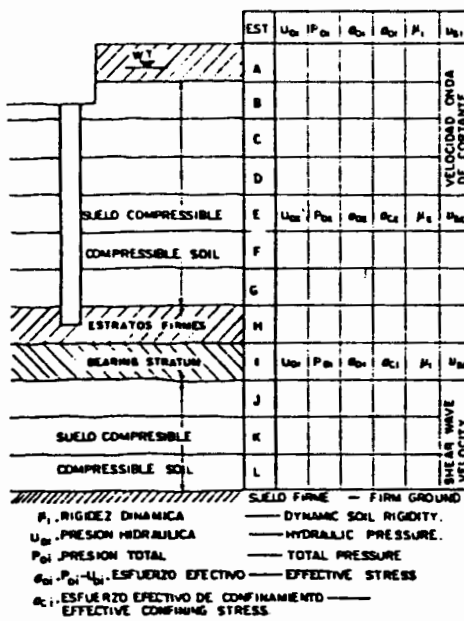


FIG.3-PROPIEDADES ESTRATIGRÁFICAS Y DINÁMICAS
ESTRATIGRAPHICAL AND DYNAMICAL PROPERTIES

Así también la transferencia total del esfuerzo vertical ($\bar{\sigma}_{oi-1} - \sigma_{i-1}$) a la profundidad $z = (i-1)$ es proporcional a la carga de fricción negativa sobre la pila ($(NF)_{i-1}$). Llamando \bar{a}_i el área tributaria equivalente cerca del vástago de la pila donde se efectúa la transferencia del esfuerzo podemos escribir⁽⁴⁾

In the same way, the vertical stress transfer ($\bar{\sigma}_{oi-1} - \sigma_{i-1}$) at depth $z = (i-1)$ is proportional to the negative friction load on the pier ($(NF)_{i-1}$). Calling \bar{a}_i the equivalent tributary area close to the pile shaft where the transfer of stresses takes place, we write

$$(NF)_{i-1} = (\bar{\sigma}_{oi-1} - \sigma_{i-1}) \bar{a}_{i-1} \quad (9)$$

y en forma semejante para la profundidad $z = i$

in similar form, for depth $z = i$

$$(NF)_i = (\bar{\sigma}_{oi} - \sigma_i) \bar{a}_i \quad (10)$$

combinando las ecuaciones 6, 8 y 9 se obtiene el esfuerzo vertical residual debido a la transferencia de carga

combining equations 6, 8 and 9, we obtain the residual vertical stress because of the load transfer

$$\sigma_i = A_i \bar{\sigma}_{oi} - B_i \sigma_{i-1} - C_i (NF)_{i-1} - D_i \quad (11)$$

donde los coeficientes son

in which the coefficients are

$$A_i = \frac{\bar{a}_i}{\bar{a}_i + m_i \Delta z_i}$$

$$B_i = \frac{m_i \Delta z_i}{\bar{a}_i + m_i \Delta z_i}$$

$$C_i = \frac{1}{\bar{a}_i + m_i \Delta z_i} \quad (12)$$

$$D_i = \frac{\bar{w}_i \cdot C_i}{\bar{a}_i + m_i \Delta z_i}$$

Los coeficientes A_i , B_i , C_i y D_i representan los valores medios del estrato del suelo de espesor Δz_i pueden calcularse de las propiedades mecánicas del suelo. Las condiciones de frontera en la cabeza de la pila son generalmente $\sigma_{i-1} = 0$ y $(NF)_{i-1} = 0$. Por lo tanto la transferencia de esfuerzos en la base del primer estrato puede calcularse por medio de la (11), esto es $(\bar{c}_{oi} - \sigma_i)$. Con este valor se obtiene la fuerza de fricción negativa al mismo nivel i , según la ecuación (10), tenemos

$$(NF)_i = (\bar{c}_{oi} - \sigma_i) \bar{a}_i \quad (13)$$

Los nuevos valores de σ_i y $(NF)_i$ se usan en la ecuación (11) para obtener σ_{i+1} y en la ecuación (13) para el valor de $(NF)_{i+1}$. La integración se hace paso a paso hasta alcanzar la longitud total de la pila expuesta a las fuerzas verticales de arrastre, obteniéndose así la fricción negativa total $(NF)_d$ a la profundidad requerida d . La reducción del esfuerzo de confinamiento vertical a la elevación de la base de la pila se estima de la transferencia de esfuerzos $(\bar{c}_{od} - \sigma_d)$ y se revisa la capacidad de carga estática.

La distribución de esfuerzos bajo la base de la pila debido a la carga axial en conjunto con la fricción negativa puede utilizarse para estimar los desplazamientos verticales estáticos de la pila. Sin embargo se hace notar que cuando las pilas o pilotes se encuentran muy separados y las áreas tributarias equivalentes no se interfieren, la reducción del esfuerzo vertical medio de confinamiento sobre el estrato firme de apoyo deberá investigarse para fines de capacidad de carga, como se indica en Ref. (4), capítulo VIII p. 361, sección 3.2.

III COMPORTAMIENTO SISMICO DEL SUBSUELO

La valorización de la respuesta sísmica de la cimentación se efectúa por un análisis cuantitativo del comportamiento sísmico del subsuelo. Para lograr lo anterior será necesario conocer las propiedades estratigráficas, hidráulicas y dinámicas del subsuelo. Consideremos que las características estratigráficas del

The coefficient A_i , B_i , C_i and D_i are average values representative of every soil stratum of thickness Δz_i and may be computed with the soil mechanical properties. The boundary conditions at the head of the pile are generally $\sigma_{i-1} = 0$ and $(NF)_{i-1} = 0$. Therefore, the transfer of stresses at the base of the first stratum may be computed by means of (11), that is $(\bar{c}_{oi} - \sigma_i)$. With this value one obtains the negative friction forces at same level i according to equation (10), we have

The new values of σ_i and $(NF)_i$ are used in equation (11) to obtain σ_{i+1} and in equation (13) for the value $(NF)_{i+1}$. The integration is performed step by step to the length of the pier exposed to the vertical drift forces, obtaining with this method the total negative friction $(NF)_d$ at depth d . The reduction of the vertical confining stress at the elevation of the base of the pier may be estimated from the transfer of stresses $(\bar{c}_{od} - \sigma_d)$, and the static bearing capacity is revised.

The stress distribution under the base of the pier because of the axial load added by the negative friction may be used to estimate the static vertical displacement of the pier. Nevertheless, one should notice that when the piers or piles are widely separated, and the equivalent tributary areas do not interfere to each other the reduction of the vertical average stress of confinement on the firm stratum where they are bearing should be investigated for bearing capacity purposes as indicated in reference (4), Chapter VIII, page 361, section 3.2.

III SEISMIC BEHAVIOR OF THE SUBSOIL

The seismic response of the foundation is achieved by means of a quantitative analysis of the seismic behavior of the subsoil. In order to proceede with this analysis it is necessary to know the stratigraphical, hydraulic and dynamic properties of the subsoil. Let us consider that the stratigraphical conditions of the

subsuelo son como se muestra en la Fig. 3. Para el análisis dinámico es indispensable conocer la rigidez dinámica del suelo μ , representativa de cada uno de los estratos que lo forman. Este parámetro dinámico del suelo puede determinarse por medio del "Péndulo de Torsión Libre" diseñado por el autor para este objeto.⁽⁸⁾ Foto 5.

La definición de módulo dinámico de rigidez del suelo es

$$\mu = \tau/\gamma \quad (14)$$

en donde τ es el esfuerzo cortante y γ la distorsión angular inducida en el suelo por las ondas sísmicas equivolumétricas o de cortante que viajan del suelo firme hacia la superficie. Las ondas sísmicas tienen diferentes velocidades v_s según los valores de μ para cada estrato. La velocidad de la onda está dada por $v_{si} = \sqrt{\mu_i/\rho_i}$, donde ρ_i es la masa unitaria. Así pues, el tiempo que toma la onda para recorrer el estrato i de espesor d_i es d_i/v_{si} , y para recorrer todos los estratos del suelo suave tomará un tiempo igual a 1/4 del periodo fundamental del depósito del suelo, esto es:

$$T_s = 4 \sum_1^n \frac{d_i}{v_{si}} \quad (15)$$

El valor de T_s representa el mayor periodo libre de vibración del suelo, el cual genera esfuerzos cortantes y desplazamientos máximos en la masa del suelo. Por consiguiente, cualquier elemento rígido que se construya en el subsuelo quedará sujeto a los desplazamientos horizontales originados por el empuje dinámico de la masa del suelo.⁽⁵⁾

Consideremos, Fig. 4, el desplazamiento relativo de la masa del suelo apoyada sobre la base firme. Se observa que un estrato a cierta profundidad se distorsiona por las ondas sísmicas que producen esfuerzos cortantes en planos horizontales. El equilibrio dinámico de un elemento de espesor d_i requiere:

1) por distorsión

$$\frac{\delta_i - \delta_{i+1}}{d_i} = \frac{\tau_i + \tau_{i+1}}{2\mu} \quad (16)$$

2) por la fuerza de inercia

$$\tau_{i+1} - \tau_i = (\rho d)_i p_n^2 \frac{1}{2} (\delta_i + \delta_{i+1}) \quad (17)$$

subsoil are like those shown in Fig. 3. For the dynamic analysis it is necessary to learn on the dynamic soil rigidity μ , representative of each one of the strata forming the subsoil. This dynamic parameter of the soil may be determined by means of the "Free Torsion Pendulum" designed by the author for this purpose.⁽⁸⁾ Photo 5.

The definition of the dynamic soil rigidity is

in which τ is the shear stress and γ the angular distortion induced in the soil by the seismic equivolumetric or shear waves that travel from the firm soil to the surface. The seismic waves have different velocities v_s according to the values of μ for each stratum. The wave velocity is given by $v_{si} = \sqrt{\mu_i/\rho_i}$, in which ρ_i is the unit mass. Hence, the time taken by the wave to travel the stratum i of thickness d_i is d_i/v_{si} , and to travel all the soft soil strata will take a time equal to 1/4 of the fundamental period of the soil deposit that is

The value of T_s represents the largest free period of vibration of the ground, that also creates the largest shear stresses and displacements of the soil mass. Therefore, any rigid element constructed in the subsoil will be subjected to the dynamic drift induced by the horizontal displacements of the soil mass.⁽⁵⁾

Let us consider, Fig. 4, the relative displacement of the soil mass supported on the firm base. We observe that the stratum at certain depth is disturbed by the seismic waves producing shear stresses in a horizontal plane. The dynamic equilibrium of an element of thickness d_i requires:

1) for distortion

2) for the inertia force

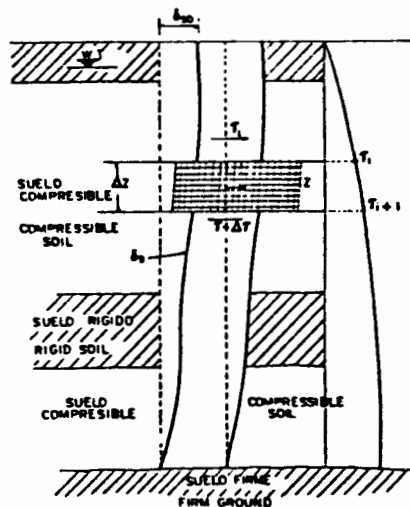


FIG.4 - COMPORTAMIENTO SISMICO DEL SUBSUELO
SEISMIC BEHAVIOR OF SUBSOIL.

Efectuando arreglos algebraicos se encuentran las expresiones que gobiernan el movimiento del subsuelo para una frecuencia circular p determinada y aceleración asignada de la superficie del suelo⁽⁵⁾

Making algebraic arrangements we find the expressions governing the subsoil movement with circular frequency p for the assigned surface acceleration⁽⁵⁾

$$\delta_{i+1} = A_i \delta_i - B_i \tau_i \quad (18)$$

$$\tau_{i+1} = C_i (\delta_i + \delta_{i+1}) + \tau_i \quad (19)$$

en donde

in which

$$A_i = \frac{1 - N_i}{1 + N_i}, \quad B_i = \frac{1}{1 + N_i} \cdot \frac{d_i}{\mu_i}$$

$$C_i = \frac{1}{2} (pd_i) p_n^2, \quad N_i = \frac{pd_i^2 \cdot p_n^2}{4\mu_i} \quad (20)$$

Con las ecuaciones (18) y (19) y conociendo la aceleración asignada a la superficie del suelo se puede encontrar la configuración de la masa del subsuelo durante el movimiento. La aceleración máxima de la superficie del suelo se designa por a_m y p_n la frecuencia circular, por consiguiente el desplazamiento en la superficie será $\delta_{so} = a_m/p_n^2$, con esta información se efectúa la integración paso a paso por medio de las ecuaciones (18) y (19) hasta encontrar que el desplazamiento relativo del suelo sea nulo en la base firme donde se generan las ondas sísmicas, obteniendo así la verificación de la frecuencia circular

With equations (18) and (19) and knowing the assigned acceleration at the ground surface we can find the configuration of the subsoil mass during the movement. The maximum acceleration of the ground surface we designate a_m and p_n the circular frequency, therefore the surface displacement will be $\delta_{so} = a_m/p_n^2$ with this information we can proceed with the integration step by step by means of equations (18) and (19) until we find that the relative displacement of the soil is zero at the firm base where the seismic waves are generated, obtaining by this method a confirmation of the free circular frequency of the soil mass and the

libre de la masa del suelo, la configuración de desplazamientos y los esfuerzos cortantes generados por la aceleración asignada en la superficie.

IV. PERIODO EQUIVALENTE ESTRUCTURA-CIMENTACION

La respuesta sísmica de la cimentación depende del conocimiento de las propiedades estratigráficas y dinámicas del subsuelo, así como del espectro de respuesta sísmico de la región.

Con el objeto de fijar los conceptos para el diseño sísmico de una cimentación con pilas, supongamos que la Fig. 5 representa la cimentación de un edificio alto cuyo centro de masa se encuentra localizado a una altura h_M del desplante de la cimentación. Se considera que la cimentación es rígida de tipo cajón que alberga un sótano formando una estructura rígida de cimentación. Las descargas se efectúan directamente sobre las pilas de gran capacidad apoyadas a cierta profundidad sobre un estrato resistente.

displacements and shear stresses configuration created by the assigned surface acceleration.

IV. EQUIVALENT PERIOD OF THE STRUCTURE AND FOUNDATION

The seismic response of the foundation is related with the knowledge of the stratigraphical and dynamical properties of the subsoil, and from the response spectrum of the region.

With the purpose of fixing the seismic design concepts of a pier foundation, let us assume, Fig. 5 represents the foundation of a tall building with the center of mass localized at height h_M from the foundation grade elevation. We consider a rigid foundation of the box type holding a basement and forming a rigid foundation structure. The building loads are acting directly on the piers of large bearing capacity at certain depth on a strong stratum.

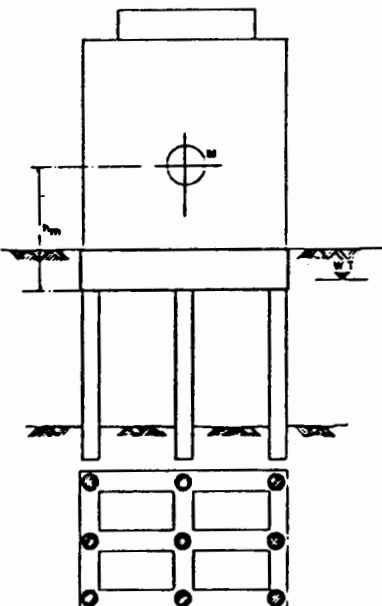


FIG. 5. CIMENTACION RIGIDA DE UN EDIFICIO SOBRE PILAS.
RIGID FOUNDATION OF BUILDING ON PIERS.

Para determinar la respuesta sísmica de la cimentación se hace necesario conocer el espectro envolvente de diseño sísmico de la zona en cuestión, Fig. 6, en términos del factor de amplificación f_a , de la relación T_o/T_s y de la fracción del amortiguamiento crítico equivalente ζ_0 de la estructura y cimentación. En donde T_o es el período acoplado de la estructura y su cimentación y T_s el período dominante del suelo. Este último se investiga como se ha descrito en la sección

In order to determine the seismic response of the foundation it is necessary to know the seismic design envelope spectrum of the area in question Fig. 6 in terms of the amplification factor f_a , against the ratio T_o/T_s , and the equivalent fraction of critical damping ζ_0 of the structure and its foundation. Here, T_o is the coupled period of the structure and its foundation and T_s is the dominant period of the ground. The last one is investigated as already described in

anterior. El período acoplado T_0 puede obtenerse como sigue con apoyo de la Fig. 7.

the last section. The coupled period T_0 may be obtained as follows with help of Fig. 7.

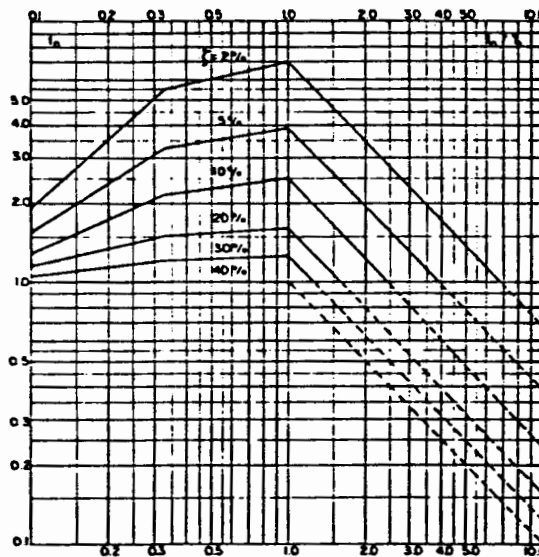


FIG. 6- ESPECTRO ENVOLVENTE DE DISEÑO SISMICO.
ENVELOPE SEISMIC DESIGN SPECTRUM.

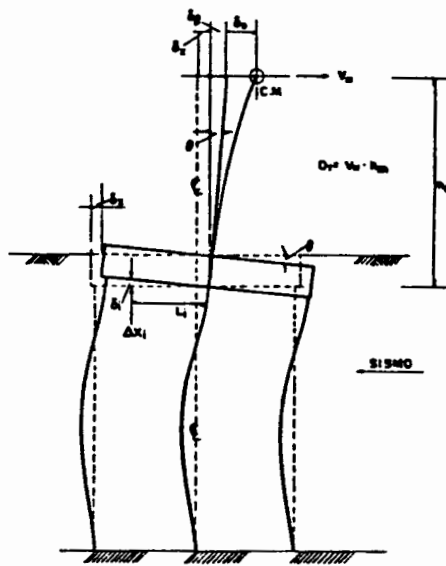


FIG. 7- COMPORTAMIENTO DE LA CIMENTACION.
FOUNDATION BEHAVIOR

Al venir el empuje sísmico sobre los pilotes se ocasiona un desplazamiento de la cimentación δ_x en el sentido opuesto al empuje sísmico, por la inercia de la masa del edificio, así también, un desplazamiento

When the seismic action on the piles creates displacements of the foundation the value δ_x has an opposite sense of the direction of the seismic action, because of the inertia of the mass of the building,

δ_θ por giro de la cimentación δ_B por flexión de la estructura del edificio, por consiguiente el desplazamiento relativo total en el centro de masa es

also the displacement δ_θ because rotation of the foundation, and δ_B because the flexibility of the structure of the building, therefore the total relative displacement at the center of mass is

$$\delta_o = \delta_B + \delta_\theta + \delta_x \quad (21)$$

Llamando ω_0 a la frecuencia libre equivalente del sistema estructura-cimentación se encuentra que la inercia de la masa M del sistema producirá un momento de volteo

Calling ω_0 the equivalent free circular frequency of the structure-foundation system we find the overturning moment because of the inertia force induced in the mass of the system,

$$O_T = M \delta_o \omega_0^2 \cdot h_m \quad (22)$$

Por otro lado, la fuerza de restitución de la cimentación por el giro es $O_T = K_B \cdot \theta$. En donde K_B es el módulo dinámico por balanceo de la cimentación y θ es la amplitud del giro, así pues

On the other hand, the restitution force of the foundation because the rotation is $O_T = K_B \cdot \theta$. In which K_B is the dynamic rocking modulus of the foundation, and θ is the amplitude of the rotation, therefore

$$M \omega_0^2 (\delta_B + \delta_\theta + \delta_x) \cdot h_m = K_B \frac{\delta_\theta}{h_m} \quad (23)$$

Además, designando por K_B la rigidez de la estructura y K_x la del suelo para el desplazamiento horizontal de la cimentación se obtienen las siguientes ecuaciones:

$$\begin{aligned} K_B \delta_B \cdot h_m &= K_B \frac{\delta_\theta}{h_m}, & \frac{\delta_B}{\delta_\theta} &= \frac{K_B}{K_B} \frac{1}{h_m^2} \\ K_x \delta_x &= K_B \frac{\delta_\theta}{h_m^2}, & \frac{\delta_x}{\delta_\theta} &= \frac{K_B}{K_x} \frac{1}{h_m^2} \end{aligned} \quad (24)$$

La ec. (23) puede escribirse en forma conveniente

Moreover, calling K_B the rigidity of the structural frame corresponding to the center of mass, and K_x that of the soil for the horizontal displacement of the foundation we obtain the following equations:

The eq. (23) may be written in convenient form

$$\frac{1}{\omega_0^2} = \frac{M}{K_B} h_m^2 \left\{ \frac{\delta_B}{\delta_\theta} + 1 - \frac{\delta_x}{\delta_\theta} \right\} \quad (25)$$

Sustituyendo en (25) los valores de (24) y arreglando términos se obtiene

Substituting in (25) the values of (24) and arranging terms we obtain

$$\frac{1}{\omega_0^2} = \frac{M}{K_B} + \frac{M}{K_B} h_m^2 + \frac{M}{K_x} \quad (26)$$

de la expresión (26) se puede observar que

From expression (26) we can observe that

$\frac{M}{K_B} = \frac{1}{\omega_B^2}$, donde ω_B es la frecuencia circular de la estructura del edificio

$\frac{M}{K_B} = \frac{1}{\omega_B^2}$, where ω_B is the circular frequency of the building

$$\frac{M}{K_B} h_m^2 = \frac{1}{\omega_0^2}, \text{ donde } \omega_0 \text{ es la frecuencia circular por rotación de la cimentación}$$

$$\frac{M}{K_x} = \frac{1}{\omega_x^2}, \text{ donde } \omega_x \text{ es la frecuencia circular por desplazamiento horizontal de la cimentación}$$

De lo anterior la expresión (26) toma la forma

$$\frac{M}{K_B} h_m^2 = \frac{1}{\omega_0^2}, \text{ where } \omega_0 \text{ is the circular frequency for the foundation rocking}$$

$$\frac{M}{K_x} = \frac{1}{\omega_x^2}, \text{ where } \omega_x \text{ is the circular frequency for the horizontal displacement of the foundation}$$

From above expressions (26) we obtain

$$\frac{1}{\omega_0^2} = \frac{1}{\omega_B^2} + \frac{1}{\omega_0^2} + \frac{1}{\omega_x^2}$$

pero como $\omega = 2\pi/T$, se tiene

but $\omega = 2\pi/T$, then we obtain

$$T_0^2 = T_B^2 + T_0^2 + T_x^2 \quad (27)$$

Así pues, conociendo el periodo acoplado T_0 estructura-cimentación y el dominante del suelo T_s se encuentra la relación T_0/T_s y se entra al espectro envolvente de diseño sísmico, con el amortiguamiento equivalente ζ_0 , Fig. 6, de donde se encuentra el factor de amplificación f_a . La fuerza cortante en el centro de masa es

Hence, knowing the equivalent period T_0 of the structure and its foundation and the dominant period of the subsoil T_s , we find the relation T_0/T_s and enter the seismic design envelope spectrum with the equivalent fraction of critical damping ζ_0 , Fig. 6. There we find the amplification factor f_a . The shear force at the center of mass is

$$V_m = (f_a a_m) \cdot M \quad (28)$$

y el momento de volteo

and the overturning moment

$$O_T = (f_a a_m) \cdot M \cdot h_m \quad (29)$$

Aquí a_m representa la aceleración máxima que se le asigna a la superficie del suelo. De los cálculos anteriores expuestos se puede reconocer que para valorizar la respuesta del edificio y su cimentación será necesario determinar los valores de los períodos individuales de la cimentación T_θ , T_x y el de la estructura T_B , así como el amortiguamiento crítico equivalente ζ_0 el cual se puede obtener por medio de la siguiente ecuación

Here a_m represents the maximum assigned surface acceleration. From the above mentioned calculations we can recognize that in order to estimate the response of the building and its foundation it is necessary to determine the values of the independent periods of the foundation T_θ , T_x and that of the structural frame T_B , also the equivalent critical damping of the system ζ_0 that may be obtained by means of the following equation

$$\zeta_0^2 = \frac{\zeta_\theta^2 T_\theta^2 + \zeta_x^2 T_x^2 + \zeta_B^2 T_B^2}{(1 - \zeta_x^2 - \zeta_n^2) T_\theta^2 + (1 - \zeta_\theta^2 - \zeta_n^2) T_x^2 + (1 - \zeta_0^2 - \zeta_x^2) T_B^2} \quad (30)$$

en donde, ζ_B es la fracción de amortiguamiento crítico del edificio, que puede tener valores del orden de 2% a 10% o más, dependiendo de la estructuración del

in which ζ_B is the fraction of the critical damping of the building, that may be between values on the order of 2% to 10% or more, depending on the structure

edificio y elementos de relleno. Por otro lado ζ_e y ζ_x son las fracciones de amortiguamiento crítico del suelo, que puede alcanzar los siguientes valores:

design of the building and secondary elements. On the other hand ζ_e y ζ_x represent the fraction of critical damping of the soil, they obtain approximately the following values:

SUELOS	% AMORTIGUAMIENTO	SOILS	% CRITICAL DAMPING
Muy blandos	40 % o mayor	Very soft	40% or more
Blandos	30%	Soft	30%
Semi-blandos	20%	Semi-rigid	20%
Rígidos	15%	Rigid	15%
Muy rígidos	10%	Very rigid	10%
Duros	5% o menor	Hard	5%

V. INTERACCION SUELO-CIMENTACION POR BALANCEO

Para determinar el periodo T_0 y las recargas axiales sobre las pilas durante el sismo por momento de volteo $O_T = \theta K_p$, será necesario formar la matriz de flexibilidad de las pilas y del suelo donde éstas apoyan. Para lograr esta acción es necesario conocer el módulo dinámico de rigidez μ del suelo y del material de las pilas. La matriz tiene la forma⁽⁶⁾

V. SOIL-STRUCTURE INTERACTION FOR ROCKING

To determine the rocking T_0 and consequently the increment of loads on the piers or piles during the seismic action because of the overturning moment $O_T = \theta K_p$ it is necessary to form the flexibility matrix of the piers and soil strata where they are supported. To achieve this action it is necessary to know the dynamic soil rigidity μ and that of the material of the piers. The matrix has the following form⁽⁶⁾

$$[\bar{\delta}_{ji}] + [1/K_p]_D \quad (31)$$

en donde $[\bar{\delta}_{ji}]$ representa la matriz de flexibilidad unitaria del suelo bajo las pilas y $[1/K_p]_D$ es la matriz diagonal que representa la deformabilidad axial unitaria de las pilas. Si llamamos X_i las reacciones incógnitas axiales sobre las pilas por el momento de volteo, entonces se puede escribir,

in which $[\bar{\delta}_{ji}]$ represents the unit flexibility matrix of the soil under the piers and $[1/K_p]_D$ is the diagonal matrix representing the unit axial deformation of the piers. When we call X_i the unknown axial reactions on the piers because of the overturning moment then we can write

$$\{[\bar{\delta}_{ji}]_\mu^T + [1/K_p]_D\} \begin{vmatrix} X_i \end{vmatrix} = \begin{vmatrix} \delta_i \end{vmatrix} \quad (32)$$

aquí $|\delta_i|$ representa el vector el desplazamiento vertical de las pilas. El momento de volteo de la cimentación rígida queda representado por una rotación simétrica, Fig. 7, por tanto se puede escribir para el desplazamiento vertical en un punto i ; $\delta_i = \theta L_i$. Susituyendo en la expresión (32) se tiene

here $|\delta_i|$ represents the vector of the vertical displacements of the piers. The overturning moment of the rigid foundation is represented by a symmetrical rotation, Fig. 7. Therefore, for the vertical displacement at point i we have $\delta_i = \theta L_i$. Substituting in expression (32) we have

$$\{[\bar{\delta}_{ji}]_\mu^T + [1/K_p]_D\} \begin{vmatrix} \frac{X_i}{\theta} \end{vmatrix} = \begin{vmatrix} L_i \end{vmatrix} \quad (33)$$

resolviendo la ec. (33) se obtienen los valores de $\frac{X_i}{\theta}$, de donde el momento de volteo es

solving the equation (33), we obtain the values of $\frac{X_i}{\theta}$, and the overturning moment is

$$O_T = \sum_{i=1}^n \left(\frac{X_i}{\theta} \right) \cdot L_i \cdot \epsilon$$

El módulo de cimentación por balanceo por definición es $K_B = O_T/\theta$, por consiguiente

The rocking foundation modulus by definition is $K_B = O_T/\theta$, therefore

$$K_B = \sum_i \left(\frac{X_i}{\theta} \right) \cdot L_i \quad (34)$$

y el periodo de balanceo

and the rocking period

$$T_B = 2\pi h_m \sqrt{\frac{M}{K_B}} \quad (35)$$

El valor de K_x se obtiene como se indica más adelante.

The value of K_x may be obtained as indicated in further paragraphs.

VI. ARRASTRE HORIZONTAL SISMICO SOBRE LA CIMENTACION

El arrastre horizontal sísmico sobre la cimentación se origina por el empuje que la masa del suelo ejerce sobre las pilas y en el cajón de la cimentación, Fig. 8. Consideremos que las pilas se encuentran empotradas en la estructura de la cimentación y en el estrato resistente donde la base puede girar de acuerdo con la rigidez dinámica del suelo donde apoya. Consideremos que el empuje del suelo sobre las pilas queda representado por las fuerzas horizontales incógnitas X_i aplicadas en tantas secciones de la pila como sea necesario para obtener la precisión requerida. Haciendo $X_i = 0$ se obtendrá el desplazamiento libre de la pila y del suelo. Llamamos a ésta acción la Condición $X_i = 0$, Fig. 9. El desplazamiento libre del suelo y de la pila en un punto cualquiera i será $(\Delta_{io} + \delta_{si})$ y en el apoyo (b) el giro es θ_{bo} (7),(8).

Los desplazamientos anteriores deben ser compatibles con las acciones que en el punto i producen las fuerzas o reacciones incógnitas X_i . Por tanto, la acción de una fuerza unitaria aplicada en el punto (i) es la Condición $X_i = +1$, Fig. 10, que induce los desplazamientos $(S_{ij} + \bar{\delta}_{ij})$ en el punto i y en la base un giro $\bar{\theta}_{bi}$. En un punto (j) es $(S_{jj} + \bar{\delta}_{jj})$. Así también al aplicar la condición unitaria en (j), para $X_j = +1$ se obtiene en el punto (i); $(S_{ij} + \bar{\delta}_{ij})$, y en (j); $(S_{jj} + \bar{\delta}_{jj})$, en la base el giro es $\bar{\theta}_{bj}$. Por otro lado al aplicar un momento unitario en la base, Condición $X_b = +1$ se tiene en (i) $\bar{\delta}_{ib}$, en (j) $\bar{\delta}_{jb}$ y en (b) un giro $(\bar{\theta}_{bb} + \bar{\theta}_{sb})$, en donde $\bar{\theta}_{bb}$ representa el giro unitario en la base de la pila, y $\bar{\theta}_{sb} = 1/K_b$ en el suelo.

VI. SEISMIC HORIZONTAL DRIFT ON THE FOUNDATION

The seismic horizontal drift on the foundation is created because of the soil mass displacements on the piers and on the foundation box, Fig. 8. Let us consider that the piers are fixed to the foundation beams and supported on the firm ground where their bases can rotate according to the dynamic rigidity of the soil where they are bearing. Let us further consider that the action of the soil on the piers is represented by the unknown horizontal forces X_i applied in so many sections of the pier as necessary to obtain the required accuracy. When we make $X_i = 0$, we obtain the free displacements of the pier and of the soil. Call this action, the Condition $X_i = 0$, Fig. 9. The free displacement of the soil and the pier at any point i will be $(\Delta_{io} + \delta_{si})$, and at the base (b) the rotation will be θ_{bo} (7),(8).

The above mentioned displacements shall be compatible with the actions that at a point i are induced by the unknown reactions force X_i . Hence, the action of a unit force applied at point i , we call the Condition $X_i = +1$, Fig. 10, and produces the displacements $(S_{ij} + \bar{\delta}_{ij})$ at points i , and at the base the rotation $\bar{\theta}_{bi}$. At point (j) we have $(S_{jj} + \bar{\delta}_{jj})$. When we apply the unit condition in (j), for $X_j = +1$ we obtain at point (i); $(S_{ij} + \bar{\delta}_{ij})$, and at (j); $(S_{jj} + \bar{\delta}_{jj})$, and at the base the rotation $\bar{\theta}_{bj}$. On the other hand, when we apply a unit moment at the base; Condition $X_b = +1$ we obtain in (i) $\bar{\delta}_{ib}$, and in (j) $\bar{\delta}_{jb}$ and at (b) the rotation $(\bar{\theta}_{bb} + \bar{\theta}_{sb})$, in which $\bar{\theta}_{bb}$ represents a unit rotation of the pier base elements, and $\bar{\theta}_{sb} = 1/K_b$ in

El valor de K_b es la rigidez del suelo al giro, por el momento unitario $X_b = +1$ aplicado al suelo.

the value of K_b is the soil rigidity to the rotation of a unit moment $X_b = +1$, applied to the supporting soil.

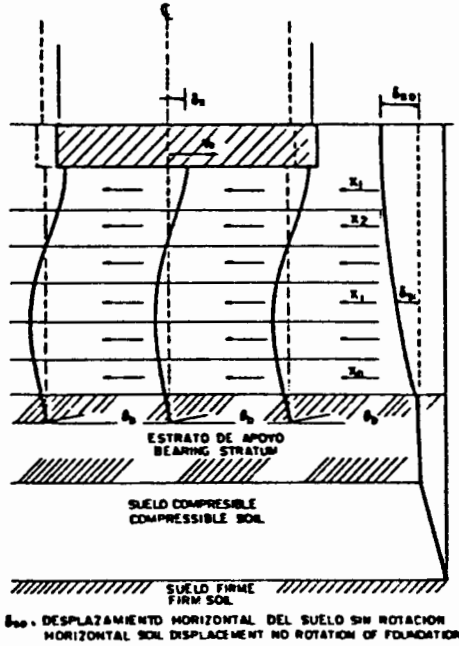


FIG. 8. ARRASTRE DEL SUELDO SOBRE LAS PILAS
SOIL DRIFT AGAINST THE PILES.

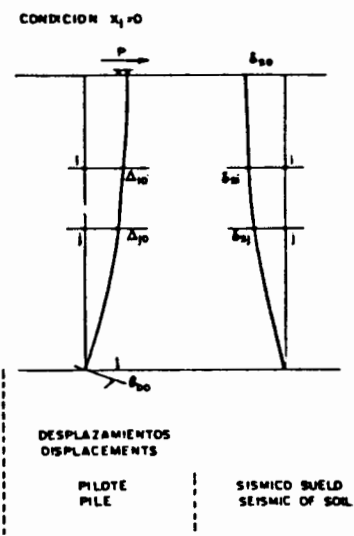


FIG. 9. DESPLAZAMIENTOS HORIZONTALES.
HORIZONTAL DISPLACEMENTS.

Por el método anterior se pueden escribir las condiciones de compatibilidad para todos los puntos (i) y (j), y para la base de la pila (b) respectivamente.

Using the method just described we can write the compatibility equations for all the points (i) and (j), and for the pier base (b), respectively.

$$\text{Pts. } i : (\bar{s}_{ii} + \bar{\delta}_{ii}) x_i + (\bar{s}_{ij} + \bar{\delta}_{ij}) x_j + \bar{s}_{ib} x_b = \Delta_{io} + \varepsilon_{si}$$

$$\text{Pts. } j : (\bar{s}_{ji} + \bar{\delta}_{ji}) x_i + (\bar{s}_{jj} + \bar{\delta}_{jj}) x_j + \bar{s}_{jb} x_b = \Delta_{jo} + \varepsilon_{sj}$$

$$\text{Base } b : \bar{\theta}_{bi} x_i + \bar{\theta}_{bj} x_j + (\bar{\theta}_{bb} + \frac{1}{K_b}) x_b = \theta_{bo}$$

en forma matricial

in matrix form

$$\begin{bmatrix} (\bar{s}_{ii} + \bar{\delta}_{ii}) & (\bar{s}_{ij} + \bar{\delta}_{ij}) & \bar{s}_{ib} \\ (\bar{s}_{ji} + \bar{\delta}_{ji}) & (\bar{s}_{jj} + \bar{\delta}_{jj}) & \bar{s}_{jb} \\ \bar{\theta}_{bi} & \bar{\theta}_{bj} & \bar{\theta}_{bb} + \frac{1}{K_b} \end{bmatrix} \times \begin{bmatrix} x_i \\ x_j \\ x_b \end{bmatrix} = \begin{bmatrix} \Delta_{io} + \varepsilon_{si} \\ \Delta_{jo} + \varepsilon_{sj} \\ \theta_{bo} \end{bmatrix} \quad (36)$$

Resolviendo la ecuación matricial (36) para las reacciones horizontales x_i , se podrán calcular los elementos mecánicos de la pila, así también los desplazamientos horizontales por medio de la matriz de flexibilidad unitaria del suelo

Solving the matrix equation (36) for the unknown horizontal reactions x_i , we can compute the mechanical elements of the pier also the horizontal displacements by means of the unit flexibility matrix of the soil

$$\begin{bmatrix} \bar{\delta}_{ii} & \bar{\delta}_{ij} & 0 \\ \bar{\delta}_{ji} & \bar{\delta}_{jj} & 0 \\ 0 & 0 & \frac{1}{K_b} \end{bmatrix} \times \begin{bmatrix} x_i \\ x_j \\ x_b \end{bmatrix} = \begin{bmatrix} \delta_i \\ \delta_j \\ \theta_b \end{bmatrix} \quad (37)$$

Así pues, de la Ec. (37) se encuentra el desplazamiento horizontal δ_x de la pila en el apoyo con la estructura de la cimentación. Llamando V_B la fuerza constante sísmica que actúa en la cabeza de la pila se obtiene el valor

$$k_x = \frac{V_B}{\delta_x} \quad (38)$$

de la Ec. (38) se puede calcular el periodo por desplazamiento horizontal de estructura de la cimentación

Therefore, from Eq. (37) we find the horizontal displacement δ_x of the pier at the support with the foundation structure. Calling V_B the base seismic shear force acting at the head of the pier we obtain

from Eq. (38) we can compute the period because of the horizontal displacement of the foundation structure

$$T_x = 2\pi \sqrt{\frac{M}{K_x}} \quad (39)$$

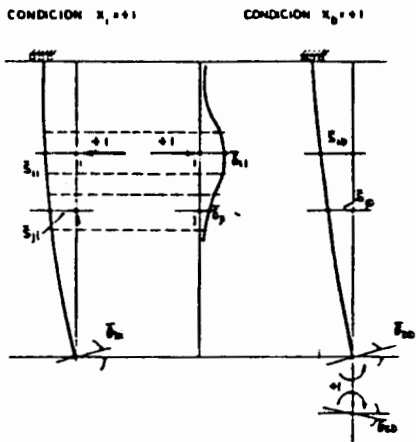


FIG. 10- INTERACCION PILOTE-SUELDO
PILE-SOIL INTERACTION.

VII. RESPUESTA SISMICA

Por medio de los procedimientos de cálculo antes indicados se encuentran los valores de T_B y T_x . El valor T_B se conoce del análisis estructural sísmico del edificio, por consiguiente

$$T_0 = \sqrt{T_B^2 + T_\theta^2 + T_x^2} \quad (40)$$

de la Ec. (40) conociendo T_0/T_s y ζ_0 se obtiene del espe-
ctro de diseño sísmico el factor de amplificación
 f_a , Fig. 6.

Con la aceleración máxima a_m asignada a la superficie del suelo se encuentra la fuerza cortante en la base $V_B = f_a(a_m M)$, y el momento de volteo $O_T = V_B \cdot h_m$, de donde la amplitud del giro de la cimentación es $\theta = O_T/K_B$ y los incrementos en carga axial sobre las pilas por sismo son

$$\left| \Delta Q_s \right| = \left| \left(\frac{X_i}{\theta} \right) \right| \cdot \left| \frac{O_T}{K_B} \right| \quad (41)$$

Por medio de la interacción sísmica suelo-pilote, Ec. 36, se podrá ajustar al valor K_x y por iteración determinar el ajuste final para la aceleración asignada.

VII. SEISMIC RESPONSE

By means of the computation method here indicated we find the values of T_B and T_x . The value of T_B may be obtained from the structural frame seismic analysis of the building, therefore

from Eq. (40) knowing T_0/T_s y ζ_0 , we enter the seismic design envelope spectrum and obtain the amplification factor f_a , Fig. 6.

With the maximum assigned acceleration a_m of the ground surface we find at the pile head a base shear; $V_B = f_a(a_m M)$, and the overturning moment $O_T = V_B \cdot h_m$, from which the amplitude of rocking of the foundation is $\theta = O_T/K_B$ and the axial load increments on the piles because of the seismic action are

By means of the seismic soil-pile interaction Eq. (37), we can adjust the value of K_x and finished the final adjustment for the assigned acceleration.

Incluyendo la carga en las pilas por el momento de volteo sísmico, las pilas extremas quedan sujetas a una carga axial máxima de

Including the load on the piers due to the overturning moment, the edge piers are subjected to an axial maximum load of

$$Q = Q_a + (NF) + \Delta Q_{sis} \quad (42)$$

A la acción axial sobre las pilas deberán incluirse los momentos flexionantes y fuerzas cortantes generadas en las pilas por el desplazamiento sísmico del subsuelo, los que se obtienen con los resultados finales de las fuerzas horizontales de interacción ocasionadas por el empuje sísmico de la masa del suelo, Ec. (36).

To the axial action on the piers given by Eq. (42) we shall add the moments and shear forces on the piers generated because of the seismic horizontal displacements of the soft soil mass, obtained with the final results of the interacting horizontal forces X_i , created during the seismic action of the soil mass, Eq. (36)

VIII. CONCLUSIONES

Del análisis aquí presentado para obtener la respuesta sísmica de una cimentación con pilotes o pilas; de las acciones sísmicas axiales sobre éstas, el arrastre horizontal sísmico, y la fricción negativa, se reconoce la necesidad de obtener con precisión razonable las condiciones estratigráficas y geotécnicas del subsuelo y en especial las propiedades dinámicas; o sea, el módulo dinámico de rigidez μ representativo de todos y cada uno de los estratos hasta la base firme. Este parámetro dinámico del suelo puede ser obtenido con precisión práctica haciendo uso del "Péndulo de Torsión Libre" diseñado por el autor⁽⁹⁾ para este objeto. La precisión de las matrices de flexibilidad se encuentra dentro de la precisión con que puedan conocerse los parámetros del suelo y el módulo de deformación elástico $1/E_c$ del material de las pilas. La flexibilidad del suelo tanto en sentido vertical como horizontal tiene una precisión que queda dentro de los procedimientos ortodoxos para la determinación de esfuerzos en la masa del suelo usados en la mecánica de suelos convencional. Se hace notar que en el diseño de cimentaciones se deberá lograr que los esfuerzos inducidos en el subsuelo por la acción sísmica sean del orden cuasi-elástico para evitar las deformaciones permanentes y así el desplome del edificio durante el sismo.

Se concluye además, que para poder calibrar las teorías y procedimientos de cálculo se hace necesario la investigación de campo a escala natural en pilotes instrumentados, así también como mejorar los procedimientos de muestreo inalterado, las técnicas y equipos de laboratorio que permitan en el futuro obtener parámetros del suelo más cercanos a las condiciones de campo dentro del rango del estado de esfuerzos sísmicos esperados.

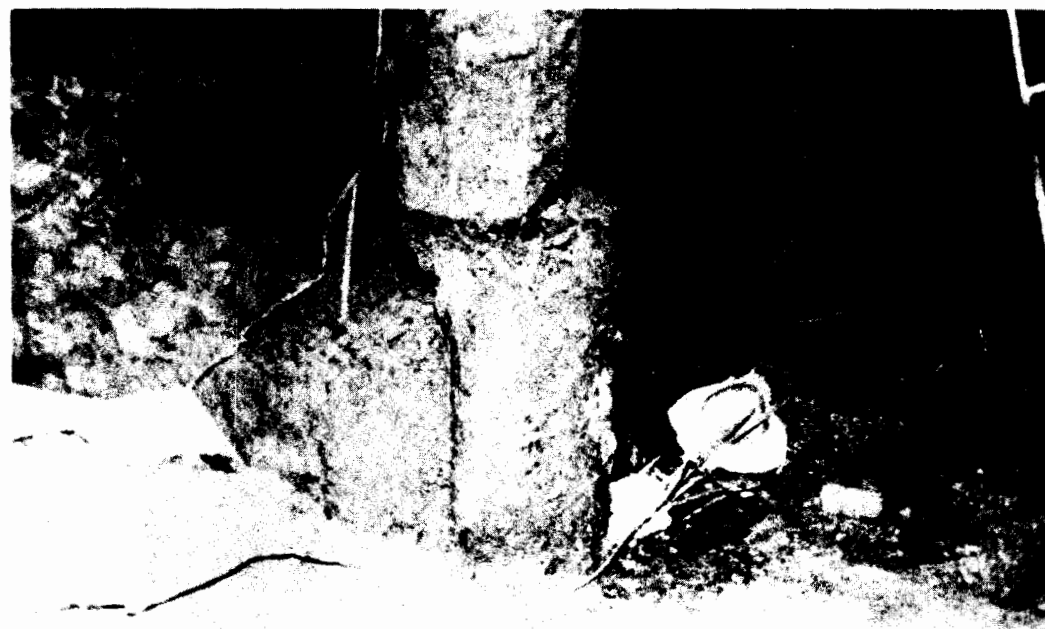
VIII. CONCLUSIONS

From above mentioned analysis presented here to obtain the seismic response of a foundation on piles or piers, the axial forces on them, the seismic horizontal drift and the negative friction, we can recognize the need to obtain with reasonable precision the stratigraphical and geotechnical conditions of the soil mass and specially the soil dynamic properties, that is to say, the dynamic soil rigidity μ representative for each one of the strata to firm base. This dynamic parameter of the soil may be obtained with practical accuracy making use of the "Free Torsion Pendulum" designed by the author for this purpose. The accuracy of the flexibility matrixes of the piers may be found under the same precision that may be obtained in the soil parameters and the elastic strain modulus $1/E_c$ of the pier or pile material. The soil flexibility either in the vertical direction or the horizontal direction have a precision that is within the orthodox procedures for the determination of stresses in the soil mass used in conventional soil mechanics methods. It may be noticed, however, that the stresses induced in the subsoil by the seismic action should be considered within a quasi-elastic behavior, to avoid large permanent plastic deformations and damage or tilting of the foundation and building during seismic action.

Furthermore, we conclude that in order to calibrate theories and methods of calculation it is necessary to investigate in the field on natural scale in instrumented piles or piers the seismic action, also, to improve the methods of undisturbed sampling, the laboratory equipment and the test techniques, that will permit in the future to obtain soil parameters closer to the field conditions within the expected state of the dynamic stresses.

REFERENCIAS

- (1) Zeevaert, L. (1976)
"Dragging Forces on Pier Foundations" ("Fuerzas de arrastre en cimentaciones con pilas"),
Memorias de la reunión conjunta Cimientos Profundos Colados en Sitio, SMMS-Association of
Drilled Shaft Contractors (ADSC), pp. 38-75, Sociedad Mexicana de Mecánica de Suelos,
México, D.F., Junio (English and Spanish)
- (2) Zeevaert, L. (1973)
"Deep Foundations, Including Pile Foundations (Design and New Methods of Construction)":
Section 1, 2 and 3. Proc. VIII Inter. Conf. Soil Mech. and Foundation Engineering,
Session 3, Moscow, USSR
- (3) Reese, C.L. (1973)
"Bored Piles Installed by Slurry Displacement", Proceedings of the VIII Inter. Conf. Soil
Mech. and Foundation Engineering, Vol. 3, pp. 203-209, Moscow
- (4) Zeevaert, L. (1982)
"Foundation Engineering for Difficult Subsoil Conditions", Second Edition, Van Nostrand-
Reinhold Co., New York, U.S.A., Chapter VIII, pp. 352-370
- (5) Referencia (4), Chapter XII, pp. 511-522
- (6) Zeevaert, L. (1980)
"Interacción Suelo-Estructura de Cimentaciones Superficiales y Profundas Sujetas a Cargas
Estáticas y Sísmicas", Editorial LIMUSA, México, D.F., parte 3, pp. 122-125
- (7) Referencia (4), Chapter XII.6, pp. 567-577
- (8) Referencia (6), parte 3, pp. 122-125
- (9) Zeevaert, L. (1982)
"Teoría y Práctica del Péndulo de Torsión (FTP)" ("Theory and Practice of the Torsion
Pendulum"), División de Estudios de Posgrado, Facultad de Ingeniería, UNAM, México, D.F.,
Febrero (Spanish and English)



DESPLAZAMIENTO DE JUNTA POR FALTA DE REFUERZO
JOINT DISPLACEMENT DUE TO LACK OF REINFORCEMENT



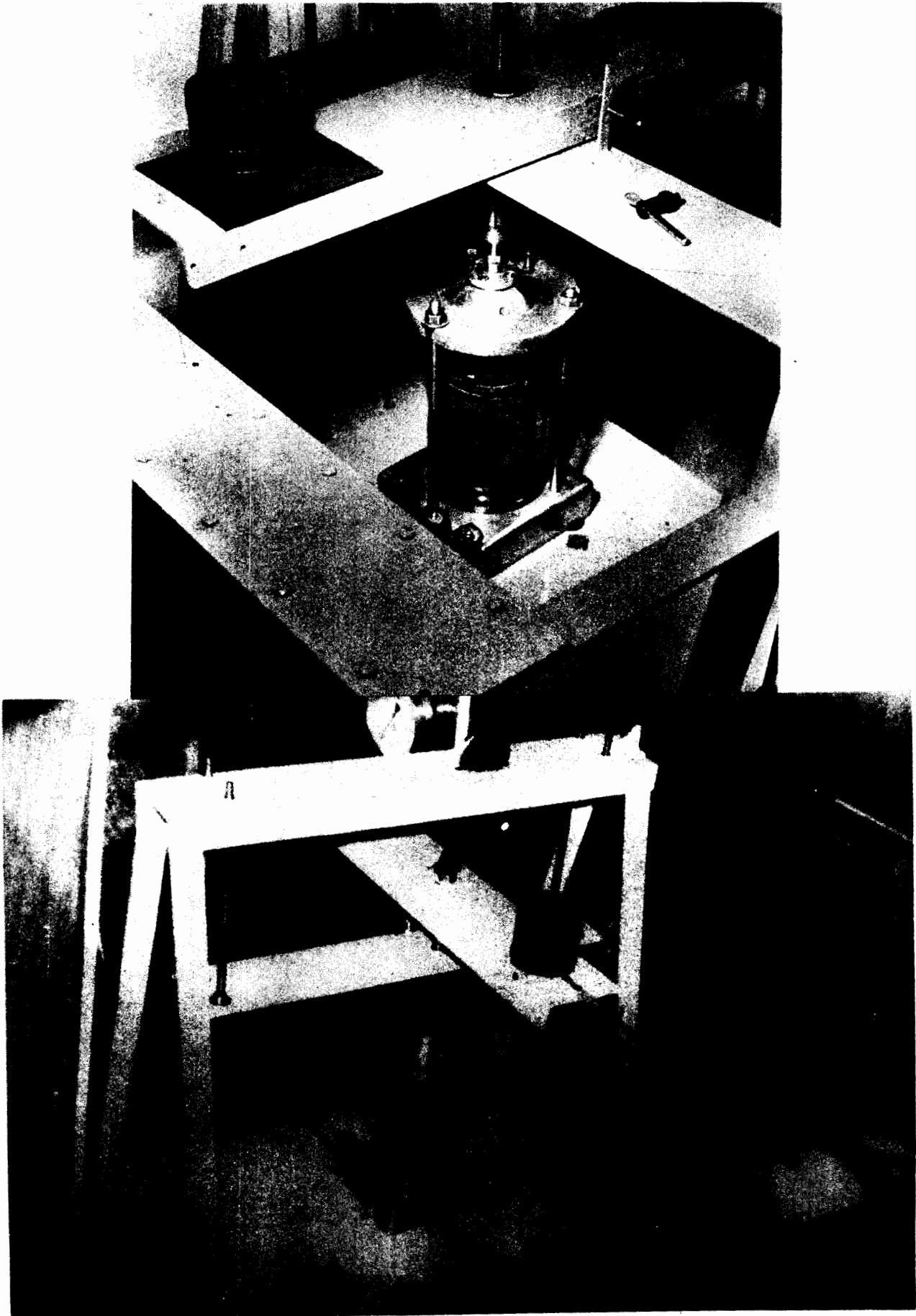
ROTURA POR FLEXION Y CORTANTE
FAILURE DUE TO HIGH BENDING AND SHEAR



FORMACION DE JUNTA POR ESFUERZOS ALTOS DE FLEXION
JOINT FORMATION DUE TO HIGH BENDING STRESSES



ROTURA TOTAL DEL APOYO POR ESFUERZOS EXCESIVOS
TOTAL FAILURE OF SUPPORT DUE TO HIGH STRESSES



Sección de Sistemas

COORDINADOR
M. en I. Gonzalo Negroe Pérez.

Programas Académicos

Profesores de Carrera y Líneas de Investigación

MAESTRIA
Investigación de operaciones
Planeación

DOCTORADO
Investigación de operaciones

Tiempo completo

FUENTES ZENON, ARTURO. Maestro en ingeniería. Universidad Nacional Autónoma de México. Teoría del conocimiento y su aplicación en el proceso de planeación.

GARCIA OLVERA, JOSE IGNACIO. Maestro en ingeniería. Universidad Nacional Autónoma de México. Teoría y modelado de sistemas, teoría de optimización de sistemas y confiabilidad.

NEGROE PEREZ, GONZALO. Maestro en ingeniería. Universidad Nacional Autónoma de México. Metodología de la planeación, planeación del sistema de transporte.

SANCHEZ GUERRERO, GABRIEL. Maestro en ingeniería. Universidad Nacional Autónoma de México. Metodología de la planeación, evaluación de sistemas.

TELLEZ SANCHEZ, RUBEN. Maestro en ingeniería. Universidad Nacional Autónoma de México. Calidad y/o productividad, evaluación de proyectos.

Medio tiempo

ACOSTA FLORES, JOSE DE JESUS. Doctor en ingeniería de investigación de operaciones. Universidad Nacional Autónoma de México. Análisis de decisiones, simulación de sistemas.

ALVAREZ CASO, FRANCISCO. Maestro en ingeniería. Universidad Nacional Autónoma de México. Dinámica de sistemas, modelado de sistemas urbanos.

COBIAN SELA, JOSE MIGUEL. Doctor en ciencias. Universidad de Michigan, E.U.A., Análisis de inventarios.

MORENO BONETT, ALBERTO. Maestro en ingeniería. Universidad Nacional Autónoma de México. Análisis de inversiones, técnicas discretas de la ingeniería de sistemas.

Publicaciones

FUENTES A , SANCHEZ G , *Metodología de la Planeación Normativa*, Revista Contaduría y Administración, F.C.A. UNAM, No. 151, nov-dic.

SANCHEZ G , *La función de evaluación en el proceso de solución de problemas de planeación. Investigaciones asociadas sobre el proceso de evaluación*, Tercer seminario teórico sobre evaluación, Informe final, CREFAL, OEA, Pátzcuaro, Mich., México, mayo.

Convenios

CONACYT-UNAM. Proyecto Investigación en ciencia y tecnología de la ingeniería .

Artículo reproducido

GARCIA, I., GELMAN, O., FUENTES, J., *Optimal strategies for dam construction under the flood risk*, Quality, Control and Reliability, International Association of Science and Technology for Development, IASTED Anaheim, Cal. E.U.A.

OPTIMAL STRATEGIES FOR DAM CONSTRUCTION UNDER THE FLOOD RISK

José Ignacio García O., Ovsei Gelman M. & Javier Fuentes M.

Instituto de Ingeniería, UNAM
Apdo. Postal 70-472, Coyoacán
México, D.F., 04510
México

ABSTRACT

A method for obtaining the optimal velocities of a dam wall curtain construction process has been elaborated to minimize the total expenses including the proper cost of construction as well as the expected damage by floods. A markovian model and a finite dynamic programming algorithm has been employed.

1. INTRODUCTION.

In the last stage of dam construction, i.e., during the wall curtain final closure, a problem of the determination of its optimal velocity is appearing. From one side, with the velocity increase and the higher altitude of the curtain, the hazard of its destruction by the flood is decreasing but the consequent cost of damage is higher; from another, with the decrease of the velocity, the altitude of the curtain is smaller and the hazard is higher, but the cost is lesser. Moreover, the own cost of the dam construction depends from its velocity.

Thus in the practice of dam construction it turns out to be very important the solution of the problem of the velocity optimization of the process of the wall curtain erection under the usual cost and time restrictions, taking into account the hazard of the floods that could overrun and destroy it during this stage of the construction process.

2. PROBLEM CONCEPTUALIZATION.

Using the conceptual framework developed in the area of the Interdisciplinary Disaster Research [1], it has been important to distinguish the Perturbating and Exposed Systems (fig. 1).

The Perturbating System (PS), i.e., the one that is producing the destructing phenomena, is formed by the rain that being integrated by the river basin is transformed into flood that increases the water level in the storage reservoir and thus could destroy the constructed part of the curtain.

The curtain is a component of the Exposed System (ES) that is composed by the both front and back cofferdams, personnel, machinery and construction devices, as well as by the people, goods and productive zones allocated in downstream area.

To define the optimal velocity of the curtain construction it is important to evaluate the risk related with the dam failure due to the surpassing of its actual level by the river rai-

sing water, i.e., the expected whole damage that includes the construction cost as well as the value of other damaged components of the ES.

Moreover, the risk assessment implies the necessity to take into account the hazard of the failure, i.e., the probability that the water level would overtop the wall curtain due to the rains.

To assess the hazard of the dam failure it is important to define the states of the PS and ES at the corresponding moment of time t .

Let's introduce the following denominations. According the discrete approach, the whole time T of the wall curtain construction is normally considered in the monthly periods ($k = 1, 2, \dots, T$); likewise, the whole elevation H of the wall curtain that would be reached by volume W of the filling materials to assure the struck capacity V of the water storage reservoir are divided into s levels, respectively. Thus:

$$\begin{aligned} V_i &= i \Delta V, \\ H_i &= g(V_i), \\ W_i &= e(V_i), \end{aligned} \quad \dots(1)$$

where $\Delta V = V/s$, $i = 1, 2, \dots, s$ and the functions $g(v)$ and $e(v)$ are allowing to calculate the curtain elevation H_i and the volume of the filling materials W_i that are corresponding to a certain capacity V_i of the storage reservoir (fig. 2).

Let's denote by X_k the variable that determines the level of the wall curtain that corresponds to the construction period K . Another variable that defines the system state is the actual water level N_k that is measured in the established scale (1), of the wall curtain altitudes H_i , i.e., its domain is

$$N_k = H_1, \dots, H_s, H_o$$

The wall curtain could be in two main states: normal and failure. The failure at the period k means that the water level N_k overtops the wall curtain, meanwhile it has not been surpassed before, i.e.:

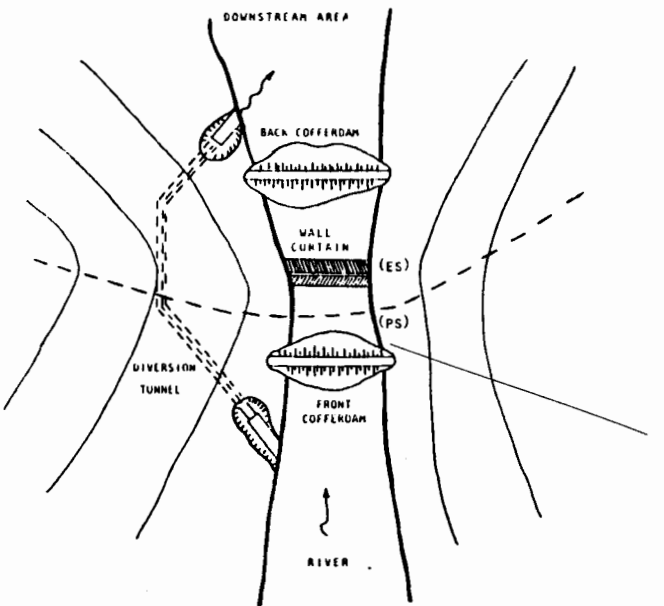


FIG 1 PERTURBATING (PS) AND EXPOSED (ES) SYSTEMS

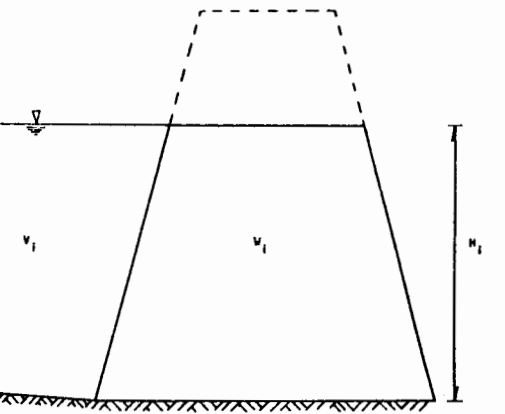


FIG 2 THE BASIC SCALE

diversion tunnel and could be estimated easily by the conventional hydrological means [3].

Thus considering that the change from the state i to state j is a result of arriving of $(j-i) \Delta V$ and a loss of Q quantities of water:

$$v_k = (j-i) \Delta V + Q,$$

it has been obtained:

$$\begin{aligned} \pi_{ij}^k &= P[v_k = (j-i) \Delta V + Q] \\ &= P[(j-i) \Delta V + Q \leq v_k \leq 2(j-i) \Delta V + Q] \quad \dots(6) \\ &= F_{v_k}[2(j-i) \Delta V + Q] - F_{v_k}[(j-i) \Delta V + Q] \end{aligned}$$

For $k=1, 2, \dots, T$; and $i, j = 1, 2, \dots, s, s$, the π_{ij}^k constitute T Markov matrices of the $(s+1) \times (s+1)$ order, and for the condition (2)

$$p^k = \prod_{r=1}^k M^r \quad \dots(7)$$

Now it is possible to evaluate the probability of the failure $P_f(k)$, taking into account (2) for all $x_k = h_n$, where $n=1, 2, \dots, s$

$$\begin{aligned} P_f(k) &= Pr[N_k > x_k = h_n] \\ &= \sum_{i=n+1}^s p_i^k = 1 - \sum_{i=1}^n p_i^k \quad \dots(8) \end{aligned}$$

For other side, every possible set $\{x_k : k=1, 2, \dots, T\}$ permits to obtain the velocity of wall curtain construction by its monthly increments:

$$(x_1, x_2 - x_1, \dots, x_k - x_{k-1}, \dots, x_T - x_{T-1})$$

$N_k > x_k$,
 $N_m < x_m, \quad (m < k) \quad \dots(2)$

As far as N_k depends from random factors such as the intensity of rains in the basin and evaporation, as well as other factors that are defining the hydrological balance, it is a random variable that could be described by the probability vector p_k :

$$p^k = (p_1^k, p_2^k, \dots, p_s^k, p_0^k) \quad \dots(3)$$

where,

p_i^k is the probability that $N_k = h_i$ for $i=1, \dots, s$
 p_0^k is the probability that $N_k = h_0$

$$\text{and } \sum_{i=1}^s p_i^k = 1$$

Supposing that the set of vectors $\{p : k = 1, 2, \dots, T\}$ determines a Markov chain with $s+1$ states [2], a usual technique of the transition probabilities π_{ij}^k could be utilized.

Let π_{ij}^k is the probability of the transition from the state i at the period $k-1$, to the state j at the next one, i.e.,

$$\pi_{ij}^k = Pr[N_k = j | N_{k-1} = i] \quad \dots(4)$$

This probability has been calculated taking into account, in the first approximation, the probability of the water income to the storage reservoir:

$$F_{v_k}(v_k) = Pr[v_k \leq v_k], \text{ for } k=1, \dots, T \quad \dots(5)$$

that is supposed to be known, as well as the quantity Q of water that is leaving through to

To facilitate the consequent analysis, the construction velocity is determined as a vector

$$U^i = (x_1^i, x_2^i, \dots, x_T^i) \quad \dots(9)$$

where x_k^i is a level of the wall curtain reached to the end to the period k , and $x_T^i = H_i$ for every $i = 1, 2, \dots, I^2$.

Thus, according (2), for every velocity U^i at the moment k , the set of all possible N_k could divided in two subsets, one of which is responsible for the failure.

Defining the state of the general system that integrates PS and ES as:

$$E(k) = (i, j) \quad \dots(10)$$

where $i = N_k$ and $j = x_k$

it could be seen that the set $\{E(k)\}$ is forming the bi-dimensional space that could be divided in two subspaces of normal $\{E_N(k)\}$ and failure $\{E_F(k)\}$ states, respectively (fig 3)

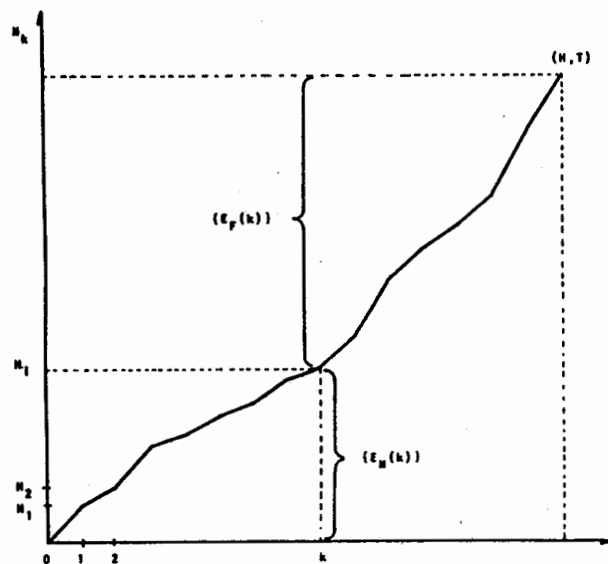


FIG 3 EXAMPLE OF THE DISTRIBUTION OF THE NORMAL AND FAILURE STATES.

The velocity U^i implies certain cost C_k^i of the construction process that has permitted to reach the altitude x_k^i at the moment k ; as well as the cost of damage CF_k^i due to the possible failure. The last one could be estimated by:

$$CF_k^i = CR_k^i + CL + CE + CA_k^i \quad \dots(11)$$

where:

- CR_k^i is the cost of rebuilding of the destroyed part of the wall curtain H_i ,
- CL is the cost of cleaning of the destructed zone from debries,

- CE is the cost of personnel, machinery, construction devices and material damages,

- CA_k^i is the cost of the third party damages, produced by the flood in the downstream area.

The previous definitions are permitting now to evaluate the expected cost of the wall curtain construction with the velocity U^i , considering it as a sum of the costs of every stage k

$$W(U^i) = \sum_{k=1}^T w_k^i \quad \dots(12)$$

where the cost w_k^i is formed by two parts: the proper cost of the construction C_k^i and the expected damage, i.e.

$$w_k^i = C_k^i + CF_k^i P_f(k) \quad \dots(13)$$

Thus the problem could be stated as an optimization problem to obtain the optimal velocity U^* , or well the values $(x_1^*, x_2^*, \dots, x_T^*)$ that minimize the expression (12)

$$\min \{W(U^i)\} = \min \left\{ \sum_{i=1}^T w_k^i \right\} \quad \dots(14)$$

under next restrictions

1. $0 \leq T \leq T_{\max}$
2. $0 \leq x_k^i \leq X$ for all $i=1, \dots, s$, $k=1, \dots, T$... (15)
3. $C_k^i \leq C_{\max}$ for all $i=1, \dots, I$

3. PROBLEM SOLUTION.

The solution of the equation (14) could be realized by different techniques. However, considering the markovian process that has been used it is convenient to apply the finite dynamic programming procedure [4].

According this approach, let introduce $B_n(i)$, that corresponds to the minimal expected cost of the part of the construction process, calculated for n consequent stages, beginning with the wall curtain altitude H_i (fig 4).

The next step consist in the determination of the vector $U^* = (x^*, x^*, \dots, x^*)$ that in case of $i=0$ is producing $B_T(0)$ as the desired total cost that minimize the equation (12), under the given restrictions (15). To find it, it is necessary to solve the next optimal equations [5].

$$B_n(i) = \min_{1 \leq j \leq s} \{ w_k^i + B_{n-1}(j) \}, \quad \dots(15)$$

$$B_1(i) = w_{T-1}^i, \quad i < T, \quad \dots(16)$$

$$B_k(s) = 0 \quad \text{for all } k \leq T$$

Considering that the solution of equations (9) y (14) for the practical problems is very complicated, two computer programs compiled in Basic for PC and denominated PROFALLA and VELOP have been elaborated. The first is calculating the failure probability and the second the optimal velocity.

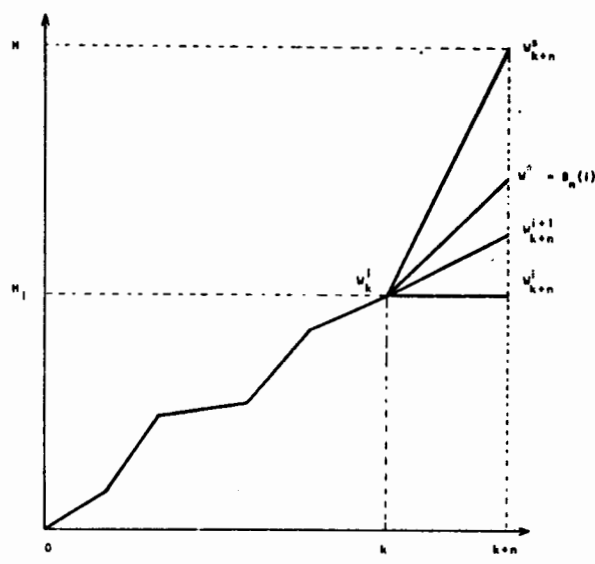


FIG 4 EXAMPLE OF THE DYNAMIC PROGRAMMING PROCEEDING.

The total process of the model elaboration as well as the optimal velocities calculations is shown in fig 5.

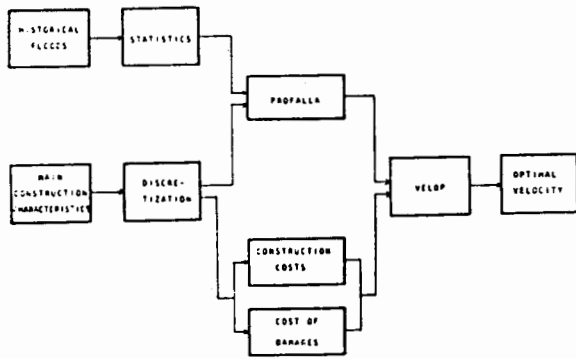


FIG 5 OPTIMAL VELOCITIES CALCULATION

Based on system approach and the Interdisciplinary Disaster Research a problem to optimization of the wall curtain construction velocity, has been formulated considering the importance to minimize the total expences that are including the proper cost of construction as well as the expected damage that could be produced by floods.

The conceptualization of the Perturbating and Exposed Systems has permitted to develop a markovian model and its study implied the use of finite dynamic programming algorithm. For the practical applications two PC programs in Basic have been elaborated.

The method has been employed for a concrete case of The Sabinal dam in the Sinaloa State of Mexico.

NOTES.

- 1 H corresponds to the level of water that are overpassing the full dam altitude H ($H_0 > H$).
- 2 I is a maximum number of all possible alternatives of the dam construction velocities.
- 3 A total destruction is considered like the worst case.
- 4 The maximum level of the restrictions (1), (2) and (3) are corresponding to the limit of construction time, the maximum level increase that could be reached during one period and the budget available, respectively.

REFERENCES.

- Gelman, O., Macias, S. Toward a Conceptual Framework for the Interdiiplinary Disaster Research, Ekistics, Vol 51, No. 309, Nov/Dec, 1984.
- Papoulis, A. Probability, Random Variables and Stochastic Processes, Mc Graw Hill, Japan, 1984.
- Raghunath, H.M. Hidrology, Wiley, New York, 1985.
- Bellman, R. Dynamic Programming, Princeton University Press, 1957.
- White, H. Finite Dynamic Programming, Wiley Interscience, 1978.
- Gelman, O., Garcia, J.I., Fuentes, J. Estudio de Cierre en Presas, cap 3, Informe Interno, Instituto de Ingenieria, México, 1986.

4. CONCLUSIONS.

This research is forming a part of a Project sponsored by SARII (Mexican Ministry of Agriculture and Hydraulic Recourses), responsible for the major number of mexican dams. This project has been dedicated to study the engineering and management aspects of the dam closure process [6].

**Departamento de
Ingeniería Electromecánica**

Programas Académicos

Profesores de Carrera y Líneas de Investigación

JEFE
Dr. Federico Kuhlmann Rodríguez.

COORDINADORES DE SECCION

ELECTRICA
Dr. Andrés Buzo de la Peña.

MECANICA
Dr. Alejandro Romero López.

ESPECIALIZACION
Proyecto de Instalaciones Eléctricas
Proyecto de Instalaciones Mecánicas

MAESTRIA
Ingeniería Eléctrica con opciones en:

Potencia
Control
Electrónica
Comunicaciones

Ingeniería Mecánica con opciones en:

Diseño y manufactura
Termofluidos
Mecánica de sólidos
Sistemas mecánicos
Metalurgia mecánica

DOCTORADO
Ingeniería Eléctrica
Ingeniería Mecánica

Tiempo completo

ALCANTARA SILVA, ROGELIO. Doctor en ingeniería eléctrica. Escuela Nacional de Telecomunicaciones de París, Francia. Electrónica digital, señales.

BALLESTEROS BAROCIO, PORFIRIO. Doctor en ingeniería mecánica estructural. Universidad de Northwestern, E.U.A. Mecánica de sólidos, estabilidad estructural.

BUZO DE LA PEÑA, ANDRES. Doctor en ingeniería eléctrica. Universidad de Stanford, E.U.A. Reconocimiento y codificación de voz, procesamiento digital de señales, compresión de datos, identificación de sistemas, control estocástico.

CHICUREL UZIEL, RICARDO. Doctor en ingeniería mecánica. Universidad de Princeton, E.U.A. Diseño mecánico y vibraciones.

FERRER ARGOTE, LUIS. Doctor en ingeniería mecánica. Universidad Católica de Washington, E.U.A. Análisis experimental de esfuerzos.

GARCIA UGALDE, FRANCISCO. Doctor en ingeniería eléctrica. Escuela Superior de Electricidad de Rennes, Francia. Códigos correctores de errores, diseño de sistema con microprocesadores, digitalización de imágenes.

HERNANDEZ ORTEGA, LUIS MARCIAL. Maestro en ciencias. Universidad de Michigan, E.U.A. Electrónica de potencia, electrónica industrial, comunicaciones.

GRINBERG FINKELSTEIN, ADOLFO. Doctor en fisicoquímica. Universidad de Buenos Aires, Argentina. Propiedades mecánicas de materiales y metalurgia mecánica.

GRINBERG, DORA M.K. de. Doctora en fisicoquímica. Universidad de Buenos Aires, Argentina. Tratamientos térmicos y transformaciones de fases.

JAUREGUI CORREA, JUAN CARLOS. Doctor en ingeniería mecánica. Universidad de Wisconsin, Milwaukee, E.U.A. Diseño mecánico, vibraciones.

KELLY MARTINEZ, RAFAEL DE J. Doctor en ingeniería eléctrica, Instituto Politécnico de Grenoble, Francia. Control adaptable, robótica.

KUHLMANN RODRIGUEZ, FEDERICO. Doctor en ingeniería eléctrica. Universidad de Texas, Austin, E.U.A. Teoría de la información, diseño de redes para teleproceso, modelado y simulación de sistemas estocásticos.

NERI VELA, RODOLFO. Doctor en ingeniería eléctrica. Universidad de Birmingham, Inglaterra. Teoría de antenas y propagación, enlaces de microondas terrestres, comunicaciones por satélite.

REYES AVILA, LUIS. Doctor en ingeniería mecánica. Universidad Nacional Autónoma de México. Elasticidad, teoría del medio continuo.

ROMERO LOPEZ, ALEJANDRO. Doctor en ingeniería mecánica. Universidad de Munich-Alemania-UNAM. Radiación térmica, transferencia de calor, propiedades termofísicas de la materia.

SARMIENTO URUCHURTU, HECTOR G., Doctor en ingeniería eléctrica. Concordia Universidad, Canadá. Sistemas de potencia, diseño de redes eléctricas de distribución.

Medio tiempo

MURRAY LASSO, MARCO ANTONIO, Doctor en ingeniería eléctrica. Instituto Tecnológico de Massachussets, E.U.A. Simulación, educación asistida por computadora, sistemas.

Publicaciones

Sección de Ingeniería Eléctrica

BADAN A , NERI R , *Operaciones oceanográficas desde el espacio*, Ciencia y Desarrollo, CONACYT, México, enero.

BEGOVICH O , ORTEGA R , LOZANO R , FERNANDEZ G , *On the destabilizing effects of unmodeled plant delay in a simple adaptive controller: Simulation and local stability results*, Control-Theory and Advanced Technology, Japón, Vol. 3 No. 2, junio.

ESPINOSA L , R , *Sistemas eléctricos de distribución*, DEPFI, UNAM, junio.

GARCIA U F , *Parallel Processing on sequential decoding*, Memoria de la Conferencia AAECC-5, Mahon, Menorca, España, junio.

GARCIA U F , *Coding and decoding algorithms of RS codes executed on a M68000 microprocessor*, Springer-Verlag LNCS, París, Francia, 3J/C, octubre.

HE N , BUZO A , KUHLMANN F , *Propiedades de cuantización vectorial de mínimo error cuadrático medio para fuentes con ruido*, Memoria del XIII Congreso de la Academia Nacional de Ingeniería, Guadalajara, México, septiembre.

HERNANDEZ L , *Enlaces satélites en control distribuido*, Memoria de IEEE, MEXICON, Acapulco, México, octubre.

HERNANDEZ L , *Redes satélites con acceso por división de código*, Memoria del Congreso Nacional de Bases de Datos y Redes de Comunicación, México, octubre.

KELLY R , *Experiments on adaptive control of a DC motor*, Fifth Yale Workshop on Applications of Adaptive Systems Theory, New Haven, C T. E.U.A., mayo.

KELLY R , *A linear state feedback plus adaptive feedforward control for DC servomotors*, IEEE Industrial Electronics, VOL. IE-34, Nueva York, E.U.A., mayo.

KELLY R , *Continuos-time adaptive control of linear periodical systems*, First Int. Conf. on Industrial and Applied Mathematics, Paris, Francia, junio.

KELLY R , *Control adaptable continuo usando estimación de mínimos cuadrados*, VI Coloquio de la Asociación de México de Control Automático, México, septiembre.

KELLY R , ORTEGA R , CARELLI R , *Análisis de un controlador adaptable para robots manipuladores usando el enfoque entrada-salida*, VI Coloquio de AMCA, México, septiembre.

KELLY R , MUÑOZ H , *Aplicación de técnicas adaptables al control de robots manipuladores*, IEEE-MEXICON, Acapulco, México, octubre.

KELLY R , *Panorama sobre el control de robots manipuladores*, IEEE-MEXICON, Acapulco, México, octubre.

KUHLMANN F , BUCKLEW J A , *Piecewise uniform approximations to vector quantizers*, Proceedings of the 1987 International Conference on Acoustics Speech and Signal Processing, Dallas, Texas, E.U.A., abril.

KUHLMANN F , BUZO A , *Redes de computadoras: estado actual y perspectivas*, Memoria del 1er. Congreso Nacional de Redes y Bases de Datos (Conferencia plenaria), México, octubre.

LEPE F , BUZO A , KUHLMANN F , *Modelado y filtrado de señales digitales*, Memoria de IEEE México, octubre.

NERI R , *Resultados de los experimentos mexicanos en el orbitador Atlantis*, Ciencia y Desarrollo, CONACYT, México, enero.

NERI R , libro: *El Planeta Azul, Misión 61-B*, EDAMEX/CONACYT, México, marzo.

NERI R , libro: *El Pequeño Astronauta*, NUFALI/CONACYT, México, septiembre.

ORTEGA R , PRALY, TANG Y , *Direct adaptive tuning of robust controllers with guaranteed stability properties*, System & Control Letters, Vol. 8, mayo.

ORTEGA I , NERI R , *Transportación de nutrientes en microgravedad*, Ciencia y Desarrollo, CONACYT, México, marzo.

ORTEGA R , KELLY R , AMESTEGUI M , IBARRA J M , *Robustness enhancement of computed torque robot control via adaptive compensation*, Int. Conf. on Robotics and Automation, Raleigh, N C , E.U.A., abril.

ORTEGA R , TANG Y , *Theoretical results on robustness of direct adaptive controllers: A Survey*, 10th World Congress IFAC, Munich, Alemania, julio.

ORTEGA R , KELLY R , *On detuned model reference adaptive control: Decision and Control*, Los Angeles, CA, E.U.A., diciembre.

RODRIGUEZ R , NERI R , *Aplicación geológica de estereopares fotográficos de México tomados desde el Atlantis*, Ciencia y Desarrollo, CONACYT, México, enero.

SARMIENTO H , ESPINOSA R , BOLADO R , HERNANDEZ S , BASAVE A , PEREZ F , *Apuntes para el curso tutorial: Temas Selectos en Sistemas de Distribución*, Congreso IEEE, Ixtapa, México, diciembre.

TANG Y , ORTEGA R , KELLY R , *Adaptive control of a heat exchanger*, IEEE Control Systems Magazine, VOL. 4, No. 1, febrero.

TANG Y , ORTEGA R , *A robust feedforward adaptive control*, VI Coloquio de Control Automático, AMCA/CIEA-IPN, México, septiembre.

TANG Y , ORTEGA R , *Sintonización adaptable de sistemas lineales variables en el tiempo*, VI Coloquio de Control Automático AMCA/CIEA-IPN, México, septiembre.

TANG Y , ORTEGA R , *On the adaptive stabilization of linear time-varying systems*, IEEE Control and Decision Conference, Los Angeles, CA. E.U.A., diciembre.

VILCHES A , NERI R , *Germinación de semillas en microgravedad*, Ciencia y Desarrollo, CONACYT, México, marzo.

ZENG C , KUHLMANN F , BUZO A , *Algunos resultados nuevos de la teoría de la información de multi-usuario y sus aplicaciones*, Memoria del XIII Congreso de la Academia Nacional de Ingeniería, Guadalajara, México, septiembre.

Publicaciones Sección de Ingeniería Mecánica

- FERRER L , RIOS M DE J , VELAZQUEZ J , *Caracterización de la resina poliéster 8016 como material fotoelástico IV Reunión Nacional de Análisis de Esfuerzos*, Querétaro, México.
- FERRER L , DORANTES A , URIBE G , *Strain and Stress Fields on Shells of Complicated shape and Boundary Conditions*, 5th Interna International Modal Analysis Conference, Londres, Inglaterra, abril.
- FERRER L , VAZQUEZ R , VELAZQUEZ J , *Desarrollo a nivel nacional de una película fotosensible que permite la implementación de Método de Moré para análisis de desplazamientos, deformaciones y esfuerzos*, Memoria XIII Congreso ANIAC, Guadalajara, septiembre.
- GALLEGO M A , y CERVANTES DE G J , *Aparato para medir conductividad térmica en materiales metálicos*, Memoria XIII Congreso ANIAC, Guadalajara.
- GRINBERG A , Y GRINBERG D M , *Azul maya: Una hipótesis sobre su estabilidad fisicoquímica*, XI Coloquio Internacional de Mayistas, Campeche, México, agosto, (en prensa).
- GRINBERG A , ROBERTO T , *El efecto Bauschinger en el Acero Inoxidable ferrítico AISI 430*, IX Encuentro de Investigación Metalúrgica, Saltillo, México, septiembre.
- GRINBERG A , COLAS R , *Aspectos fractográficos e inestabilidad plástica en una aleación de aluminio termotratable*, Memoria del XIII Congreso de la Academia Nacional de Ingeniería, A.C. (ANIAC), Guadalajara, México, septiembre.
- GRINBERG A , GRINBERG D M , *Sobre la naturaleza físico-química de azul maya*. XX Mesa Redonda de la Sociedad Mexicana de Antropología. México, octubre (en prensa).
- GRINBERG D M GASCA A , *La soldadura: evidencia de su uso entre los tarascos*. Metalurgia moderna Vol. 3 No. 1, Buenos Aires, Argentina, enero-marzo.
- GRINBERG D M , *Dureza de temple en aceros nacionales al carbono para maquinaria*, Memoria del XIII Congreso de la Academia Nacional de Ingeniería, Guadalajara, México, agosto.
- GRINBERG D M , *Metalurgia prehispánica tarasca*, Memoria de la IX Inter-American Conference on Material Technology, Santiago, Chile, octubre.
- GRINBERG D M , GRINBERG A , *Selección de materiales para usos mecánicos*, Memoria de la IX Inter-American Conference on Material Technology, Santiago, Chile, octubre.
- GRINBERG D M , FRANCO F , BELTRAN O , *Técnicas de elaboración de las hachas y escoplos metálicos prehispánicos, I-Hachas de Tamán, San Luis Potosí*, XX Mesa Redonda de la Sociedad Mexicana de Antropología, México, octubre, (en prensa).
- GRINBERG D M , GASCA A , *¿Conocían los aborígenes mesoamericanos la soldadura?*, Primer Congreso Nacional de Soldadura en Morelia, México, noviembre.
- GRINBERG D M , FRANCO F , *Estudio de cuatro cascabeles de falso alambre provenientes de las excavaciones del tren subterráneo de la ciudad de México*, Antropología y Técnica No. 2, UNAM.

JAUREGUI J, *Aplicación de la distribución Weibull al Cálculo numérico de la confiabilidad de elementos de máquinas*, Memorias del XIII Congreso ANIAC, agosto.

JAUREGUI J, *Análisis de soldaduras usando el método del elemento finito*, Memoria de la II Reunión Nacional de Inv. Metalmeccánica.

MANERO B, E, CERVANTES de G, J, DURST F, *Aplicación del anemómetro laser-doppler al estudio de flujo bifásico con partículas en suspensión*, Memoria XIII Congreso ANIAC, Guadalajara, México, septiembre.

MENDEZ F, TREVIÑO C, LIÑAN A, *Combustión del carbón. Parte I: Etapas de calentamiento inerte e ignición. Parte II Etapas transitorias y de equilibrio, controladas por difusión*, Memoria XIII Congreso ANIAC, Guadalajara, México, septiembre.

REYES L, *Sobre la modelación mecánica, numérica y aproximación de una barra en extensión simple*, Memoria de la IV Reunión Nacional de Análisis de Esfuerzos, ITQ Querétaro, México, mayo.

REYES L, *Une justification du modèle dynamique de plaques élastiques avec inertie rotationnel*, Memoria del Primer Seminario Internacional de Conceptos Modernos y la Tribología en el Diseño de Maquinaria y los Procesos de Manufactura. Tecnológico de Querétaro, CIATEQ, México, septiembre.

RIESCO J M, ROMERO A, *Absorción de energía solar en cuerpos de agua*, Memoria XIII Congreso ANIAC, Guadalajara, México, septiembre.

RIESCO J M, GEITZ R, CERVANTES J, *Condensador de vapor enfriado por aire*, Memoria XIII Congreso ANIAC, Guadalajara, México, septiembre.

ROMERO A, *Numerical modelling of microgravity venting*. V International Conference on Numerical Methods in Thermal Problems, junio-julio, Montreal, Canadá, (sometido para su publicación en "Communications in Applied Numerical Methods").

ROMERO A, GALLEGOS, M A, *Descarga de recipientes cilíndricos a microgravedad y micropresión*, Memoria XIII Congreso ANIAC, Guadalajara, México, septiembre.

ROMERO A, MERTE Jr H, *Low Gravity Venting of R-11, A Model*, Proceedings, ASME Winter Annual Meeting, Boston, MA, E.U.A.

RUBIO C, CERVANTES J, GEITZ R, *Obtención de datos experimentales y diseño preliminar de un secador de cuero*, Memoria XIII Congreso ANIAC, Guadalajara, México, septiembre.

SANCHEZ S, CERVANTES DE G J, *Construcción y prueba de un lecho fluidizado por aire*, Memoria XIII Congreso ANIAC, Guadalajara, México, septiembre.

VALLEJO G, ROMERO A, *Distribución de temperatura mediante conducción inversa del reactor de Laguna Verde*. Memoria XIII Congreso ANIAC, Guadalajara, México, septiembre.

Convenios

CONACYT. Fortalecimiento al posgrado, ingeniería eléctrica. F. García Ugalde.

S.C.T., Monitoreo y detección de señales de R.F. F. Kuhlmann.

**I.I.E.-C.F.E. Fortalecimiento al posgrado, ingeniería electromecánica.
F. Kuhlmann, A. Buzo.**

CONACYT, Diseño mecánico. A. Romero.

CONACYT, Ciencias Sociales, Metalurgia prehispánica. D. K. de Grinberg.

**Convenio de colaboración SEMIP, Consejo de Recursos Minerales, SEMIP.
D. K. de Grinberg.**

CONACYT, Difusión maestría en metalurgia mecánica. A. Grinberg.

Artículos reproducidos

KELLY R, A Linear State Feedback Plus Adaptive Feedforward Control for DC Servomotors. IEEE Transactions on Industrial Electronics, Nueva York, mayo

GARCIA UGALDE F. J , MORELOS ZARAGOZA R. H, Design of a Viterbi decoder with microprocessor-based serial implementation, LNCS by Springer Verlag, Conference AAECC-4, Karlsruhe University, Alemania, noviembre 1987.

ROMERO L A, MERTE Jr H, Low gravity venting of R-11, a model, Proceedings ASME Winter Annual Meeting 87, Boston, Ma., diciembre 1987.

A Linear-State Feedback Plus Adaptive Feed-Forward Control for DC Servomotors

RAFAEL KELLY

Abstract—This paper proposes a linear-state feedback plus adaptive feed-forward control to control position for DC servomotors. The aim is to control DC servomotors submitted to inertia and Coulomb friction variations. Conditions for stability depending on the frequency richness of the reference input are presented. Experimental results show the improvement with respect to classical tachometric feedback.

I. INTRODUCTION

THE DC motors used in robotics and some industrial applications are submitted to frequent environment changes. As a consequence the motor model has time-varying parameters; therefore, the performance is poor when linear controllers are used.

Position control of DC servomotors is considered in this paper. It is assumed that the motor is submitted to inertia and/or Coulomb friction variations.

Adaptive control was motivated to treat plants with uncertain or time-varying parameters [1]. In this paper, an adaptive control for DC motors is proposed. This consists of a linear-state feedback plus an adaptive feed-forward. It is derived from an adaptive servo-controller proposed in [2]. Adaptive techniques for DC motor control have been considered before [4]–[8]. The proposed scheme differs in the adaptive control law that is used. Some advantages of the adaptive scheme introduced are the following: 1) the inclusion of the adaptation feed-forward on classical tachometric feedback requires simple modifications; 2) the adaptive feed-forward operates only in servo mode; and 3) in regulation mode, only the tachometric feedback is used.

Conditions that assure boundedness of all the signals in the adaptive system are presented in terms of frequency richness of the reference input.

Experiments were performed with the adaptive scheme on a DC servomotor submitted to Coulomb friction value changes. The results obtained show the improvement in position control with respect to classical tachometric feedback.

The paper is organized as follows: a DC motor model and the tachometric feedback are presented in Section II; Section III describes the tachometric feedback plus adaptive feed-forward control; the adaptive system analysis is performed in Section IV; experimental results on a DC motor with

tachometric feedback and the proposed control scheme are shown in Section V; and some conclusions are given in Section VI.

II. DC MOTOR MODEL AND TACHOMETRIC FEEDBACK

A classical description of an armature-controlled DC motor is given by the following set of equations [3]:

$$J\ddot{\theta}(t) + f\dot{\theta}(t) = K_i I(t) \quad (1a)$$

$$L\dot{I}(t) + RI(t) + e(t) = v(t) \quad (1b)$$

$$K_b\dot{\theta}(t) = e(t) \quad (1c)$$

where $v(t)$ is the input voltage which drives the angular position output $\theta(t)$, $I(t)$ is the motor current, J is the total moment of inertia reflected to the motor axis, and f is the friction torque. The constants K_i , K_b , R , and L are electrical characteristics of the motor.

For most purposes, the inductance effects are neglected ($L = 0$). The reduced model can be rewritten in a state form

$$\dot{\theta}(t) = A_1\theta(t) + b_1v(t) \quad (2a)$$

$$\theta(t) = c^T\theta(t) \quad (2b)$$

where

$$\theta(t) = [\theta(t) \ \dot{\theta}(t)]^T \quad (2c)$$

$$A_1 = \begin{bmatrix} 0 & 1 \\ 0 & -\frac{Rf + K_b K_i}{JR} \end{bmatrix}$$

$$b_1 = \begin{bmatrix} 0 & K_i \\ 0 & RJ \end{bmatrix}^T$$

$$c = [1 \ 0]^T \quad (2d)$$

The motor transfer function $G_{DC}(s)$ is given by

$$G_{DC}(s) = c^T(sI - A_1)^{-1}b_1 = \frac{K}{s(\tau s + 1)} \quad (3a)$$

where

$$K = \frac{K_i}{Rf + K_b K_i}$$

Manuscript received July 18, 1986; revised October 22, 1986.
The author is with DEPFI, the National University of Mexico, C. Universitaria, Apdo. Postal 70-256, 04510 México, D.F., Mexico.
IEEE Log Number 8613357.

$$\tau = \frac{J\Delta}{Rf + K_b K_i} . \quad (3b)$$

Notice that the first-order model (3) depends on the values of the inertia J and friction f .

A. Tachometric Feedback

The tachometric feedback is a commonly used strategy for DC motor position control. This corresponds to state feedback. The control law is given by

$$v(t) = [-k_p - k_v]\theta(t) + k_p\theta_r(t) \quad (4)$$

where k_p and k_v are the position and velocity gains. The reference position is $\theta_r(t)$. The closed-loop system composed of the motor model (2) and the tachometric feedback (4) is given by

$$\dot{\theta}(t) = A\theta(t) + b\theta_r(t) \quad (5a)$$

$$\theta(t) = C^T\theta(t) \quad (5b)$$

where

$$A = (A_1 + b_1[-k_p - k_v])$$

$$b = b_1 k_p \quad (5c)$$

whose transfer function $G(s)$ is

$$G(s) = c^T(sI - A)^{-1}b = \frac{\omega_n^2}{s^2 + 2\xi\omega_n + \omega_n^2} \quad (6a)$$

with

$$\omega_n^2 = \frac{Kk_p}{\tau}$$

$$\xi = \frac{1 + Kk_v}{2\tau} \sqrt{\frac{\tau}{Kk_p}} . \quad (6b)$$

When the motor characteristics K and τ are known, the designer parameters k_p and k_v may be chosen to assign arbitrary values to ω_n^2 and ξ . However, when the motor characteristics, which depend on the inertia and friction, are unknown or time varying, we do not assure good performance with a tachometric feedback. In the next section, an adaptive feed-forward will be incorporated to the tachometric feedback to treat this case.

III. TACHOMETRIC FEEDBACK PLUS ADAPTIVE FEED-FORWARD CONTROL

The control of plants whose parameters are unknown or time varying is a major objective of adaptive controllers [1]. Adaptive techniques for DC control have been considered before [4]–[8]. This paper differs in the adaptive control law used.

The proposed adaptive system, depicted in Fig. 1, is composed by the following.

1. DC Motor Model (2):

$$\dot{\theta}(t) = A_1\theta(t) + b_1v(t) \quad (7a)$$

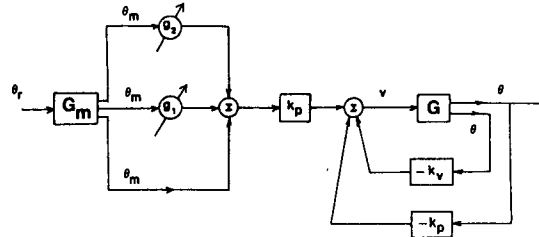


Fig. 1. Tachometric plus adaptive feed-forward control.

$$\theta(t) = c^T\theta(t) \quad (7b)$$

2. Reference Model:

$$\dot{\theta}_m(t) = A_m\theta_m(t) + b_m\theta_r(t) \quad (8a)$$

$$\theta_m(t) = c_m^T\theta_m(t) \quad (8b)$$

whose transfer function $G_m(s)$ is given by

$$G_m(s) = c_m^T(sI - A_m)^{-1}b_m = \frac{a_0}{s^2 + a_1s + a_0} \quad (8c)$$

The reference model (8) is the desired transfer function from the reference θ_r to position output θ .

3. Control Law:

$$v(t) = k_p[g^T(t)\psi(t) + \theta_m(t)] + [-k_p - k_v]\theta(t) \quad (9a)$$

with

$$g(t) = [g_1(t) \ g_2(t)]^T \quad (9b)$$

$$\psi(t) = [\phi_1(t) \ \phi_2(t)]^T = [s \ s^2]^T G_m(s)\theta_r(t) \quad (9c)$$

where $\psi(t)$ and $g(t)$ are the regressor and parameters vectors, respectively.

The control law (9) is composed of a tachometric feedback term and a feed-forward one ($g^T(t)\psi(t) + \theta_m(t)$). Notice that by choosing

$$g(t) = \left[\begin{array}{cc} 2\xi & 1 \\ \omega_n & \omega_n^2 \end{array} \right]^T \quad (10)$$

the closed-loop transfer function matches the model reference one (8c). However as ω_n and ξ depend on K and τ (6b), the latter being unknown by assumption, the constant vector (10) is unknown too. A constant-gain (gradient) [14], [15] adaptive law will be used to estimate vector (10).

4. Adaptation Law:

$$\dot{g}(t) = \gamma\psi(t)e(t) \quad (11)$$

where $e(t) = \theta_m(t) - \theta(t)$ and γ is a positive scalar, called adaptation gain. Equation (11) is used in most of adaptive systems to update the parameter vector $g(t)$ [14]–[16].

The adaptation gain γ is a design parameter which regulates the adaptation rates. However, small values are recommended to assure a stability margin [17]. In the next section, an analysis of the adaptive system in (7)–(11) will be presented.

IV. ANALYSIS

Some preliminaries will be presented before we analyze the adaptive system.

1. Definition [9]: The closed-loop adaptive system in (7)–(11) is said to be Bounded-Input Bounded-State (BIBS) stable, if uniformly bounded references (θ_r) give uniformly bounded states (θ and g).

In many works on adaptive systems, the following linear time-varying differential equation arises:

$$\frac{d}{dt} \begin{bmatrix} x \\ y \end{bmatrix} = \begin{bmatrix} \Lambda & \beta w(t)^T \\ -\gamma w(t) \delta^T & 0 \end{bmatrix} \begin{bmatrix} x \\ y \end{bmatrix} \quad (12)$$

Many properties of (12) have been reported in the literature [10]–[12]. We present a result on stability of (12) whose proof is given in [12].

2. Theorem 1 [12]: Consider (12). Assume that $w(t)$ is a vector of periodic functions of time, i.e., $w(t) = w(t + T)$ with $T \in \mathbb{R}_+$ and Fourier representation:

$$w(t) = \sum_{k=-\infty}^{\infty} \alpha_k e^{j\omega_k t}$$

$$\omega_k = \frac{2\pi k}{T}, \quad \alpha_k = \alpha_k^* \quad (13)$$

where α_k^* is the conjugate of the complex vector α_k . If

$$\sum_{k=-\infty}^{\infty} \operatorname{Re}[\delta^T(j\omega_k - \Lambda)^{-1} \beta] \cdot \operatorname{Re}\alpha_k \alpha_k^{*T} > 0 \quad (14)$$

then there exist $\gamma_0 > 0$ such that, for all $\gamma \in (0, \gamma_0]$ the zero solution of (12) is uniformly asymptotically stable (UAS).

Notice that the sufficient condition for UAS is trivially satisfied when $w(t)$ contains enough frequencies and $\operatorname{Re}[\delta^T(j\omega_k - \Lambda)^{-1} \beta] > 0$ for each ω_k .

A. Main Result

Using theorem 1, our main result given by the following proposition, can be proved.

1. Proposition: Consider the adaptive system in (7)–(11). Assume that the reference input θ_r is a periodic function of time, i.e.:

$$\theta_r(t) = \sum_{k=-\infty}^{\infty} \alpha_k e^{j\omega_k t} \quad (15)$$

if

$$\sum_{k=-\infty}^{\infty} |\alpha_k|^2 |G_m(j\omega_k)|^2 \operatorname{Re} G(j\omega_k) \begin{bmatrix} \omega_k^2 & 0 \\ 0 & \omega_k^4 \end{bmatrix} > 0. \quad (16)$$

Then, there exists $\gamma_0 > 0$ such that for all $\gamma \in (0, \gamma_0]$, the adaptive system is BIBS stable.

2. Proof: Adaptive system (7)–(11) can be described by a linear time-varying differential equation:

$$\begin{bmatrix} \dot{\theta}(t) \\ \dot{g}(t) \end{bmatrix} = \begin{bmatrix} A & b\psi(t)^T \\ -\gamma\psi(t)c^T & 0 \end{bmatrix} \begin{bmatrix} \theta(t) \\ g(t) \end{bmatrix} + \begin{bmatrix} b \\ \gamma\psi(t) \end{bmatrix} \theta_m(t). \quad (17)$$

From condition (15) and equation (9c) we have

$$\psi(t) = \begin{bmatrix} \phi_1(t) \\ \phi_2(t) \end{bmatrix} = \sum_{k=-\infty}^{\infty} \alpha_k \begin{bmatrix} j\omega_k \\ -\omega_k^2 \end{bmatrix} G_m(j\omega_k) e^{j\omega_k t}. \quad (18)$$

Applying theorem 1 to (17) and (18), we obtain the following condition for UAS of the homogeneous part of (17):

$$\sum_{k=-\infty}^{\infty} |\alpha_k|^2 |G_m(j\omega_k)|^2 \operatorname{Re}[c^T(j\omega_k I - A)^{-1} b]$$

$$\operatorname{Re} \begin{bmatrix} \omega_k^2 & -j\omega_k^2 \\ j\omega_k^3 & \omega_k^4 \end{bmatrix} > 0$$

or

$$\sum_{k=-\infty}^{\infty} |\alpha_k|^2 |G_m(j\psi_k)|^2 \operatorname{Re}[c^T(j\omega_k I - A)^{-1} b]$$

$$\begin{bmatrix} \omega_k^2 & 0 \\ 0 & \omega_k^4 \end{bmatrix} > 0.$$

The proof is completed from (6a) and the fact that UAS of a homogeneous linear equation implies BIBS stability of the nonhomogeneous linear equation (13).

When the adaptive system operates in regulation mode, i.e., the reference input $\theta_r(t)$ is a constant θ_{ro} , the adaptive system equation becomes asymptotically a linear invariant one:

$$\begin{bmatrix} \dot{\theta}(t) \\ \dot{g}(t) \end{bmatrix} = \begin{bmatrix} A & 0 \\ 0 & 0 \end{bmatrix} \begin{bmatrix} \theta(t) \\ g(t) \end{bmatrix} + \begin{bmatrix} b \\ 0 \end{bmatrix} \theta_{ro}. \quad (19)$$

Equation (19) means that the motor model is controlled by a tachometric feedback with θ_{ro} as the reference input.

V. EXPERIMENTAL RESULTS

In this section, some experimental results obtained on DC motor control are presented. The aim of the experiments is to compare the performances of tachometric feedback and tachometric feedback plus adaptive feed-forward control when the DC motor Coulomb friction is changed abruptly.

A DC motor with a permanent magnet was used in our experiments. Such motors are commonly used in robots and precision servos. Assuming a hypothetical linear armature-controlled motor model, the gain- and time-constant (3b) are $K = 247 \text{ rad} \cdot \text{s}^{-1} \cdot \text{V}^{-1}$ and $\tau = 150 \times 10^{-3} \text{ s}$. A magnetic break was used to change the Coulomb friction coefficient.

The control strategies were implemented in an analog computer. The reference input θ_r was a 55° amplitude square wave. Initially, the DC motor runs freely. At $t = 27 \text{ s}$, the magnetic break was set up. The goal was to have a second-order closed-loop system with low overshoot (see Fig. 2).

A. Tachometric Feedback

The first experiment was performed with the tachometric feedback control (4). The design parameters k_p and k_v were

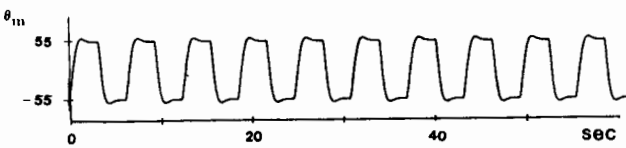


Fig. 2. Model reference output.

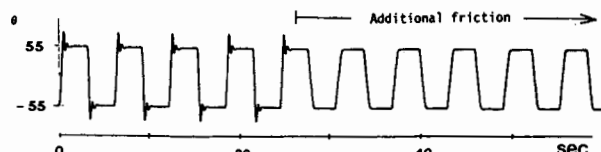


Fig. 3. Tachometric feedback control. Motor position output.

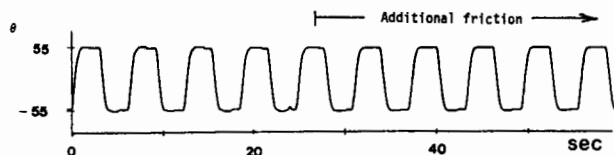
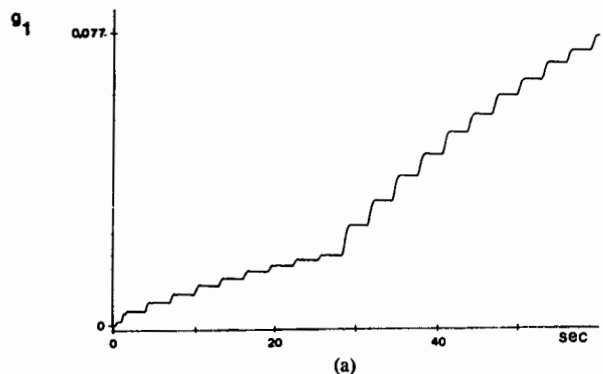
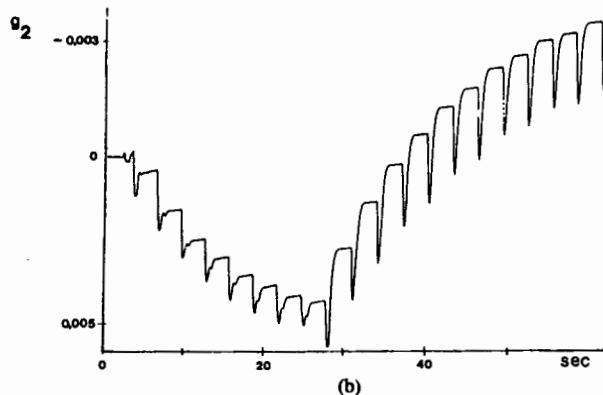


Fig. 4. Tachometric feedback plus adaptive feed-forward control. Motor position output.



(a)

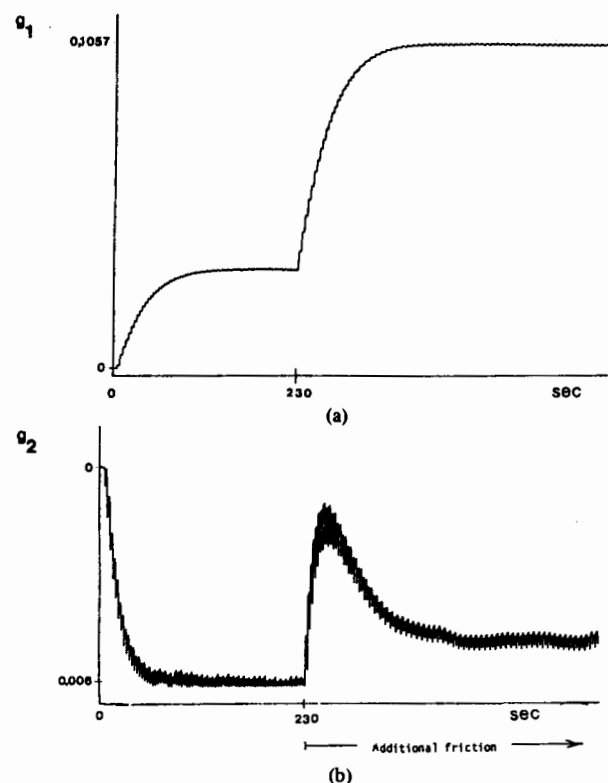
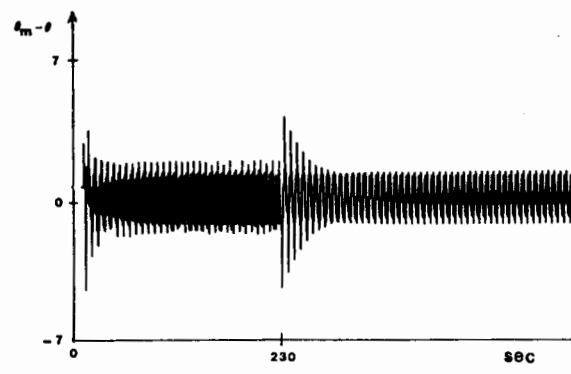


(b)

Fig. 5. (a) and (b) Adaptive parameters.

chosen to have a second-order closed-loop system with low overshoot. The design was carried considering magnetic break on the DC motor.

The experimental results are shown in Fig. 3. Clearly, bad performance is present when the DC motor runs without the magnetic break, that is until $t = 27$ s.

Fig. 6. (a) and (b) Adaptive parameters. Additional friction at $t = 230$ s.Fig. 7. Experimental error. Additional friction at $t = 230$ s.

B. Tachometric Feedback Plus Adaptive Feed-Forward

In this second experiment, the adaptive feed-forward was added to the tachometric feedback. The same values k_p and k_i of the first experiment were kept. The adaptive gain γ was 0.01.

The experimental results are shown in Figs. 4 and 5. The output position θ is depicted in Fig. 4. Compare it with Fig. 3. The improvement on a tachometric feedback is noticeable. Fig. 5 shows the evolution of adaptive parameters g_1 and g_2 .

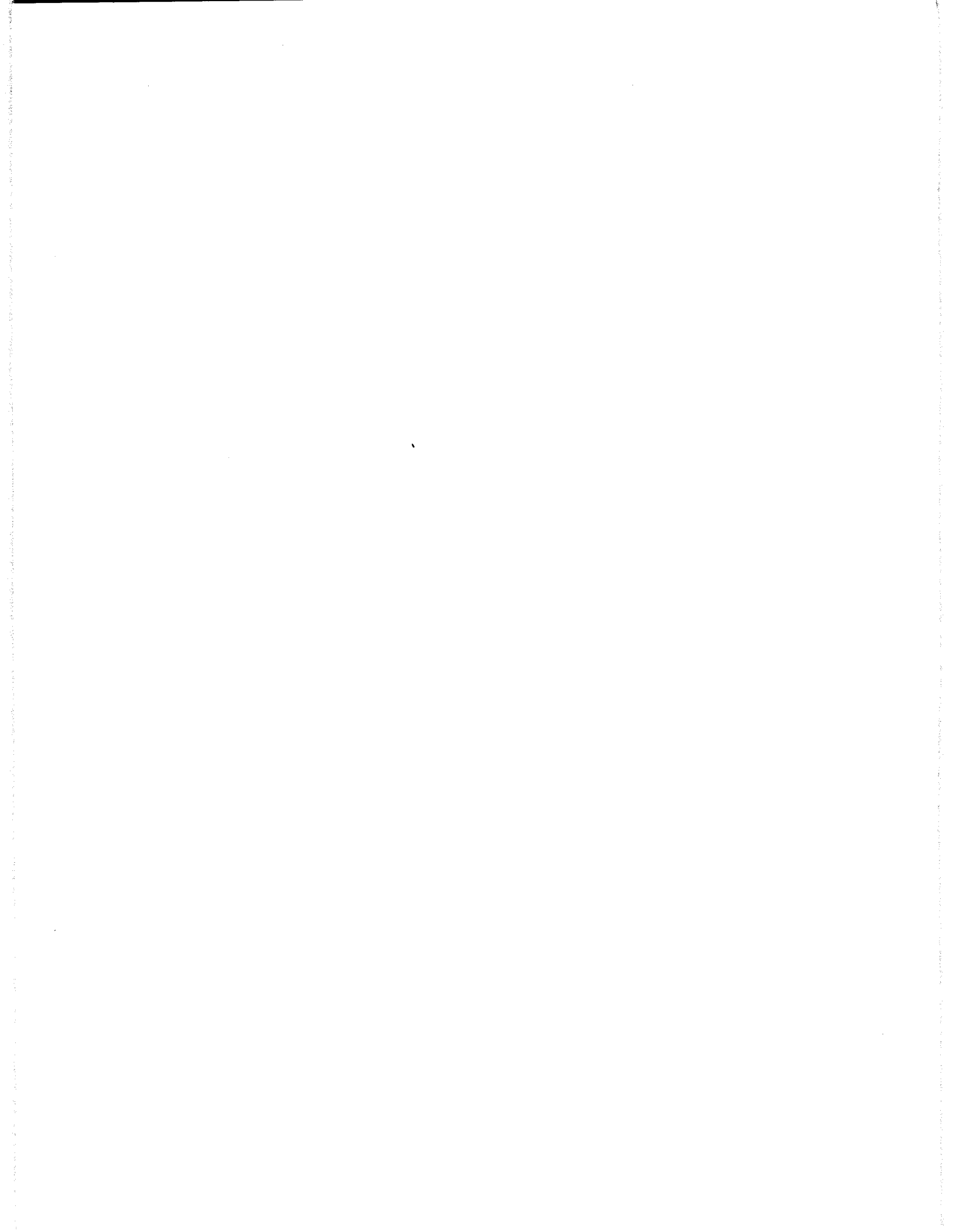
To show adaptive parameters convergence, the experiment was repeated but placing the magnetic break at $t = 230$ s. The result obtained, see Fig. 6, shows that after a transient, the adaptive parameters converge. The experimental error e , that is the error between the reference model output and motor output positions is depicted in Fig. 7.

VI. CONCLUSIONS

A linear-state feedback plus adaptive feed-forward control for DC motors has been proposed. The usefulness of this adaptive scheme appears when variations on inertia or friction are present. A stability analysis is also presented. Experimental results show improvement in precision with respect to classical tachometric feedback control.

REFERENCES

- [1] K. J. Astrom, "Theory and applications of adaptive control—A survey," *Automatica*, vol. 19, no. 5, 1983.
- [2] R. Ortega and R. Kelly, "On stability-instability conditions of a simple robust adaptive servo controller," presented at the 24th IEEE Conf. Decision, Control, Ft. Lauderdale, FL, Dec. 1985.
- [3] B. C. Kuo, *Automatic Control Systems*, 4th ed. Englewood Cliffs, NJ: Prentice-Hall, 1982.
- [4] I. D. Landau, "Model reference adaptive control systems for DC and AC drives," presented at the IEEE Industry, General Applications Group, Annu. Meeting, Detroit, MI, Oct. 1969.
- [5] J. W. Gilbart and G. C. Winston, "Adaptive compensation for an optical tracking telescope," *Automatica*, vol. 10, pp. 125–131, 1974.
- [6] C. D. Walrath, "Adaptive bearing friction compensation based on recent knowledge of dynamic friction," *Automatica*, vol. 20, no. 6, pp. 717–727, 1984.
- [7] S. D. Kraft and E. T. Wall, "Experimental microprocessor-based adaptive control system," *IEEE Contr. Syst. Magn.*, vol. CSM-6, no. 1, Feb. 1986.
- [8] C. Canudas, K. J. Astrom, and K. Braun, "Adaptive friction compensation in DC motor drives," presented at the IEEE Conf. Robotics Automation, San Francisco, CA, Apr. 1986.
- [9] B. D. Riedle and P. V. Kokotovic, "Stability analysis of an adaptive system with unmodelled dynamics," *Int. J. Contr.*, vol. 41, no. 2, 1985.
- [10] A. P. Morgan and K. S. Narendra, "On the uniform asymptotic stability of certain linear nonautonomous differential equations," *SIAM J. Contr. Optimiz.*, vol. 15, pp. 5–24, 1977.
- [11] B. D. O. Anderson, "Exponential stability of linear equations arising in adaptive identification," *IEEE Trans. Automat. Contr.*, vol. AC-22, pp. 83–88, 1977.
- [12] B. D. Riedle and P. V. Kokotovic, "A stability-instability boundary for disturbance-free slow adaptation with unmodeled dynamics," *IEEE Trans. Automat. Contr.*, vol. AC-30, no. 5, Oct. 1985.
- [13] J. K. Hale, *Ordinary Differential Equations*. Molaban, FL: Krieger, 1980.
- [14] K. S. Narendra and L. S. Valavani, "Direct and indirect model reference adaptive control," *Automatica*, vol. 15, pp. 653–664, 1979.
- [15] R. L. Kosut and C. R. Johnson, Jr., "An input-output view of robustness in adaptive control," *Automatica*, vol. 20, no. 5, pp. 569–582, 1984.
- [16] R. L. Kosut and B. Friedlander, "Robust adaptive control: Conditions for global stability," *IEEE Trans. Automat. Contr.*, vol. AC-30, no. 7, pp. 610–624, July 1985.
- [17] C. E. Rohrs, M. Athans, L. Valavani, and G. Stein, "Some design guidelines of discrete-time adaptive controllers," *Automatica*, vol. 20, no. 5, pp. 653–660, 1984.



F.J. García-Ugalde, R.H. Morelos-Zaragoza A.
División de Estudios de Posgrado
Facultad de Ingeniería, UNAM
P.A.P. 70-256 Cd. Universitaria
04510 MEXICO, D.F.

ABSTRACT

The purpose of this paper is to present the design of a Viterbi decoder, for moderate data transmission rates (hundreds of bits/sec), using a serial implementation based on a 16/32-bit microprocessor.

This design is only one experimental phase, of a final version which will be constructed to operate at a data transmission rate of 32 Kbits/sec, utilizing principally MECL and TTL integrated circuits.

1. INTRODUCTION

The Viterbi decoding algorithm has been widely used in communication systems. As a maximum-likelihood decoding scheme, it is the most practical forward-error-correcting (FEC) technique to achieve long coding gains in Gaussian channels, specifically in satellite channels [1].

In Mexico, with the place in orbit of the "Morelos" mexican domestic satellites, there is a plan to integrate data transmission, telephony and TV services with a KU-band earth stations network, throughout the country.

As a first step of this work, it started with the study of several channel coding schemes only for data transmission at a very low rate, which could be used in the above stations in its experimental phase. As a result of the present study it was stated that convolutional codes with Viterbi decoding give excellent performance, with relatively low complexity. Furthermore Viterbi decoders can easily be adapted to take advantage of soft demodulator decisions which will be a possibility in the final version of this error control system.

Only convolutional codes are considered here. Block codes which were common in early applications of digital space communication are so definitely inferior both in required complexity and in resulting performance that their further treatment is not worthwhile for the systems under consideration, other than as outer codes in a concatenated coding system.

2. GENERALITIES

To clarify some concepts used in this paper, we next present briefly the well known structure of convolutional codes and describe the Viterbi decoding algorithm, which is well known too [2]

Figure 1 shows a coder for a binary convolutional code of rate m/n and constraint length k . The information bits are fed in m -bit shifts. The code constraint length is defined as the number of information bits that influence the n output channel bits.

The shift register is initially loaded with zeros, after which the information message is coded, and followed by a "tail" of $k-m$ zeros to resynchronize the coder.

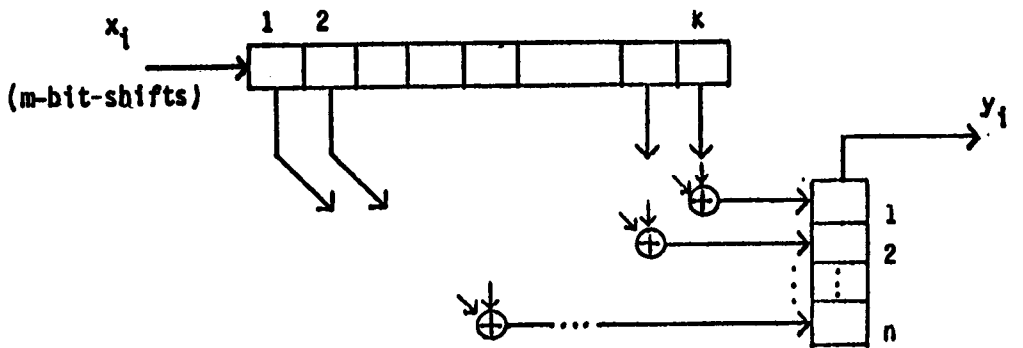


Fig. 1 A coder for a convolutional code of rate m/n and constraint length k .

To generate a n channel bits output, the coder considers m input information bits and the preceding $k-m$ information bits.

Hence the memory of the coder is $k-m$. Since the coder is a lineal and time-invariant circuit, its state is given by the contents of the $k-m$ memory elements and together with the m input bits uniquely specify the output bits.

The structure of a binary convolutional code allow us to draw the output bit sequence using a trellis diagram shown in Fig. 2., for the $1/2$ -rate $k=3$ code. The trellis diagram is a transition diagram between the $2^{(k-m)}$ states of the coder. The branches indicate the state transition due to an input bit. Conventionally, a "zero" input results on an upper branch, whereas a "one" input results on a lower branch. The output is indicated above the corresponding branch.

The Viterbi decoding algorithm takes advantage of the repetitive structure of the trellis diagram.

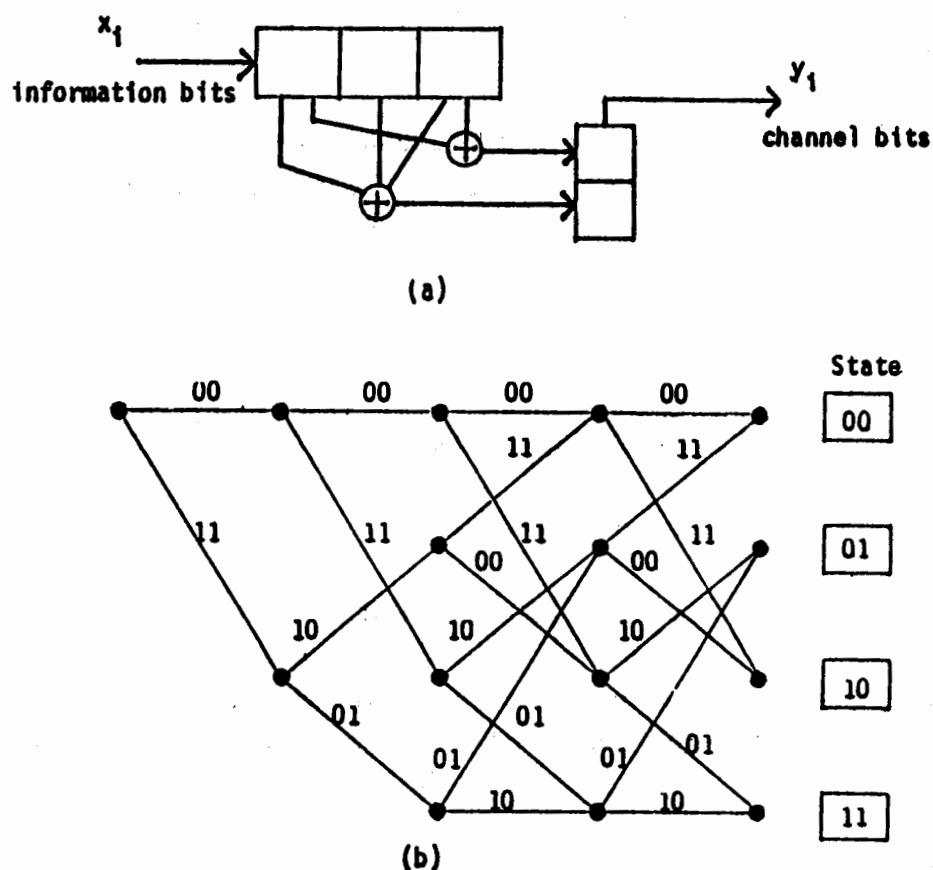


Fig. 2 (a) Coder for the convolutional code of rate $1/2$ and constraint lenght $k=3$.
 (b) Trellis diagram.

From the trellis diagram we observe that it has a repetitive structure after $k-m$ consecutive bits.

The Viterbi decoder computes the distance to the received path of each of 2^m paths that arrive to a given state, and selects that path with maximum-likelihood, eliminating all other paths. This procedure is done for each state, in a given trellis depth. This is known as a decoding step. See Fig. 3 for the block diagram of such algorithm.

When eliminating the less likely paths that arrive to a state, the Viterbi decoder does not reject branches that might be part of the transmitted code path.

To compare paths entering a given state, we use the path-likelihood function given in [3]

$$P(\bar{z}|\bar{y}^{(m)}) \quad (1)$$

where \bar{z} is the total received path and $\bar{y}^{(m)}$ is one of the possible transmitted paths.

Let us consider the binary symmetric channel (BSC). The difference between the N -bit \bar{z} , and $\bar{y}^{(m)}$ paths is d_m bits (where d_m is the Hamming distance). The probability of $\bar{y}^{(m)}$ being transformed into \bar{z} is given by:

$$P(\bar{z}|\bar{y}^{(m)}) = p^{d_m} (1-p)^{N-d_m} \quad (2)$$

where p is the BSC transition probability.

Using a log-likelihood function we have:

$$\log [P(\bar{z}|\bar{y}^{(m)})] = -d_m \log [(1-p)/p] + N \log (1-p) \quad (3)$$

it is clear from (3) that in order to minimize the error probability in a BSC, we must choose the code path with minimum Hamming distance from the received path.

As for the memory required to store the history of the selected paths in each state (survivors); it has been shown [3] that the $2^{(k-m)}$ survivor paths tend to be equal in the preceding levels of the trellis, approximately $5k$ levels away from the present level (for 1/2-rate codes).

Therefore, the amount of memory required is about $5k \cdot 2^{(k-m)}$ bits, in addition to the one needed to store the distance of the survivor paths, which is of $5 \cdot 2^{(k-m)}$ bits for 1/2-rate codes.

This path memory truncation, results on avoiding the tail of the paths and permits a continuous operation, with negligible degradation in performance.

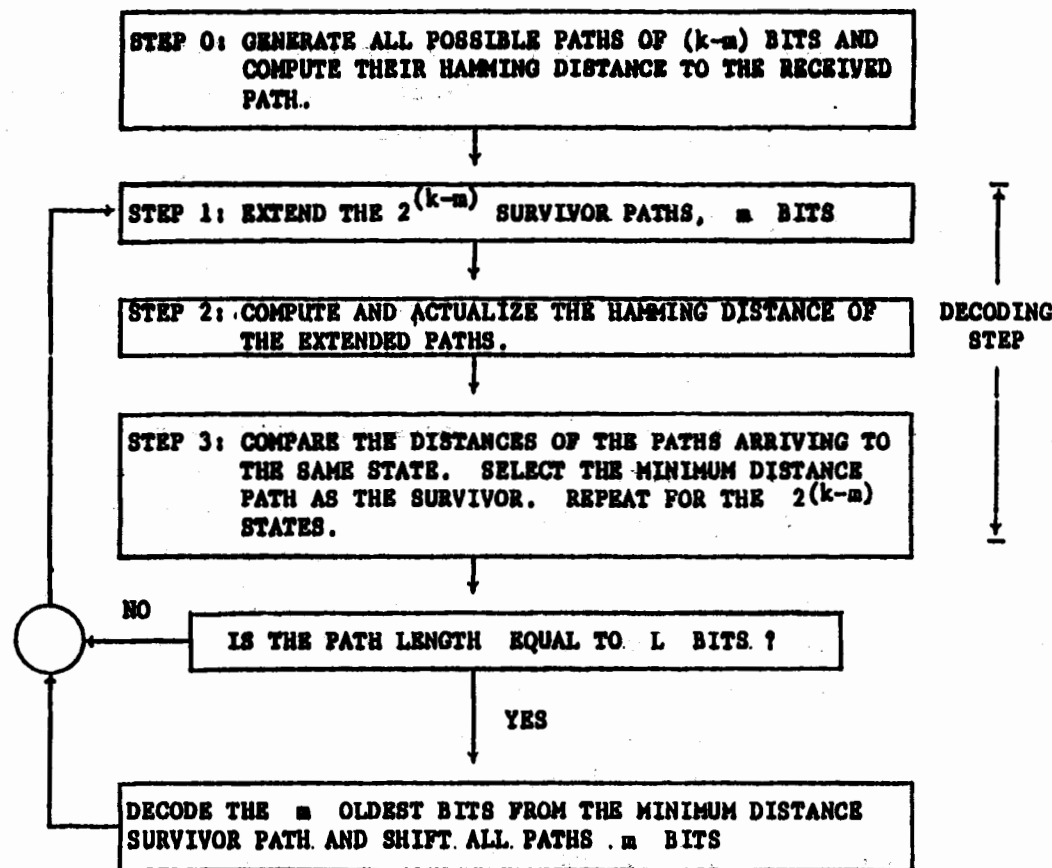


Fig. 3 Block diagram of the Viterbi decoding algorithm. The decoding lenght is L bits. k bits constraint lenght and m/n-rate code.

3. CONVOLUTIONAL CODE SELECTED

A 1×10^{-7} bit error rate (BER) corresponding to a theoretical 7.3 dB energy per bit-to-noise ratio (E_b/No) (not includes 0.5 dB margin), is one of the requirements for KU-band data link. In order to accomplish this, a 1/2-rate $k=7$ convolutional code was selected using a hard-decision Viterbi decoder. The code generators are those obtained by

Odenwalder in [4], whose generator coefficients are $171, 133|_8 = 1111001, 1011011$. These code generators were chosen to minimize the bit probability of error at large E_b/N_0 ratios, which is the range of E_b/N_0 's used here. These yields a code with a minimum free distance of 10.

In this version with hard-decisions, there is no need neither to compute more complicated likelihood functions, nor to use soft-decisions (usually of 3 bits) from the demodulator.

The choice of a rate-1/2 code allow us to use the availability of moderate bandwidth expansion, due to power limitation in the satellite. This rate also reduces significantly the decoder complexity, and we can exploit the fact that from this scheme, higher codes rates could be obtained with punctured codes [5]

As for decoder's architecture two approximations were analyzed: parallel implementation and serial implementation.

With parallel implementation, $2^{(k-m)}$ processing units are needed for each state (each unit performing the operations of likelihood metric computation, comparing, adding, selecting and updating the survivor path). Utilizing principally MECL and TTL integrated circuits, this approach achieve very high data transmission rates (up to 10 Mbits/sec), at the cost of large number of logic and memory elements. This scheme is suitable for VLSI designs, obtaining a whole decoder in a single integrated circuit, whereas traditional electronic designs would require excessive space and would be impractical.

On the other hand, the serial approach permits significant saving in the number of devices required, but at the cost of reducing transmission rate (several hundreds of Kbits/sec). In this kind of scheme a single processing unit is required for all the $2^{(k-m)}$ survivor paths. In this version we consider the serial implementation as the most suitable for satellite data communications, because the present needs in data transmission rates are not to large -32 Kbits/sec using a SCPC/QPSK/FDMA system, only for data transmission, nor telephony and TV services neither-, and also because it is a scheme easy to build with reduce number of components

This type of architecture also has the advantage of being able to increase data transmission rate, by means of hybrid configuration - serial

and parallel-, in which several processing units share the decoding task. The progressive decrement in both price and size of electronic devices is a valid justification of our selection.

4. PRESENT VERSION OF THE DESIGN

This preliminary version has been designed around a microprocessor for two reasons principally:

- * To measure the performance of a relatively recent 16/32-bit microprocessor in this kind of applications.
- * To test the correct operation of the decoding system accordingly to our theoretical calculations. Awaiting for the final version.

The key element in a serial implementation is the processing unit (PU), because it must perform the Viterbi decoding algorithm efficiently. High operation speed; efficiency in data addressing and transfer; and good instruction set are desirable features of the PU.

In the last few years more powerful microprocessors have appeared, among which we find Motorola's MC68000 series that present all characteristics mentioned above. We therefore select a microprocessor-based serial implementation using the MC68000 family.

Being the microprocessor the heart of the design, the architecture must also consider three basic elements: a read-only-memory (ROM), to store the set of instructions to implement the Viterbi decoding algorithm; a random-access-memory (RAM), for the path distance storage and the path memory; and the input (from the demodulator) and output (to the user) interface circuits. The block diagram of the proposed design is shown in Fig. 4.

The system was constructed as a single board utilizing an Educational Computer Board (ECB) from Motorola systems. The principal features of this board are:

- * A 16/32-bit microprocessor in its version of 10 MHz and N-channel technology.
- * 32K bytes of dynamic RAM
- * 8K bytes of system monitor ROM
- * Two serial I/O ports with RS-232C interface. Baud rate, strap selectable: 110, 150, 300, 600, 1200, 2400, 4800, 9600.

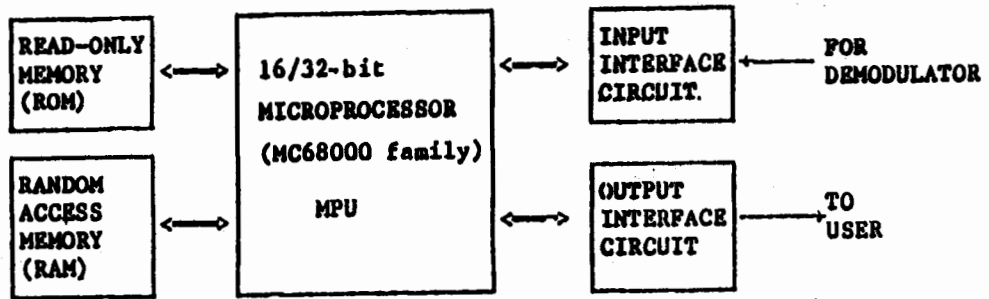


Fig. 4 Block diagram of the microprocessor-based serial implementation of Viterbi Decoder.

Therefore our choice is software implementation, using an assembler language program executed by the microprocessor. In a straight-forward implementation two sets of registers are used, containing the survivor paths and their distances, for two consecutive levels in the trellis diagram. After each decoding step, the microprocessor updates and transfers the contents of the registers sets.

The disadvantage of this procedure, as was pointed out in [6], is the reading and rewriting of long registers (32 bits in our case), which requires two buffers. Nevertheless, the speed and power of the new generation of microprocessors allow us to design without considering any restriction in memory size. Therefore, there is no need to remove double buffers for transfers between registers.

A very important feature of any decoder is the synchronization of symbols. In our case, branch synchronization is achieved by detecting when received data contain excessive number of errors. Whenever this happens, it can easily be detected by the microprocessor who shifts one bit the received branches.

To update and store the path distances we take advantage of the trellis structure, to determine state transitions [7]

The basic trellis structure is used when comparing and updating both the survivor paths and their distances, as shown in Fig. 5.

In each decoding step, a new bit is added at the beginning of each path, and the oldest bit of the minimum distance path is decoded. In our

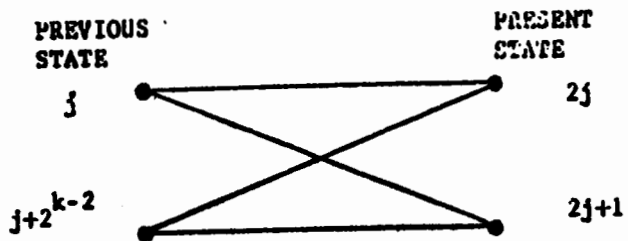


Fig. 5 Basic structure of the trellis diagram.

design, a path history of 31 bits was taken, and the 32nd bit is the decoded bit. At the end of the decoding step, the content of the registers is shifted right one bit.

With this implementation, nevertheless we could obtain a maximum data transmission rate of 495 bits/sec, which is about ten times faster than a previous work in which the Viterbi algorithm has been implemented on a Zilog Z-80 microcomputer for the (2,1)8 convolutional code [8].

Until now our design has been tested in our laboratories with a simulated channel and data transmission; the results are very encouraging, but much research still has to be done for this application, in particular with respect to the real data transmission rate (32 Kbits/sec), which will be obtained only with a logic design utilizing MECL and TTL integrated circuits or a VLSI realization.

5. CONCLUSION

In summary, a 16/32-bit microprocessor-based serial implementation of a Viterbi decoder has been designed. The scheme has the advantage of requiring a reduced number of components, and permits an increased data transmission rate by a serial-parallel approach. This work was done in the context of the design of KU-band earth stations for data transmission, telephony and TV services, using the mexican domestic satellites systems.

Nevertheless this design constitutes only one experimental phase of the final version, and although we could obtain a data transmission rate of 495 bits/sec which is about ten times faster than a previous work, it is not satisfactory for our present requirements which are of 32 Kbits/

sec for the data transmission link. To obtain this final rate a definitive version will be constructed utilizing MECL and TTL integrated circuits or a VLSI realization.

For the reason that has been explained in paragraph 1, only convolutional codes have been considered here, a 1/2-rate k=7 convolutional code has been chosen to accomplish one of the requirements for KU-band data link. To choose the code generators we have been highly influenced by the CCSDS recommendation for telemetry channel coding.

ACKNOWLEDGMENT

The authors are very grateful to the referees for valuable comments.

References

- [1] J.A. Heller and I.M. Jacobs, "Viterbi Decoding for Satellite and Space Communications", IEEE Trans. on Commun. Technol., Vol. COM-19, No. 5, Oct. 1971, pp. 835-848.
- [2] A.J. Viterbi, "Error Bounds for Convolutional Codes and an Asymptotically Optimum Decoding Algorithm", IEEE Trans. Inf. Theory, Vol. IT-13, Apr. 1967, pp. 260-269.
- [3] A.J. Viterbi, "Convolutional Codes and Their Performance in Communication Systems", IEEE Trans. on Commun. Technol., Vol. COM-19, No. 5, Oct. 1971, pp. 751-772.
- [4] J.P. Odenwalder, "Optimal Decoding of Convolutional Codes", Ph.D. thesis, University of California, Los Angeles, 1970.
- [5] J.B. Cain, G.C. Clark Jr., and J.M. Geist, "Punctured Convolutional Codes of rate $(n-1)/n$ and Simplified Maximum Likelihood Decoding", IEEE Trans. Inf. Theory, Vol. IT-25, No. 1, Jan. 1979, pp. 97-100.
- [6] C.M. Rader, "Memory Management in Viterbi Decoder", IEEE Trans. on Commun., Vol. COM-29, No. 9, Sep. 1981. pp. 1399-1401.
- [7] G.D. Forney, "The Viterbi Algorithm", Proc. IEEE, Vol. 61, Mar. 1973, pp. 268-277.
- [8] H.H. Ma, "The Multiple Stack Algorithm Implemented on a Zilog Z-80 Microcomputer", IEEE Trans. on Commun., Vol. COM-28, No. 11, Nov. 1980, pp. 1876-1882.

LOW GRAVITY VENTING OF R-11, A MODEL

ALEJANDRO F. ROMERO-LÓPEZ
PROFESSOR
DIVISIÓN DE ESTUDIOS DE POSGRADO
FACULTAD DE INGENIERÍA, UNAM
04510 MÉXICO, D.F.

HERMAN MERTE, JR.
PROFESSOR
DEPT. OF MECHANICAL ENGINEERING AND
APPLIED MECHANICS
THE UNIVERSITY OF MICHIGAN
ANN ARBOR, MI 48109-2125

ABSTRACT

An algorithm is presented to predict transient discharge phenomena at micropressure and microgravity of cylindrical vessels during short periods of time. The present work improves previous ones (1,2,3), with the incorporation to the analysis of the heat transfer phenomenon from the vessel wall, when the system is depressed to vacuum conditions, causing a transient temperature variation at the vapor-liquid interface and specially at the triple line boundary (solid-liquid-vapor), where an instantaneous evaporation results from the transient phenomena caused by the discharge process.

NOMENCLATURE

a	Thermal difusivity	m^2/s
A	Area	m^2
C_d	Discharge Coefficient	--
C_v	Specific Heat at constant volume	J/kg K
h	Specific enthalpy	J/kg
h_{fg}	Evaporation enthalpy	J/kg
k	Thermal conductivity	W/m K
m	Mass	kg
P	Pressure	Pa
q	heat flux	W/m^2
R	Ideal gas constant	J/kg K
T	Temperature	K
t	Time	s
U	Internal Energy	J
u	Specific internal energy	J/kg

Greek Symbols

δ	Penetration depth	m
γ	Specific heat ratio	C_p/C_v
<u>Subindexes</u>		
d	Discharge	
e	Exit	
i	Interface, inner	
l	Liquid	
p	Pressure	
sat	Saturation conditions	
v	Volume, vapor	
w	Wall	

INTRODUCTION

The thermodynamic behaviour of fluids bound by cylindrical pressure vessels, that are momentarily depressed to space conditions, is very important for propulsion purposes. The objective of this paper is to predict the internal pressure response of a saturated liquid-vapor closed system when depressed to vacuum for very short periods of time. The figure 1 depicts a schematic typical vessel showing a hemispherical liquid vapor interface, which is assumed in accordance to previous experimental results (2). In figure 2 a schematic of the model is presented with a flat interface but with a hemispherical surface area. The surface is a two-phase mixture within the vessel at equilibrium under saturation conditions for a vapor pressure P_v just before the discharge $t < 0$. Once the discharge is started $t > 0$, the interface temperature drops due to depressurization of the vapor space and the temperature gradient so created induces a heat transfer both from the liquid and the solid wall, which evaporates part of the fluid in a natural tendency to restore the system to its previous conditions. The analysis consists of applying the governing equations to three different control volumes (open systems), namely the vapor, vapor-liquid interface and the liquid. The

PROCEEDINGS, ASME WINTER ANNUAL MEETING '87, BOSTON, MA
DEC. 13-20, 1987

vapor is considered a uniform control volume (Fig. 3), where mass and energy conservation equations are applied. At the liquid-vapor interface, the energy equation is applied to determine the interfacial mass transfer, considering transfer of heat from the vessel wall. Finally, for the short periods of time under consideration and very small penetration depths, the liquid is considered as a semi-infinite solid boundary.

ANALYSIS

Due to the very short periods of discharge, the following assumptions hold for the model:

1. The vapor internal energy varies only with time.
2. Changes of the ullage volume are negligible.
3. The interfacial surface area remains constant.
4. The mass of liquid is very large compared to the evaporated mass.
5. All of the vapor properties are uniform and defined by T_v and P_v .
6. The interface temperature is $T_i = T_{sat}$ at P_v .
7. Initially the liquid-vapor mixture is saturated $T_i = T_{sat} = P_v$.
8. Very short periods of time are modelled ($t \leq 3s$).

A different model should be considered for longer test times. For the vapor region of the vessel:

$$\frac{d}{dt}(m_v u_v) + \dot{m}_e h_e - \dot{m}_i h_i = 0 \quad (1)$$

The time variation of mass within the vapor volume is then given by the continuity conditions:

$$\frac{dm}{dt} v = \dot{m}_i - \dot{m}_e \quad (2)$$

Whereas, for the liquid region:

$$\frac{dm}{dt} l = -\dot{m}_i \quad (3)$$

The mass variation rate in (1) is substituted by the continuity conditions (2), and the derivative of the internal energy is then evaluated as a function of the quality parameter:

$$u_v = u_f + x u_{fg} \quad (4)$$

Substituting (2) and (4) in (1):

$$m(d(u_f + x u_{fg})/dt) + \dot{m}_i (u_v - h_i) + \dot{m}_e (h_v - u_v) = 0 \quad (5)$$

The mass flow rate through the vent \dot{m}_e is calculated by using a classical choked flow analysis (4), and therefore the exiting mass flow rate is only a function of upstream vapor properties, or:

$$\dot{m}_e = P_v C_d A_T K_d (R T)^{-1/2} \quad (6)$$

Where C_d is an experimentally determined coefficient, and

$$K_d = \frac{\gamma^{1/2}}{2} \frac{2}{(\gamma+1)^{(\gamma+1)}} \quad (7)$$

Since no heat transfer to the vapor is assumed, all energy transferred to the interface by conduction in the liquid and from the wall, results in vaporization in this region:

$$\dot{m}_i h_{fg} = q_1 + q_w \quad (8)$$

If the liquid is regarded as a semi-infinite solid with one-dimensional heat conduction, then:

$$q_1 = -k_1 A_1 \left[\frac{dT}{dx} \right]_{x=0} \quad (9)$$

and for the vessel wall:

$$q_w = -k_w A_w \left[\frac{dT}{dr} \right]_{r=r_1} \quad (10)$$

then, solving for \dot{m}_i :

$$\dot{m}_i = \frac{-k_1 A_1 \left[\frac{dT}{dx} \right]_{x=0} - k_w A_w \left[\frac{dT}{dr} \right]_{r=r_1}}{h_{fg}} \quad (11)$$

A_1 is the hemispherical surface area and A_w is the radial conduction area of the vessel wall.

Therefore, in order to determine the interfacial mass transfer, two temperature gradients are required, one in the liquid and the other one at the vessel wall.

In view of the previous assumptions, the temperature distribution for the liquid region can be obtained from the solution of:

$$\left(\frac{\partial T}{\partial t} \right) = a \frac{\partial^2 T}{\partial x^2} \quad (12)$$

Initially the system is at the uniform temperature T_0 , with a sudden increase to the value T_i , therefore the initial and boundary conditions are given by:

$$T(x,0) = T_0$$

$$T(0,t) = T_i$$

$$T(\infty,t) = T_0$$

The solution to equation (12) is then given by:

$$\frac{\theta(x,t)}{\theta_i} = erfc \left(\frac{x}{2(at)^{1/2}} \right) \quad (13)$$

where: $\theta(x,t) = T(x,t) - T_0$

$$\theta_i = T_i - T_0$$

The equation for the temperature distribution at the vessel wall is given by:

$$\frac{\partial T}{\partial t} = a \frac{1}{r} \frac{\partial}{\partial r} [r \frac{\partial T}{\partial r}] \quad (14)$$

For the following initial and boundary conditions:

$$\theta(r,0) = 0 = T(r,0) - T_0$$

$$\theta(R,t) = \theta_i = T(R,t) - T_0 = T_i - T_0$$

$$\theta(\infty,t) = 0 = T(\infty,t) - T_0$$

The solution is given by:

$$\frac{\theta(r,t)}{\theta_1} = \frac{(r/R - 1)(at/R^2)^{1/2}}{4(r/R)^{3/2}} \operatorname{erfc} \left[\frac{r}{2(at/R^2)^{1/2}} \right] \quad (15)$$

The temperature at the interface is equal to the saturation temperature corresponding to the discharge pressure P_d . Since there is a

pressure change associated with the discharge, then a time varying boundary condition $T_1(t)$ is introduced in the solution. By using Duhammel's superposition integral (5):

$$\theta(z,t) = \theta_1(0)\psi(z,t) + \int_0^t \psi(z,t-s) \frac{d\theta_1(s)}{ds} ds \quad (16)$$

where:

$$\theta(z,t) = T(x,t) - T_0 \quad \text{or} \quad \theta(z,t) = T(r,z) - T_0$$

$$\theta_1(t) = T_1(t) - T_0$$

Then for the liquid:

$$\phi(z,t) = \frac{\theta(x,t)}{\theta_1(t)} \quad (17)$$

and for the vessel wall:

$$(z,t) = \frac{\theta(z,t)}{\theta_1(t)} \quad (18)$$

$\psi(z,t)$ is the unsteady temperature resulting from a stepwise unit increase in surface temperature, in relation to a uniform initial temperature. The new temperature $\psi(x,t)$, may be expressed in terms of (x,t) as:

$$\psi(z,t) = \begin{cases} 0, & t < s \\ (z,t-s), & t > s \end{cases} \quad (19)$$

The solution for (z,t) comes from equation (13) for the liquid and from equation (15) for the vessel wall, therefore:

$$\psi(z,t) = \frac{\theta(x,t)}{\theta_1} = \operatorname{erfc} \left[\frac{x}{2(at)^{1/2}} \right] \quad (20)$$

The other expression is rather large and cumbersome:

$$(z,t) = \frac{\theta(r,t)}{\theta_1} = \frac{(r/R-1)(at/R^2)^{1/2}}{4(r/R)^{3/2}}$$

$$\cdot \operatorname{erfc} \left[\frac{r/R - 1}{2(at/R^2)^{1/2}} \right] +$$

$$+ \frac{7(r/R)^2 + 2(r/R) - 9}{32(r/R)^{5/2}} (at/R^2)^{1/2} \operatorname{erfc} \left[\frac{r/R - 1}{2(at/R^2)^{1/2}} \right] \quad (21)$$

The solution of the system of equations has to be carried in discrete time steps, so that the discrete form of equation (16) is:

$$\theta(x,t) = \theta_1(0)\psi(z,t) + \sum_{m=1}^n \Delta\theta_{im} \cdot \psi(z,t-s_m) \quad (22)$$

where:

$$\Delta\theta_{im} = \theta_i(s_m) - \theta_i(s_{m-1}) \quad (23)$$

n , is the total number of time steps, m is a running time index $1 \leq m \leq n$ and $\Delta\theta_{im}$, is the increment change in surface temperature.

The solution given by (22) does not imply a precise temperature gradient, therefore a third order polynomial with a least squares fit is imposed:

$$T_1 = A + Bx + Cx^2 + Dx^3 \quad (24)$$

$$T_w = A_1 + B_1r + C_1r^2 + D_1r^3$$

The respective temperature gradients for liquid and wall are then given by:

$$\frac{dT}{dx}|_{x=0} = B \quad (25)$$

$$\frac{dT}{dr}|_{r=R} = B_1 + 2C_1R + 3D_1R^2$$

To evaluate the eight constants in the equations (24), a penetration depth was estimated for which the dimensionless temperature change given by equations (13) and (15) is 95% for the first case, or substituting in the Gauss' error function:

$$0.95 = \operatorname{erfc} \left[\frac{8}{2(at)^{1/2}} \right] \quad (26)$$

$$= 1.39 (2(at)^{1/2})$$

Equations (26) refer only to the liquid interface, a similar procedure is carried on for equation (15), only the estimation is attained by means of a digital computer.

The actual penetration depth will be somewhat less than the value predicted by (26) on the computer estimation for equation (15) due to the transient change in surface temperature. Six equally spaced nodes are taken to be within this penetration depth, a schematic diagram is shown in Fig. 3. The same procedure is accomplished with the vessel wall.

RESULTS AND CONCLUSIONS

The present paper takes into account the evaporation phenomenon at the triple interface boundary (solid-liquid-vapor), resulting from the transfer of heat from the vessel wall to the liquid, which was ignored in a previous model (1). This results in a larger evaporation and a pressure drop lower than the one predicted in previous models (1), (2) and some experimental results (6). Figure 4 shows transient vapor and saturation temperatures, while Fig. 5 shows the general system transient response (pressure, flow rate and interface evaporation).

The computer algorithm was also modified in order to incorporate the previous effects, a flow diagram is included in Fig. 6.

The pressure drop predicted by previous models was too large compared to experimental conditions. This model predicts values closer to the experimental data and even improves a previous one (1), due to the consideration of

the evaporation along the triple interline at the solid boundary of the vessel. Heat transfer from the container walls was only considered at the triple boundary for a depth twice as large as the one considered as "penetration depth", for increasing of the evaporation effect.

The results are summarized in table 1 and some runs are shown, where a comparation is made with two previous models (1), (2). Inspection of the table can lead to the conclusion that this model better approaches previously reported experimental data (6). Thermodynamic data for performance evaluation and for the evaluation of thermodynamic properties, were taken from reference (7).

REFERENCES

1. M.D. Mc. Broom and H. Merte, Jr., "Modeling of Zero Gravity Venting", internal communication, The University of Michigan, Ann Arbor, MI, 1984.
2. T.L. Labus, J.C. Aydelott, "Zero Gravity Venting of three Refrigerants", NASA TN D-7480, 1974.
3. A. F. Romero, "Numerical Modeling of Microgravity Venting", Proceedings of the Fifth International Conference on Numerical Methods in Thermal Problems, Montreal, PQ, June 29-July 3, 1987, in print.
4. White, F.M. Fluid Mechanics, Mc Graw Hill Book Co., Inc., N.Y., 1979, pp. 530-1.
5. Aspaci, V.S. Conduction Heat Transfer, Addison Wesley Publishing Co., 1966, pp. 307-14.
6. T.L. Labus, J.C. Aydelott & R.F. Lacovic, "Low Gravity Venting of Refrigerant 11" NASA TM X-2479, Feb. 1972.
7. Anonymous, "Thermodynamic Properties of Freon 11", E.I. Dupont de Nemours & Co., 1965.

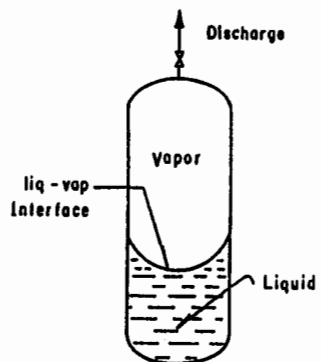


Fig 1 Typical pressure vessel

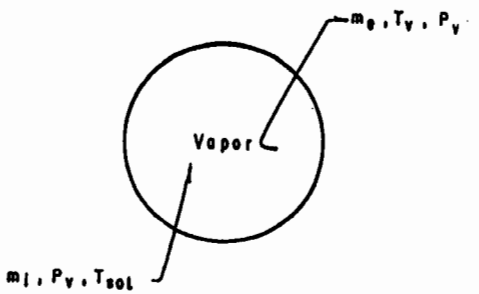


Fig 2a Vapor region

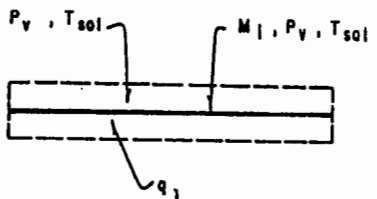


Fig 2b Two - phase region

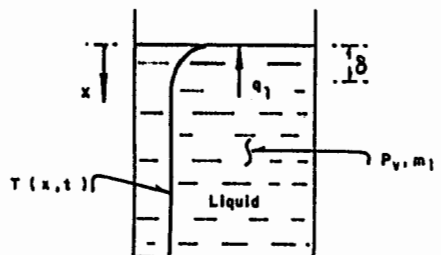


Fig 3 Liquid region and penetration depth

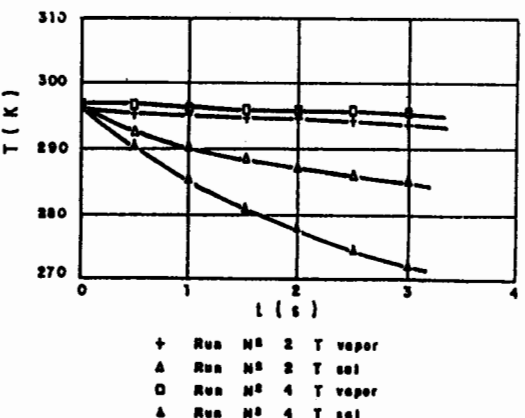


Fig 4 Transient vapor and saturation temperatures

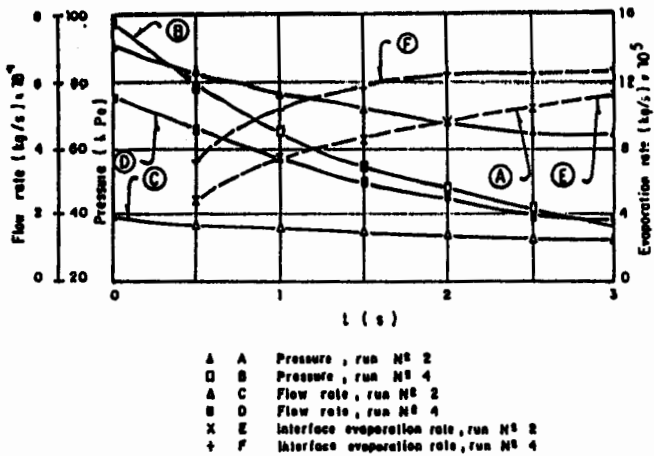


Fig. 5 Transient system response

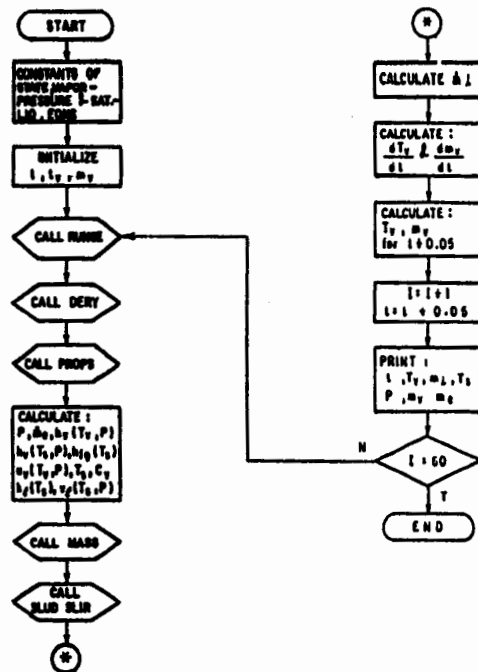
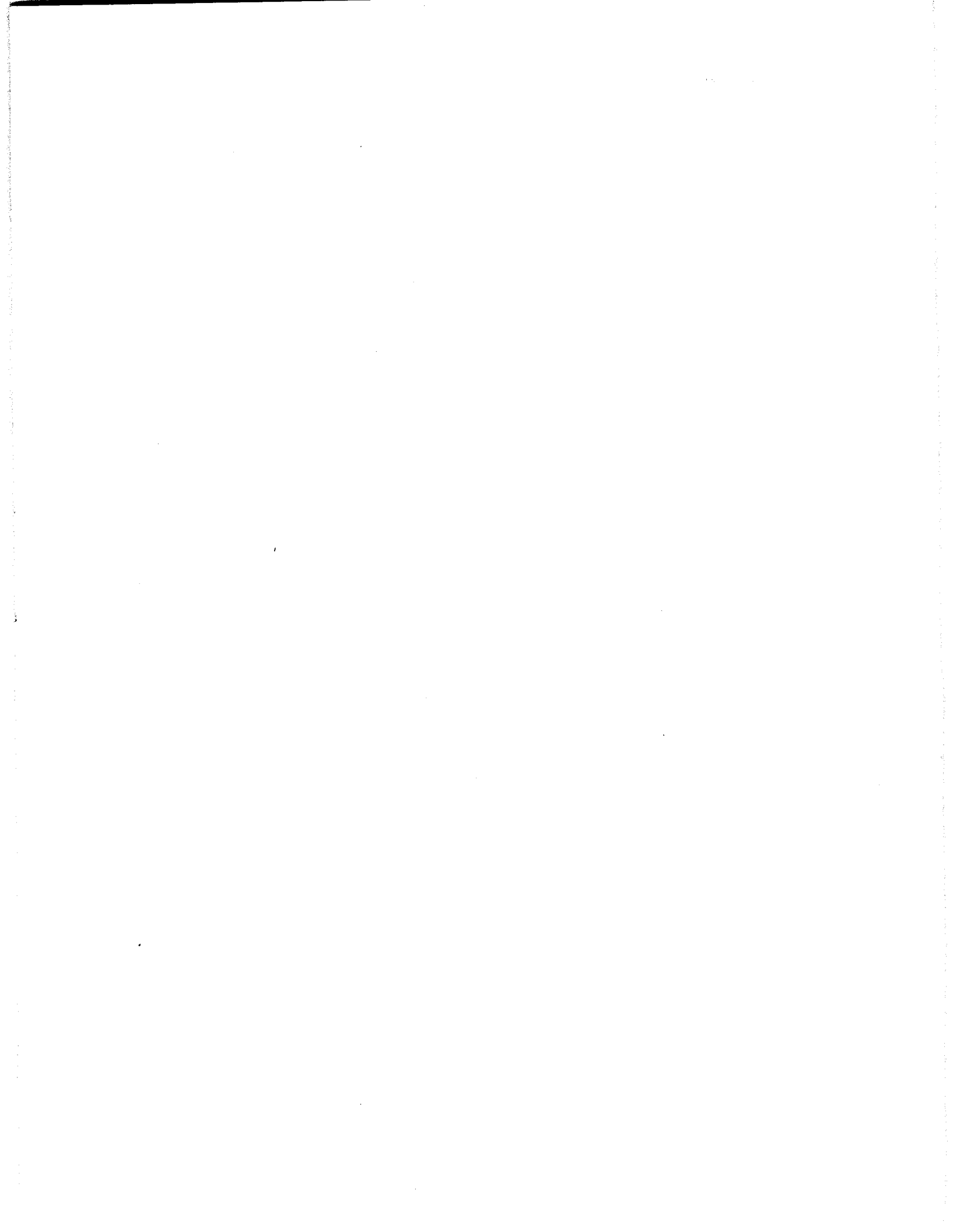


Fig. 6 ALGORITHM FLOW DIAGRAM

TABLE 1: SUMMARY OF PARAMETERS AND RESULTS

Run test.	Initial vapor volume m ³	Nozzle diameter m	Discharge Coefficient Cd	Initial vapor pressure kPa	Initial vapor temperature °K	Prel. experimental pressure (6) kPa	Present model final pressure kPa	Final pressure previous model 2 (1) kPa	Final "measured" previous model 1 (2) kPa	Dimensionless analytical pressure drop	Dimensionless experimental pressure drop
No.											
1	1.93x10 ⁻⁴	0.406x10 ⁻³	0.64	89.6	294.3	86.2	85.7	85.2	81.6	0.043	0.037
2	2.01	0.889	0.69	87.9	294.7	70.3	67.4	64.4	56.3	0.23	0.20
3	1.90	1.07	0.86	91.0	293.7	60.7	50.2	46.8	40.7	0.44	0.33
4	1.93	1.32	0.875	97.2	296.5	53.8	42.1	37.9	29.4	0.58	0.44
5	1.93	1.93	0.77	101.0	295.4	41.4	27.4	21.4	13.1	0.72	0.59



**Departamento de
Ingeniería de Recursos
del Subsuelo**

Programas Académicos

JEFE
Dr. Heber Cinco Ley

COORDINADORES DE SECCION

ENERGETICA
Dr. Fernando Rodríguez de la Garza

EXPLORACION DE RECURSOS ENERGETICOS DEL SUBSUELO
M. en C. Juan M. Brandi Purata

PETROLERA
Dr. Jesús Rivera Rodríguez

ESPECIALIZACION

Recuperación secundaria en yacimientos petroleros
Reparación y terminación de pozos
Seguridad de instalaciones industriales de explotación petrolera
Perforación de pozos petroleros
Métodos artificiales de producción

MAESTRIA

Exploración de recursos energéticos del subsuelo
Con opciones en:
Geotermia
Uranio
Petróleo
Carbón

Energética

Con opciones en:
Planeación, evaluación energética y uso eficiente de energía.
Energía nuclear
Desarrollo de nuevas fuentes de energía (Energía solar, Biomasa, Geotermia, Eólica, etc.)

Yacimientos
Perforación
Desarrollo de campos
Producción

DOCTORADO
Petrolera

Profesores de Carrera y Líneas de Investigación

Tiempo completo

BARCELO DUARTE, JAIME. Doctor en ingeniería. Universidad de Texas, Austin, E.U.A. Ambientes sedimentarios.

BRANDI PURATA, JUAN M. Maestro en ciencias. Universidad de Pierre et Marie Curie, París, Francia. Procesamiento de datos potenciales aplicados en exploración petrolera.

CINCO LEY, HEBER. Doctor en ingeniería petrolera. Universidad de Stanford, California, E.U.A. Caracterización de yacimientos, análisis de pruebas de presión, yacimientos fracturados.

RIVERA RODRIGUEZ, JESUS. Doctor en ingeniería petrolera. Universidad de Stanford, California, E.U.A. Recuperación secundaria y mejorada, ingeniería de yacimientos geotérmicos, fenómenos de transferencia.

RODRIGUEZ DE LA GARZA, FERNANDO. Doctor en ingeniería petrolera. Universidad de Stanford, California, E.U.A. Yacimientos fracturados, caracterización de yacimientos.

RUIZ CASTELLANOS, MARIO. Doctor en geología. Universidad de Dallas, Texas, E.U.A. Geocronología.

SAMANIEGO VERDUZCO, FERNANDO. Doctor en ingeniería petrolera. Universidad de Stanford, California, E.U.A., Caracterización de yacimientos, análisis de pruebas de presión, yacimientos fracturados.

Medio tiempo

CAUDILLO MARQUEZ, PEDRO. Maestro en ingeniería. Universidad Nacional Autónoma de México. Técnicas de perforación de pozos, modelos matemáticos de perforación.

CHAVEZ PEREZ, SERGIO. Maestro en ciencias. Universidad de Carolina del Sur, E.U.A. Modelado sísmico.

GARCIA GOMEZ, FRANCISCO. Maestro en ingeniería. Universidad Nacional Autónoma de México. Procesos de recuperación mejorada.

SANCHEZ ARREDONDO, FRANCISCO. Maestro en ingeniería. Universidad Nacional Autónoma de México. Flujo multifásico en tuberías, instalaciones superficiales.

ZAMORA GUERRERO, DAVID H. Maestro en ciencias. Universidad de Stanford, California, E.U.A. Geomatemáticas.

ARREOLA M A , RODRIGUEZ DE LA G F , *Efecto de la geometría de la malla sobre la estabilidad de un simulador numérico*, XXV Congreso Nacional del AIPM, Oaxaca, México, abril.

CINCO L H , *Behavior of Fractured Wells in Double Porosity Reservoirs*, Dowell-Schlumberger, Tulsa, Oklahoma, E.U.A., diciembre.

CINCO L H , *Well Test Analysis*, Notas de curso, diciembre.

CINCO L H , RAMEY Jr. H J, SAMANIEGO V F, RODRIGUEZ DE LA G F, *Behavior of Wells with Low-Conductivity Vertical Fractures*, Society of Petroleum Engineers SPE 16776, Dallas, Tex, E.U.A., septiembre.

Publicaciones Sección de Ingeniería Petrolera

DOMINGUEZ V G, *Costos de descubrimiento y desarrollo de reservas probadas de hidrocarburos en México, 1965-1984*, Revista de Ingeniería Petrolera, Vol. XXVII, México, febrero.

HERRERA R J , RODRIGUEZ DE LA G F, *Aplicaciones prácticas del simulador CONIMP-FRAC: Estudios de conificación de los pozos Bellota IA, Chuc 101 y Abkatún 20*, XXV Congreso del AIPM, Oaxaca, México, abril.

RIVERA R J , RAMIREZ S J , RODRIGUEZ DE LA G F, *Parallel Fractures Model for Tracer Flow Through Geothermal Reservoirs-Preliminary Results*, Geothermal Workshop, Stanford, CA, E.U.A., enero.

RODRIGUEZ DE LA G., F., *Un simulador numérico del flujo multifásico hacia pozos naturalmente fracturados*, XXV Congreso Nacional del AIPM, Oaxaca, México, abril.

Sección de Ingeniería en Exploración de Recursos Energéticos del Subsuelo

BERTRAND C. C., *Geoquímica orgánica aplicada a la prospección petrolera (apuntes)* DEPFI, UNAM, noviembre.

BRANDI P J M, *Continuación analítica ascendente para perfiles usando la integral de Neuman*, Boletín de la Asociación Mexicana de Geofísicos, Vol. 25, México, enero-marzo.

BRANDI P J M, *Teoría del potencial aplicada a la exploración petrolera*, DEPFI, UNAM., (en proceso).

CASTAÑEDA P M, *Reseña sobre la evolución histórica de las reservas del carbón en México*, DEPFI, UNAM, agosto.

ORTEGA C R F, *Economía nuclear*, DEPFI, UNAM, agosto.

PADILLA S R, *Geotectónica (apuntes)* DEPFI, UNAM, junio.

PADILLA S R, *Geología estructural (apuntes)* DEPFI, UNAM, junio.

VERA O , TORRES R V, *Diagénesis de carbonatos*, DEPFI, UNAM, octubre.

Convenios

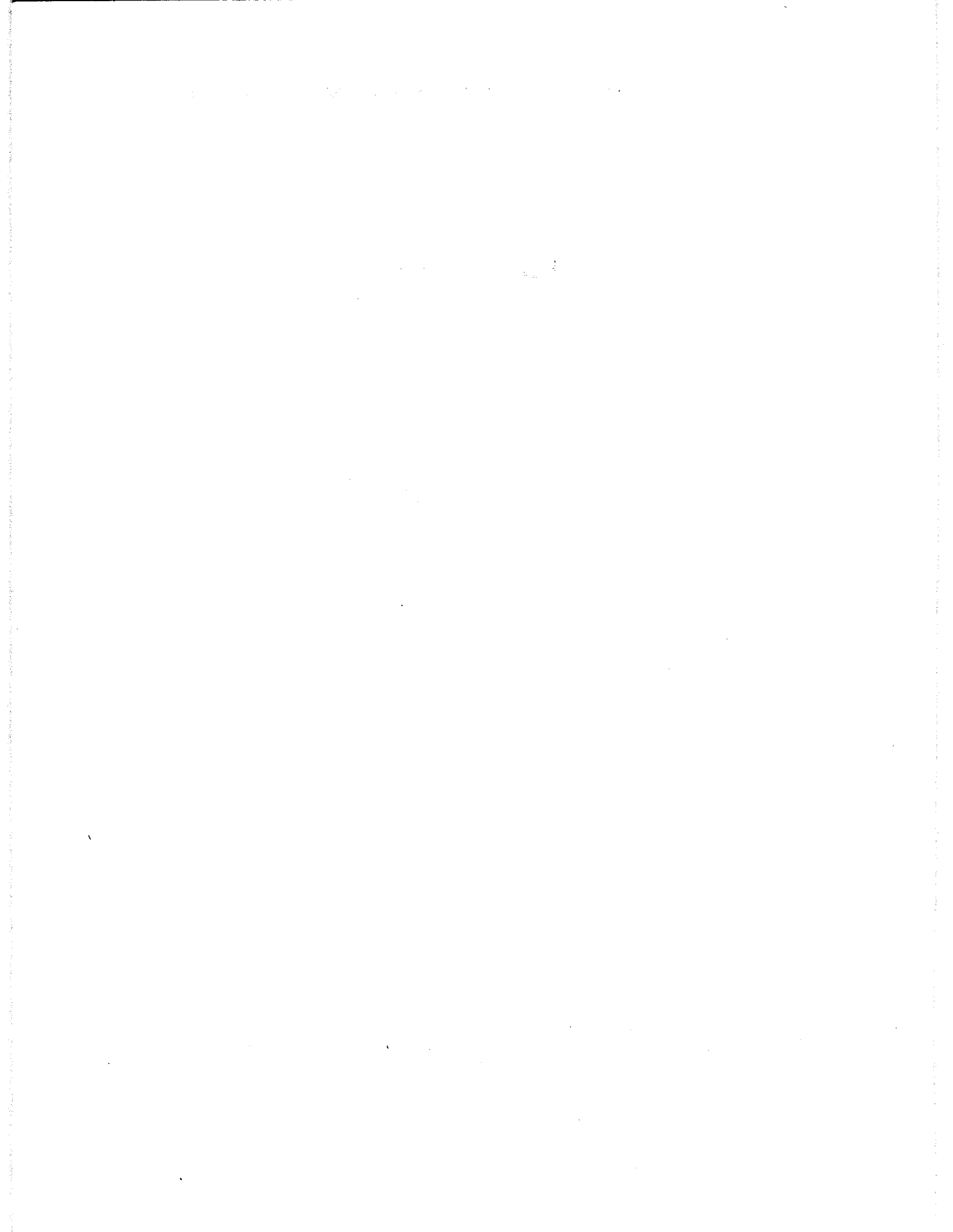
PEMEX-CIPM-IMP-UNAM. Convenio de colaboración para la superación académica de ingeniería petrolera.

UNAM-PEMEX-IMP. Convenio de colaboración para la superación académica en el área de ingeniería geológica y geofísica.

UNAM-PEMEX-IMP. Convenio de colaboración para implantar la especialización de seguridad en instituciones industriales de explotación petrolera.

Artículo reproducido

CINCO L H RAMEY Jr H J , SAMANIEGO V F , RODRIGUEZ DE
LA G F , *Behavior of Wells with Low Conductivity Vertical Fractures*,
Editorial Comitees of the Society of Petroleum Engineers, SPE, Dallas, Tex.,
E.U.A., septiembre.





SPE 16776

Behavior of Wells With Low-Conductivity Vertical Fractures

by H. Cinco-Ley, PEMEX and U. of Mexico; H.J. Ramey Jr., Stanford U.; F. Samaniego, PEMEX and U. of Mexico; and F. Rodriguez, IMP and U. of Mexico

SPE Members

Copyright 1987, Society of Petroleum Engineers

This paper was prepared for presentation at the 62nd Annual Technical Conference and Exhibition of the Society of Petroleum Engineers held in Dallas, TX September 27-30, 1987.

This paper was selected for presentation by an SPE Program Committee following review of information contained in an abstract submitted by the author(s). Contents of the paper, as presented, have not been reviewed by the Society of Petroleum Engineers and are subject to correction by the author(s). The material, as presented, does not necessarily reflect any position of the Society of Petroleum Engineers, its officers, or members. Papers presented at SPE meetings are subject to publication review by Editorial Committees of the Society of Petroleum Engineers. Permission to copy is restricted to an abstract of not more than 300 words. Illustrations may not be copied. The abstract should contain conspicuous acknowledgment of where and by whom the paper is presented. Write Publications Manager, SPE, P.O. Box 833836, Richardson, TX 75083-3836. Telex, 730989 SPEDAL.



ABSTRACT

This paper presents the transient pressure behavior for a well with a low conductivity vertical fracture, $(k_f b_f)_D \leq 0.1$; these cases include low $k_f b_f$ fractures, long fractures or wells in relatively high permeability formations.

It appears that this type of systems exhibits two flow periods only: bilinear flow and pseudo-radial flow. It is demonstrated that for these fracture conductivities the effective wellbore radius is given by $r_w^* = 0.28 (k_f b_f / k)$; that means that there is a maximum value of the effective wellbore radius achieved by hydraulic fracturing for a given value of $(k_f b_f / k)$.

A new single line type curve is presented for analysis of pressure transient tests.

INTRODUCTION

Evaluation of hydraulic fracturing has been attained successfully through the

analysis of pressure test in the last few years. These has been possible because of the introduction of new models for fractured wells such as the finite conductivity fracture¹⁻⁴ and the fractured well in a layered reservoir^{5,6} among others.

The use of the pressure derivative⁷⁻⁹ has enhanced the interpretation reducing the uniqueness problem when the type curve matching procedure is applied. Pressure transient analysis allows the estimation of fracture half length x_f , fracture conductivity $k_f b_f$, fracture skin s_f and effective wellbore radius r_w^* .

It has been established⁴ that a well intersected by a fully-penetrating finite conductivity vertical fracture exhibits in general the following flow periods. Initially, there is a fracture linear flow; after a transition flow period may or may not exhibit a bilinear flow period might develop. Eventually, in all cases, the system reaches a pseudoradial flow period.

All cases published in the literature consider fracture conductivities equal to or higher than 0.1. Solutions for smaller fracture conductivities are not reliable when obtained through the use of finite difference simulators mainly because for these cases, pressure gradients within the fracture become extremely high as fluid is approaching the wellbore.

The purpose of this work is to present the pressure behavior and welltest interpretation for a well with a vertical fracture of conductivity less than or equal to 0.1. In addition a discussion on the maximum effective wellbore radius is included. A new single line type curve is introduced for this kind of systems.

MAXIMUM EFFECTIVE WELLBORE RADIUS

One way to express the well conditions (damage or stimulation) is by using the concept of effective wellbore radius. Prats¹⁰ showed that a well intersected by an infinite conductivity vertical fracture exhibits an effective wellbore radius equal to half of a wing length of the fracture; in addition he presented a graph of effective well radius versus the relative fracture conductivity parameter $a = \pi k x_f / 2k_f b_f$ (See Figure 1). Here the parameter a is inversely proportional to the conductivity of the fracture. It can be observed in this figure that as the fracture conductivity decreases the r'_w/x_f ratio decreases.

As Raghavan¹¹ pointed out, the effective wellbore radius ratio r'_w/x_f varies linearly with the parameter a in a log-log graph for large values of a (Low conductivity fractures), the straight line representing this relationship has a

slope equal to minus one. That means that, for these conditions, r'_w/x_f can be expressed as:

$$\frac{r'_w}{x_f} = \frac{c}{a} \quad (1)$$

$$\text{or } \frac{r'_w}{x_f} = \frac{2C_1 k_f b_f}{\pi k x_f} \quad (1-a)$$

$$\text{or } r'_w = \frac{2C_1 k_f b_f}{\pi k} \quad (1-b)$$

where C is a constant. In Eq. 1-b we observe that the effective wellbore radius appears to be independent of fracture length.

In Appendix it is shown by using a model proposed by Muskat, for naturally fractured reservoirs, that the effective wellbore radius for a well intersected by a low conductivity vertical fracture ($(k_f b_f)_D = k_f b_f / k x_f \leq 0.1$) is given by:

$$r'_w = 0.2807 \frac{k_f b_f}{k} \quad (2)$$

this means, as indicated by Raghavan¹¹, that given $k_f b_f / k$ there is a critical fracture length beyond which there is no increase in well productivity for practical purposes. The critical fracture length is:

$$(x_f)_{\text{critical}} = 10 \frac{k_f b_f}{k} \quad (3)$$

From Eqs. 2 and 3,

$$r'_w \approx \frac{(x_f)_{\text{critical}}}{35} \quad (4)$$

SPE 16776

CINCO-LEY, H., RAMEY, H.J., JR., SAMANIEGO, F. AND RODRIGUEZ, F.

FRACTURE FLUX DISTRIBUTION

The distribution of low rate q_f towards a vertical fracture depends on both time and dimensionless fracture conductivity³. However, it has been shown that the flux distribution along the fracture becomes stabilized during the pseudoradial flow and appears to be identical to the flux distribution under steady state flow conditions.

For low conductivity fractures q_f can be calculated from the model presented by Muskat¹². The fractional flow rate q/q_w within the fracture at a distance x from the wellbore is given by:

$$\frac{q(x)}{q_w} = \frac{2\cosh \epsilon}{\pi} \int_0^{\infty} \frac{\sin xz/b_f \sinh z/2}{z \sinh(z/z + \epsilon)} dz \quad (5)$$

where $\epsilon = \tanh \frac{k}{k_f b_f}$. Hence the fracture flux distribution in dimensionless form $q_f(x)/q_w$ for large values of x_D can be approximated by:

$$\frac{q_f(x)}{q_w} = - \frac{\partial q(x)/q_w}{\partial x} \approx \frac{(k_f b_f)_D^3}{\pi x_D^2} - \frac{3(k_f b_f)_D^3}{2\pi x_D^4} \quad (6)$$

here $(k_f b_f)_D$ is the dimensionless fracture conductivity. Figure 3 shows a graph of q_f/q_w versus x_D for several values of fracture conductivity. As this parameter decreases the contribution of flow from regions far from the wellbore becomes negligible; that implies that most of the fluid goes into the fracture near the wellbore. For instance for a conductivity $(k_f b_f)_D = 0.01$ about 99 percent of the fluid produced at the wellbore enters

the fracture within one third of the fracture length close to the wellbore.

It can be shown that reservoirs with low conductivity fractures exhibit radial flow pressure distribution (logarithmic variation) along the fracture beyond a distance equal to $(x_f)^{critical}$; this fact indicate that fracture tips do not affect the behavior of the system under these conditions.

TRANSIENT PRESSURE BEHAVIOR

At early time, a well intersected by a finite conductivity vertical fracture exhibits the bilinear flow behavior⁴; that is:

$$P_{WD} = \frac{2.45}{\sqrt{(k_f b_f)_D}} t_D^{1/2} x_f \quad (7)$$

the bilinear flow period occurs when

$$t_{Debf} \approx \frac{0.1}{(k_f b_f)_D^2} \text{ for } (k_f b_f)_D \geq 3$$

$$t_{Debf} \approx 0.0205[(k_f b_f)_D - 1.5]^{-1.53}$$

$$\text{for } 1.6 \leq (k_f b_f)_D \leq 3$$

and

$$t_{Debf} \approx \left[\frac{4.55}{\sqrt{(k_f b_f)_D}} - 2.5 \right]^{-4} \quad (8)$$

A good approximation for the time of end of the bilinear flow, for low conductivity fractures $((k_f b_f)_D \leq 0.1)$, is

*Definition of dimensionless variables is given in Nomenclature.

$$t_{Debf} \approx 0.0023(k_f b_f)^2 D$$

(9)

$$\text{or } (t_{Dr'_w})_{ebf} \approx 0.03 \quad (10)$$

In terms of dimensionless time based on effective wellbore radius, the pressure behavior during the bilinear flow period is:

$$P_{WD} = 1.298 \cdot t_{Dr'_w}^{\frac{1}{2}} \quad (11)$$

According to this equation a single curve gives the behavior of the system during the bilinear flow in terms of r'_w .

As mentioned before, the fracture tips do not affect the pressure behavior of the system; that means that the pseudoradial flow follows the bilinear flow after a transition flow period.

During the pseudoradial flow a fractured well acts as a well with an effective wellbore radius r'_w given by Eq. 2. Hence

$$P_{WD} = \frac{1}{2} [\ln t_{Dr'_w} + 0.80907] \quad (12)$$

An analytical solution for the behavior of finite conductivity fractures^{3,13} was used to evaluate the pressure transient behavior for low conductivities cases. Very small fracture segments had to be used to simulate properly the transient pressure behavior. Figure 4 shows a graph of P_{WD} versus the group $t^{\frac{1}{2}} / (k_f b_f)^{\frac{1}{2}}$, for several values of conductivity; the curves for different $(k_f b_f)_D$ merge from the single curve representing the cases where $(k_f b_f)_D \leq 0.1$

At early time, as expected, the curves exhibit a straight line portion that goes through the origin representing the bilinear flow period; the curves for $(k_f b_f)_D > 1.6$ are concave upwards, as pointed out by Cinco-Ley et al⁴, and the curves for $(k_f b_f)_D \leq 1.6$ are concave downwards.

According to Eqs. 7 and 8 P_{WD} can be expressed as a function of the dimensionless time $t_{Dr'_w}$ only. Figure 5 shows a log-log graph of P_{WD} versus $t_{Dr'_w}$ for different $(k_f b_f)_D$. Here the curves are r'_w between two limiting cases, $(k_f b_f)_D = 0.1$ and $(k_f b_f)_D = 300$.

The beginning of the pseudoradial flow occurs at $t_{Dr'_w} = 2000$, in such a way that there is a r'_w long transition period (five log cycles) between the bilinear flow and the pseudoradial flow.

ANALYSIS OF PRESSURE DATA

The interpretation of pressure test data can be accomplished with a high confidence if a flow regime diagnosis is included in the analysis. This basic step uses the type curve matching technique including both the pressure change and the pressure derivative function.

Figure shows a type curve for a low conductivity vertical fracture $(k_f b_f)_D \leq 0.1$ in terms of dimensionless time bases on effective wellbore radius. This graph include both pressure and pressure derivative function. Two single curves represent all values of $(k_f b_f)_D$ less than 0.1. The application of these technique requires that both curves must be matched to obtain data from a match point $(\Delta P)_M$, $(P_{WD})_M$, $(t)_M$ and $t_{Dr'_w}$. Hence we can estimate:

$$kh = \frac{\alpha q B u (P_{WD})_M}{(\Delta P)_M} \quad (13)$$

SPE 16776

CINCO-LEY, H. RAMEY, H.J., JR., SAMANIEGO, F. AND RODRIGUEZ, F.

$$\text{and } r'_w = \sqrt{\frac{\beta k(t)M}{\phi \mu c_t (t_{Dr'_w})M}} \quad (14)$$

we can also compute:

$$k_f b_f = \frac{k r'_w}{0.2807} \quad (15)$$

A unique match is obtained when data fall on either the transition period or the pseudo radial flow.

If data exhibit the bilinear flow behavior only, the analysis can be achieved, as illustrated by Cinco and Samaniego⁴ through the use of a graph of p_w vs $t^{1/4}$. This type of graph yields a straight line of slope m_{bf} inversely proportional to $(k_f b_f)^{1/2}$.

If data fall on the pseudoradial flow the semilog graph applies giving a straight line of slope m inversely proportional to kh of the formation. The skin factor s is estimated using conventional methods, then

$$r'_w = r_w e^{-s} \quad (16)$$

$$\text{and } k_f b_f = 0.2807 k r_w e^{-s} \quad (17)$$

in addition a minimum value for x_f can be calculated from:

$$(x_f)_{\min} = 10 \frac{k_f b_f}{k} \quad (18)$$

CONCLUSIONS

The results obtained in the present work indicate that:

1. A low conductivity vertical fracture, $(k_f b_f)_D \leq 0.1$, exhibits three flow periods: bilinear flow, transition region and pseudoradial flow.
2. The pressure transient behavior for the low conductivity fracture is given by a single curve.

3. The effective wellbore radius for a fractured well with $(k_f b_f)_D \leq 0.1$ is independent of fracture length and can be estimated as $0.2807 k_f b_f / k$.
4. The use of type curve matching is essential to analyze pressure transient test in low conductivity fractures.

NOMENCLATURE

- b_f = fracture width, m
- B = formation volume factor, m^3/m^3
- c_t = total compressibility, $1/\text{kPa}$
- c_1 = constant of proportionality
- h = formation thickness, m
- k = formation permeability, md
- k_f = fracture permeability, md
- $(k_f h_f)_D$ = dimensionless fracture conductivity $(\frac{k_f b_f}{k x_f})$
- p = Pressure, kPa
- p_{wD} = dimensionless wellbore pressure $(\frac{kh\Delta p_w}{\alpha q B \mu})$
- q_f = fracture flux, $\text{m}^3/\text{Day}/\text{m}$
- q_w = Well flow rate
- r_w = Wellbore radius, m
- r'_w = effective wellbore radius, m
- s = skin factor
- t = time, hours
- t_{Dxf} = dimensionless time $(\frac{\beta k t}{\phi \mu c_t x_f^2})$
- $t_{Dr'_w}$ = dimensionless time $(\frac{\beta k t}{\phi \mu c_t r'_w^2})$
- t_{Dcbf} = time for end of bilinear flow

BEHAVIOR OF WELLS WITH LOW CONDUCTIVITY VERTICAL FRACTURES

SPE 16775

t_{Dbpr} = time for beginning of pseudo-radial flow

x = distance, m

x_f = half fracture length, m

ϕ = porosity

μ = viscosity, E-6 Pa.s

Subscripts

b_f = bilinear flow

D = dimensionless

f = fracture

i = initial

w = well

REFERENCES

1. Agarwal, R.G. y Carter, R.D. and Pollock, C.B.: "Evaluation and Prediction of Performance of Low Permeability Gas Wells Stimulated by Massive Hydraulic Fracturing", J. Pet. Tech. (March 1979) 362-372; Trans., AIME, 267.
2. Barker, B.J. and Ramey, H.J., Jr.; "Transient Flow to Finite Conductivity Vertical Fractures", paper SPE 7489 presented at SPE 53rd Annual Conference and Exhibition, Houston, Oct. 1-3, 1978.
3. Cinco Ley, H., Samaniego V.F., and Dominguez N.: "Transient Pressure Behavior for a Well with a Finite-Conductivity Vertical Fracture", Soc. Pet. Eng. J. (Aug. 1978) 253-264.
4. Cinco Ley, H., and Samaniego V.F.: "Transient Pressure Analysis for Fractured Wells", J. Pet. Tech. (Sept. 1981) 1749-1766.
5. Bennett, C.O. et al.: "Approximate Solutions for Fractured Wells Producing Layered Reservoirs", SPEJ (Oct. 1985) 729-742.
6. Camacho V., R.G., Raghavan R., and Reynolds, A.C.: "Response of Wells Producing Layered Reservoirs: Unequal Fracture Length", SPE Formation Evaluation (March 1987) 9-28.
7. Puthiagai, S.K., and Tiab, D.: "Application of P_D^t Function to Vertically Fractured Wells-Field Cases". Paper SPE 11028 presented at SPE 57th Annual Conference and Exhibition, New Orleans, Sept. 26-29, 1982.
8. Alagoa, A., Bourdet, D., and Ayoub, J.A.: "How to Simplify the Analysis of Fractured Well Tests", World Oil (Oct. 1 1985) 97-102.
9. Wong, D.W., Harrington, A.G., and Cinco Ley, H.: "Application of the Pressure Derivative Function in the Pressure-Transient Testing of Fractured Wells". SPE Formation Evaluation (Oct. 1986), 470-480.
10. Prats, M.: "Effect of Vertical Fractures on Reservoir Behavior-Incompressible Fluid Case". Soc. Pet. Eng. J. (June 1961), 105-118.
11. Raghavan, R.: "Pressure Behavior of Wells Intercepting Fractures". Proceedings, Invitational Well-Testing Symposium, October 19-21, 1977, pp. 117-160.
12. Muskat, M.: "The Flow of Homogeneous Fluids Through Porous Media". McGraw-Hill Book Company Inc., New York and Londres, 1937.

SPE 16776

CINCO-LEY, H., RAMEY, H.J., JR., SAMANIEGO, F. AND RODRIGUEZ, F.

13. Rodriguez, F. Horne, R.N. and Cinco-Ley, H.: "Partially Penetrating vertical Fractures: Pressure Transient Behavior of a Finite-Conductivity Fracture", paper SPE 13057 presented at the 59th Annual Technical Conference and Exhibition of SPE of AIME, Houston, Tx, Sept. 16-19, 1984.

APPENDIX

MAXIMUM EFFECTIVE WELLBORE RADIUS OF A FRACTURED WELL

We can use a model described by Muskat to estimate the effective wellbore radius for a well with a low conductivity vertical fracture. Muskat assumed two porous media, one representing the fracture and the other one representing the reservoir; as shown in Figure 2. The reservoir is produced under steady-state flow conditions. According to Muskat, the pressure drop between a point at the fracture located at a distance x from the well and the wellbore is given by:

$$\begin{aligned} P_w - \Delta P_f(x) - P_f(x=0) \\ = \frac{q\mu}{2kh} \left(\frac{\pi}{2} \frac{kx}{k_f b_f} + \int_0^\infty \frac{k}{k_f} \frac{\sin^2(xz) \sinh(z-\epsilon)}{z^2 \sinh(z+\epsilon)} dz \right) \end{aligned} \quad (A-1)$$

where $\epsilon = \tanh^{-1} \left(\frac{k}{k_f} \right)$

For large values of x and small values of $\epsilon = \tanh^{-1} \left(\frac{k}{k_f} \right)$

For large values of x and small values of ϵ ($\epsilon \leq 10^{-3}$) Equation (A-1) can be approximated by the following expression:

$$P_f(x) - P_f(x=0) = \frac{\cosh \epsilon}{\epsilon} \frac{q\mu}{2\pi k_f h} [1.2704 + \ln(\epsilon x)] \quad (A-2)$$

or:

$$P_f(x) - P_f(x=0) = \frac{q\mu}{2\pi kh} \ln \left(\frac{x}{-.2807 k_f b_f} \right) \quad (A-3)$$

This equation indicates that pressure along the fracture varies with the logarithm of distance for large values of x .

The pressure drop equation for radial flow is:

$$P(r_e) - P(r'_w) = \frac{q\mu}{2\pi kh} \ln \frac{r_e}{r'_w} \quad (A-4)$$

where r'_w is the effective wellbore radius.

From comparison of Eqs. (A-3) and (A-4) we find that a well intersected by a vertical fracture of permeability k_f , width b_f and of infinite extension (length) has an effective wellbore radius given by

$$r'_w = 0.2807 \left(\frac{k_f b_f}{k} \right) \quad (A-5)$$

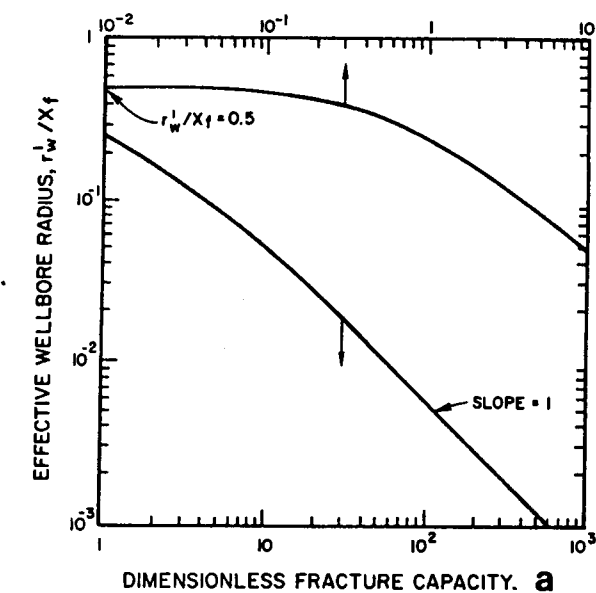


Fig. 1—Effective wellbore radius for fractured wells (after Raghavan).

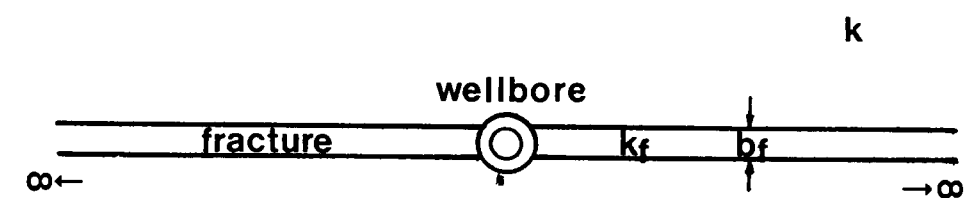


Fig. 2—Vertical fracture of infinite extent.

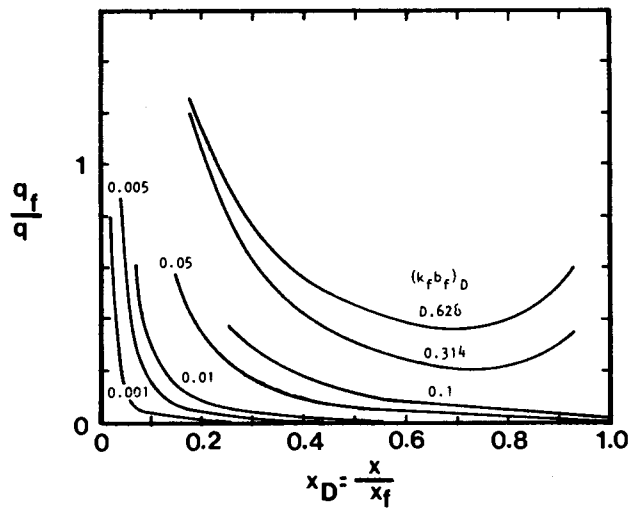


Fig. 3—Flux distribution for low-conductivity fractures.

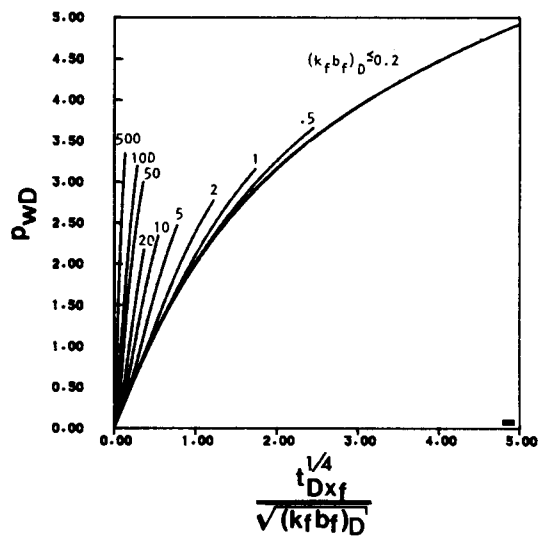


Fig. 4—Transient pressure behavior for fractured wells.

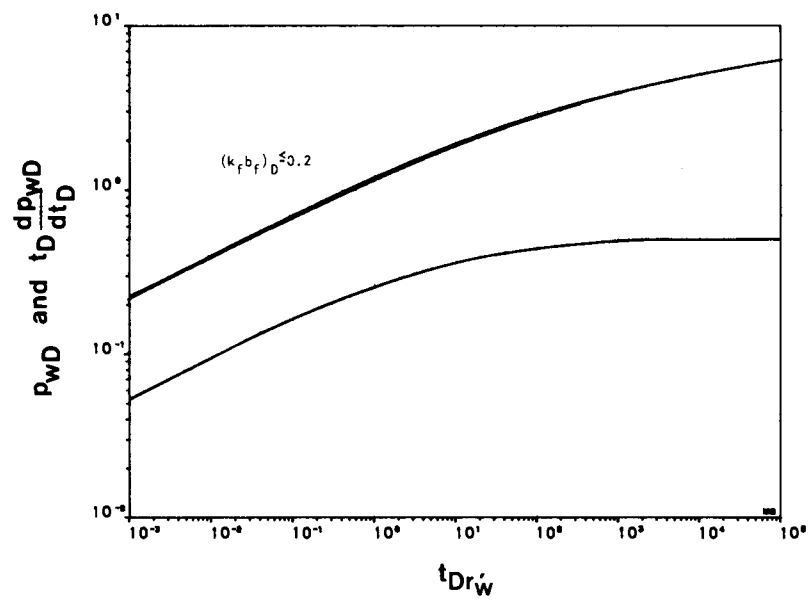
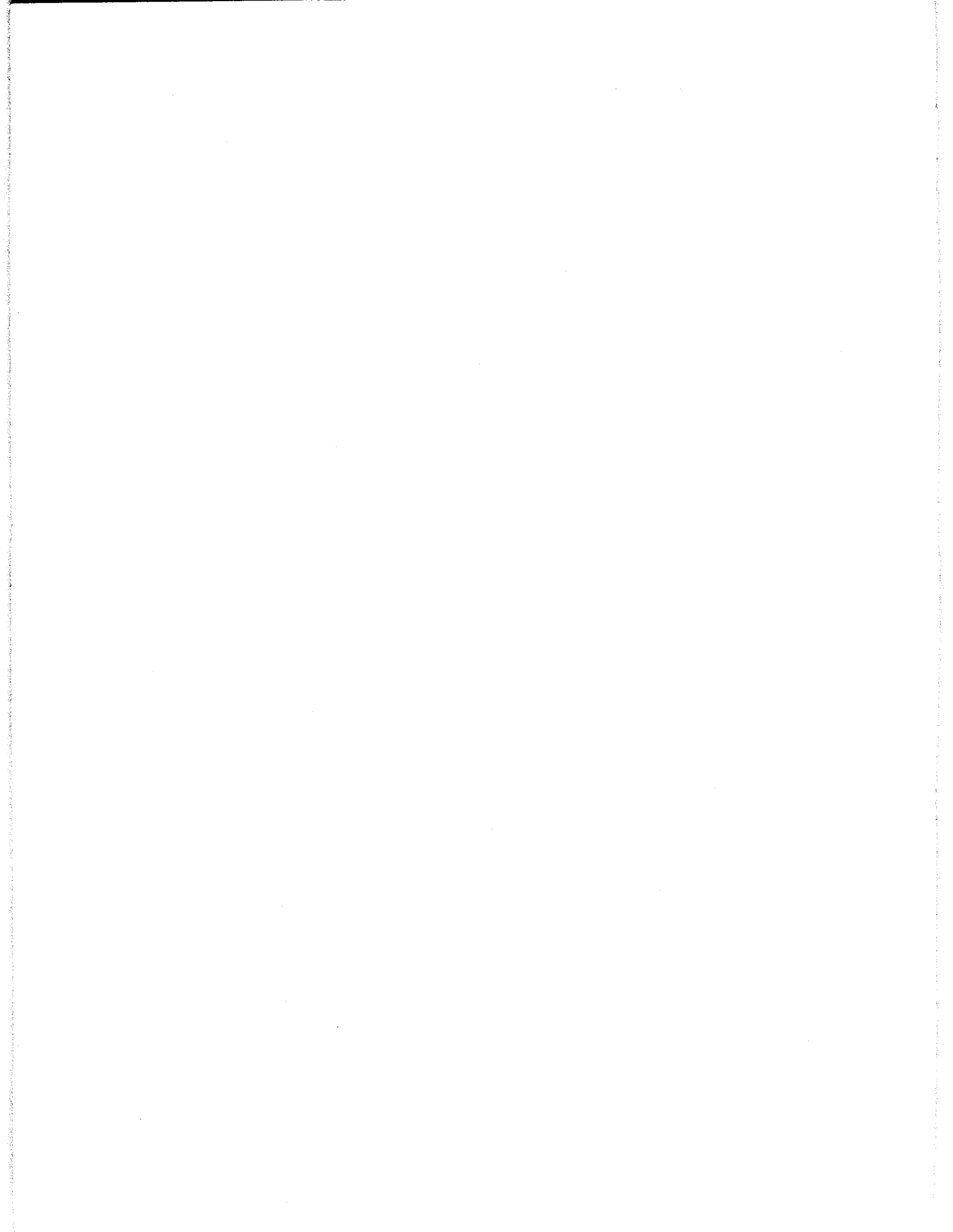


Fig. 5—Type curves for low-conductivity vertical fractures.



Departamento de Matemáticas

JEFE
Dr. Sergio Fuentes Maya

COORDINADORES DE SECCION

MATEMATICAS
Dr. Sergio Fuentes Maya

COMPUTO
M. en I. José Luis Mora Castro

Profesores de Carrera y Líneas de Investigación

Tiempo completo

CAMACHO GALVAN, ABEL. Maestro en ingeniería. Universidad Nacional Autónoma de México. Métodos numéricos aplicados a problemas de potencia y lógica.

DELGADO RODRIGUEZ, ARTURO. Maestro en ingeniería. Universidad de Harvard, E.U.A. Ecuaciones en diferencias y matemáticas aplicadas II.

FUENTES MAYA, SERGIO. Doctor en ingeniería. Universidad de Stanford, E.U.A. Optimización y modelación matemática.

MORA CASTRO, JOSE LUIS. Maestro en ciencias. Universidad Iberoamericana, México. Inteligencia artificial y sus aplicaciones.

Publicaciones

ALVAREZ M G M , SALAZAR N J M , *Diseño asistido por computadora (CAD) en la UNAM*, Tercera conferencia Internacional, Las computadoras en la educación "La educación y los sistemas de información en la frontera del siglo XIX", México, noviembre.

CAMACHO G A , *Algunas aplicaciones de métodos numéricos al flujo en medios porosos*, División de Educación Continua, Facultad de Ingeniería, UNAM, México.

DELGADO R A , *Sumas y series semitelescopicas*, División de Estudios de Posgrado, Facultad de Ingeniería, UNAM, México, abril.

DELGADO R A , *Ecuaciones en diferencias con coeficientes variables lineales y no lineales*, Notas correspondientes al segundo curso intersemestral para profesores. Departamento de Matemáticas Aplicadas de la Facultad de Ingeniería, UNAM, México, mayo.

DELGADO R A , *Solución del problema Jóvenes famosos*, (propuesto en el Boletín 82), Boletín del Departamento de Matemáticas básicas, Facultad de Ingeniería, UNAM, México, septiembre.

DELGADO R A , *Ecuaciones en diferencias parciales, sistemas con coeficientes variables y transformada geométrica*. Tercer curso intersemestral para profesores, Departamento de Matemáticas Aplicadas de la Facultad de Ingeniería, UNAM, México, octubre.

DELGADO R A , *Cálculo de integrales mediante ecuaciones en diferencias*, Boletín del Departamento de Matemáticas Básicas No. 85, Facultad de Ingeniería, UNAM, México, diciembre.

FUENTES M S ., et al, *Políticas de operación de las presas en la cuenca del Río Bravo*, División de Estudios de Posgrado, Facultad de Ingeniería, UNAM, agosto.

FUENTES M S , ALARID R J , *Programa POZO P* División de Estudios de Posgrado, Facultad de Ingeniería, UNAM, México, agosto.

FUENTES M S , *Programa POLGEN*, División de Estudios de Posgrado, Facultad de Ingeniería, UNAM, México, septiembre.

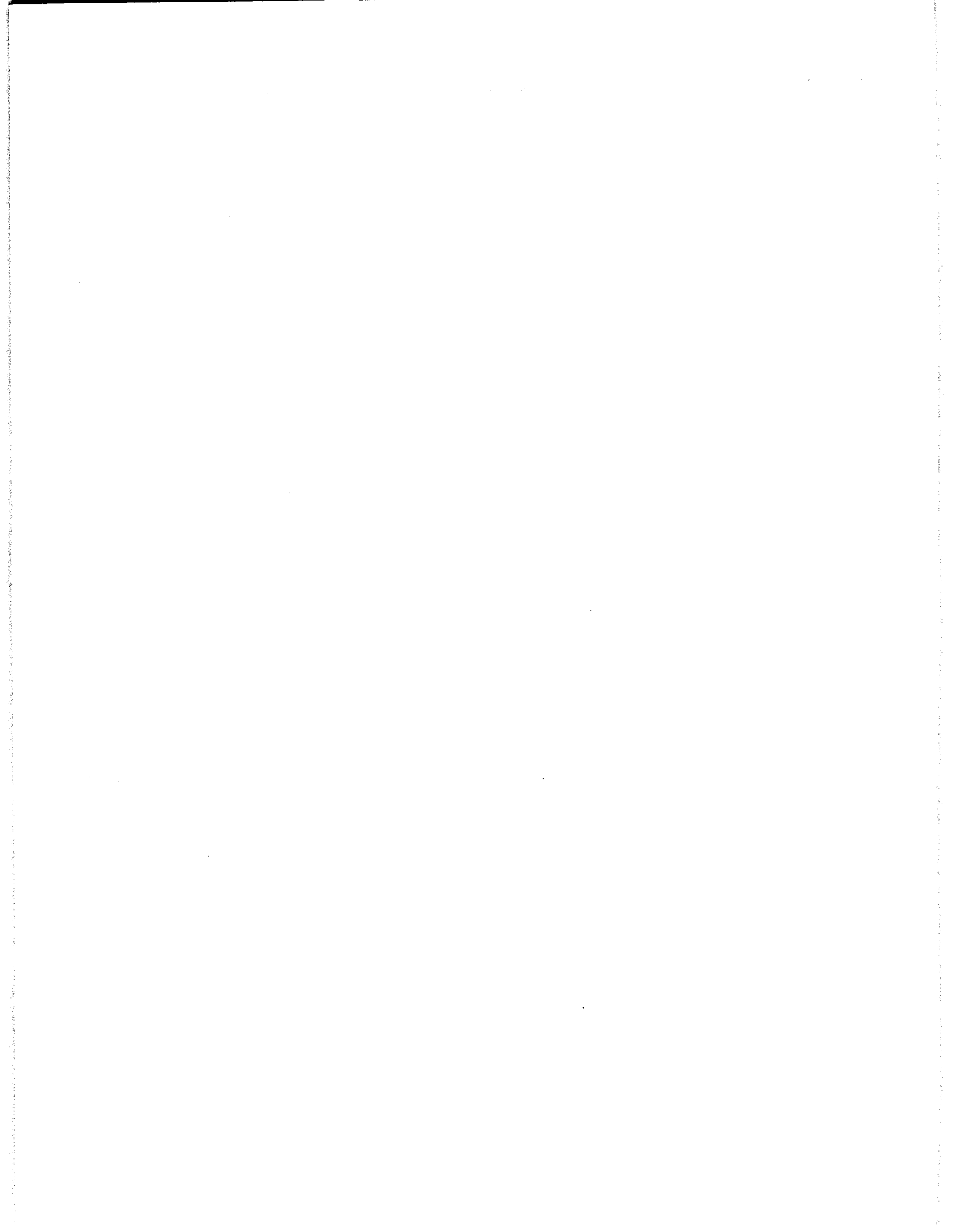
MORA C J L , *LISP: un lenguaje funcional*, Revista de Computación 010, Vol. 7, No. 9, México, mayo.

MORA C J L , *CAD CAM CAE, Un enfoque introductorio*, Revista de computación 0.10, Vol. 7, No. 16, México, diciembre.

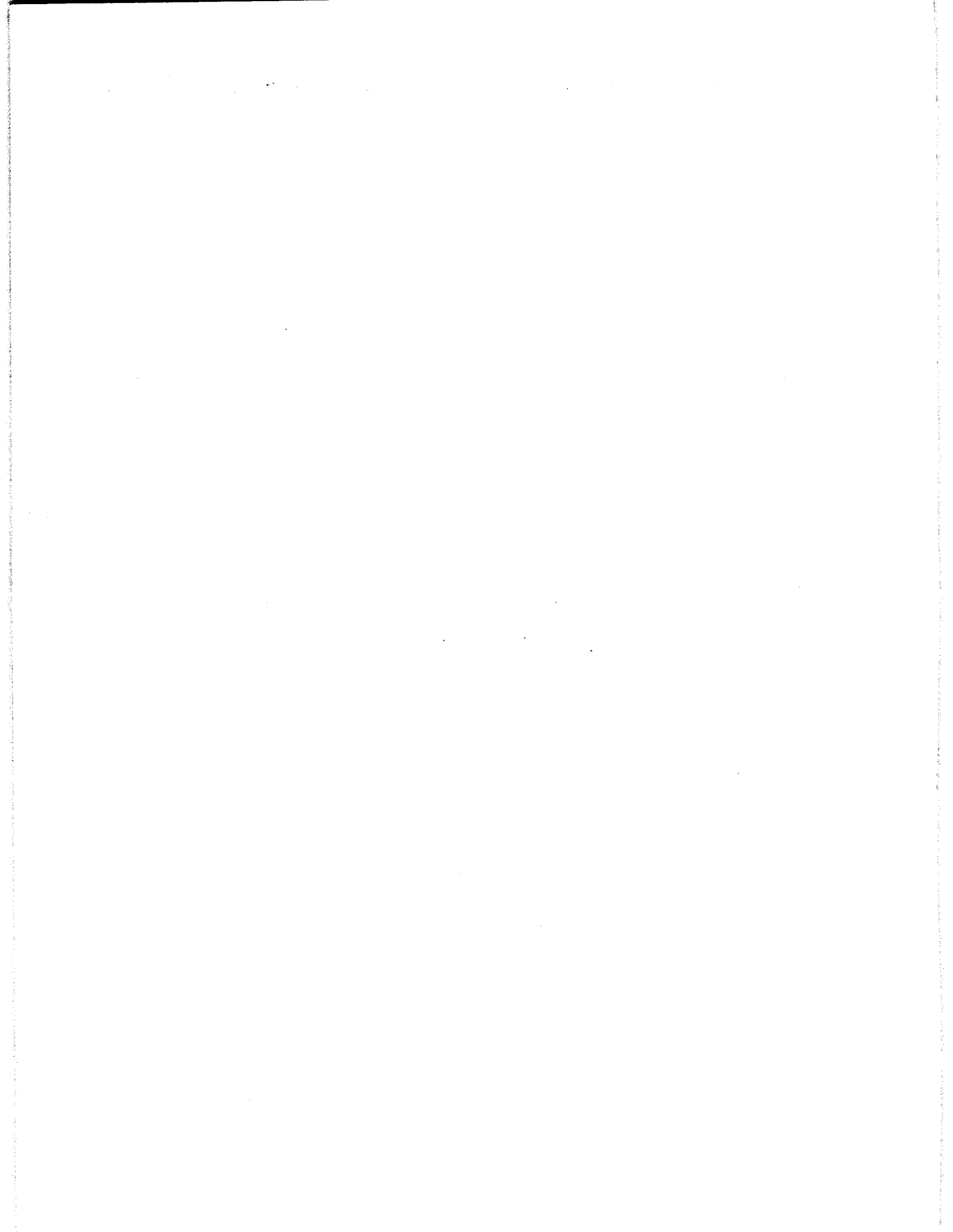
Convenios

SARH-CONACYT-UNAM. Proyecto sobre políticas de operación de las presas en la cuenca del Río Bravo.

IBM-UNAM. Administración del proyecto CAD-CAM.



Alumnos Graduados



Alumnos Graduados

ENERO

ACEVEDO ARREGUIN, L. ANTONIO

M en I ambiental. "Simulación de la contaminación de un acuífero por inyección de aguas residuales". Mexicano.

CARRO DE LA FUENTE, ADAN

M en I aprovechamientos hidráulicos. "Estimadores de máxima verosimilitud de los parámetros de los modelos arma no periódicos y con coeficientes constantes". Mexicano.

PEREZ GOMEZ, LAURA ELISA

M en I investigación de operaciones. "La teoría de conjuntos borrosos como base metodológica, alternativa para el análisis de decisiones bajo criterios múltiples". Mexicana.

REYES SANCHEZ, MARTHA LUCIA

M en I hidráulica. "Fallas de presas". Colombiana.

RIVAS RIVAS, HECTOR

M en I petrolera. "Modelo de optimización de costos en redes de tuberías". Mexicano.

RIVERA RIVERA, CARLOS

M en I eléctrica-control. "Teoría de la información con aplicaciones al procesamiento digital de señales". Mexicano.

VALDEZ DE LA RIVA, J. CLAUDIO

Especialización I construcción. "Procesamiento de reciclado de pavimentos asfálticos en México". Mexicano.

FEBRERO

En este mes no hubo obtención de grados.

MARZO

BOCANEGRA NORIEGA, MA. GUADALUPE

M en I exploración. "El paleomagnetismo y sus implicaciones con el origen y evolución del Golfo de México". Mexicana.

ESGUERRA AMAYA, C. AUGUSTO

M en I estructuras. "Confiabilidad de marcos de varios pisos ante la acción de sismos". Colombiano.

EUDAVE MUÑOZ, JORGE

M en I estructuras. "Vibración con balanceo en estructuras". Mexicano.

GARCIA JARQUI, L.J. ALONSO

M en I estructuras. "Análisis paso a paso del centro postal mecanizado con acelograma del sismo del 19 de septiembre de 1985". Mexicano.

HERNANDEZ GUTIERREZ, J. ISSAC

M en I mecánica. "Características del chorro incipiente". Mexicano.

LOYO FERNANDEZ, J. AURELIO

M en I petrolera. "Programa de cómputo para el análisis y el diseño de instalaciones de bombeo neumático continuo". Mexicano.

SANDOVAL GARCIA, MA. CLEMENCIA

M en I hidráulica. "Ajuste de parámetros de modelos autorregresivos periódicos con técnicas de optimización". Colombiana.

SOLIS GALEANA, GILBERTO

M en I petrolera. "Análisis y aplicaciones de la teoría de interpretación de pruebas de campo 'minifrac' ". Mexicano.

TRISTAN WONG, MARCELO

M en I hidráulica. "Análisis y alivio de supresiones en obras de excedencia". Panameño.

LEON ROMANOS, ARTURO

M en I electrónica. "Interpolación de áreas cromáticas entre puntos cuyos porcentajes de colores son conocidos". Mexicano.

VICENTE VIVAS, ESAU.

M en I eléctrica. "Desarrollo conjunto de procesamiento digital de imágenes y sistemas automatizados". Mexicano.

ABRIL**ARMIJO PALACIO, G. ERNESTO**

M en I mecánica de suelos. "Potencialidad a la licuación de un depósito de arena límosa mediante cono eléctrico". Argentino.

DIAZ CRUZ, ARMANDO

M en I hidráulica. "Influencia de la zona de inmersión en la concentración de una corriente de densidad en un embalse". Mexicano.

JARAMILLO FERNANDEZ, J. DIEGO

M en I estructuras. "Torsión sísmica de edificios". Colombiano.

RUIZ CARMONA, VICTOR MANUEL

M en I eléctrica. "Control adaptable de un canal de riego". Mexicano.

MAYO**AVILES OCHOA, JUAN S.**

M en I aprovechamientos hidráulicos. "Análisis de eficiencia de la estimación de los parámetros de la distribución general de valores extremos para el análisis de sequías". Mexicano.

CABRERA BORBOA, LUIS R.

M en I planeación. "Decisiones estratégicas en el procedimiento de plan empresarial". Mexicano.

CARDENAS ORDOÑEZ, HAROLD G.

M en I estructuras. "Estudio de un edificio reforzado con contravientos metálicos y muros de concreto". Colombiano.

CONTRERAS LOPEZ, ENRIQUE A.

M en I mecánica. "Investigación experimental del efecto de la temperatura sobre la permeabilidad, la porosidad y la expansión térmica de rocas areniscas". Mexicano.

DOURIET CARDENAS, JOSE C.

M en I hidráulica. "Análisis univariado de frecuencias de sequías". Mexicano.

FLORES VIVEROS, JAIME A.

M en I aprovechamientos hidráulicos. "Revisión del capítulo 7 del libro 'Mathematical modeling of hydrologic series Advanidze' ". Mexicano.

GARCIA MOLINA, GORGONIO

M en I exploración. "Aplicación de la teoría de rayos en el modelado sísmico tridimensional". Mexicano.

HERNANDEZ LLOVERA, LEONEL.

M en I mecánica. "Construcción de la parte mexicana del puente internacional". Mexicano.

HERNANDEZ RODRIGUEZ, JOSE A.

M en I planeación. "Modelo multicriterio para la evaluación social de proyectos de desarrollo regional". Mexicano.

RUIZ CASILLAS, MANUEL E.

M en I eléctrica. "Asignación de unidades hidroeléctricas en la planeación a corto plazo de la operación de los sistemas eléctricos de potencia". Mexicano.

VALDEZ PALACIOS, JOSE ALBERTO

M en I mecánica. "Concentrados solares tipo canal parabólico". Mexicano.

JUNIO**LEON LOPEZ, SAMUEL**

M en I construcción. "Criterios para la reparación de estructuras dañadas por sismos". Mexicano.

LEPE CASILLAS, FERNANDO

M en I control. "Sobre aplicaciones de la teoría de información a procesamiento digital de señales". Mexicano.

MOJICA BARRERA, RAFAEL

M en I planeación. "Deuda externa mexicana. Estrategias de solución". Colombiano.

ROJAS SALGADO, J. ANGEL A.

Doctor en I mecánica teórica aplicada. "Dinámica de sistemas articulados de cuerpos rígidos". Mexicano.

JULIO**ALVAREZ HERNANDEZ, RAFAELA G.**

M en I aprovechamientos hidráulicos. "Obras hidráulicas y acciones institucionales en el control de avenidas". Hondureña.

BELTRAN GARCIA, JORGE LUIS

M en I estructuras. "Influencia de los efectos de segundo orden en el diseño de columnas de marcos rígidos para edificios". Mexicano.

NAVAS PABON, EDGAR

M en I construcción. "Análisis de proyectos de construcción de una economía inflacionaria: un ejemplo". Colombiano.

LULE CERVANTES, GILBERTO

Especialización I construcción. "Utilización del concreto lanzado en la construcción". Mexicano.

AGOSTO**FERNANDEZ ANAYA, GUILLERMO**

M en I control. "Un ensayo sobre una teoría general de modelo de teoría general de sistemas". Mexicano.

GOMEZ DE LUNA, RUBEN

M en I aprovechamientos hidráulicos. "Estudio colectivo de metodologías de análisis de gastos máximos". Mexicano.

LOPEZ DE LARA DIAZ, EDUARDO

Especialización I construcción. "Empleo de las emulsiones asfálticas en pavimentos". Mexicano.

MARTINEZ MORENO, BRUNO

M en I estructuras. "Análisis dinámico de un edificio por dos programas de computadoras diferentes". Mexicano.

MORELOS ZARAGOZA, ROBERT H.

M en I eléctrica. "Diseño de un decodificador de Viterbi". Mexicano.

ROMO MILLARES, CESAR ALFREDO

M en I energética. "Centrales del ciclo combinado, una alternativa energética". Mexicano.

ZAMORA ARAGON, POMPILIO

M en I control automático. "Optimación en el dominio de la frecuencia para sistemas muestrados". Colombiano.

SEPTIEMBRE**CARRILLO GARCIA, MAURICIO**

M. en I. hidráulica. "Simulación del flujo en una red de canales para riego". Mexicano.

CUEVAS SALGADO, JESUS

M. en I. eléctrica. "Cogeneración industrial en México. Producción de electricidad. Estado actual y perspectivas". Mexicano.

FAJARDO FAJARDO, DIEGO

M en I planeación. "La construcción del objeto de estudio en la planeación. (Pautas para la aplicación al transporte)". Colombiano

HERNANDEZ AYUSO, CARMEN

M. en I investigación de operaciones. "Flujos y diferenciales: factibilidad y optimidad". Mexicana.

JIMENEZ RIOS, BERTHA

M en I investigación de operaciones. "Análisis de sistemas de producción-inventario". Mexicana.

OLIVERA MARTINEZ, CELIA MARGARITA

M. en I planeación. "Conducción de proyectos de consultoría". Mexicana.

RODRIGUEZ PADILLA, VICTOR

M. en I. energética. "Exploración petrolera en los países en vías de desarrollo frente a la evolución de los precios del petróleo"
Mexicano.

TURRENT DIAZ, RAFAEL

M. en I. investigación de operaciones. "Un enfoque sistémico en el sector comunicación".
Mexicano.

VARGAS BALLESTER, WALDO PERCI

M. en I. ambiental. "Estudio preliminar de la capacidad de autopurificación del agua en el río Bravo cuenca media".
Boliviano.

OCTUBRE**ALCANTARA GUTIERREZ ANA VICTORIA**

M. en I. ambiental. "La cloración en la planta de tratamiento de aguas residuales en la Ciudad Universitaria".
Mexicana.

MOGUEL POZOS, E. ERASMO

M. en I. proyecto de instalaciones eléctricas. "Puesta en servicio de sistemas de protección y medición de una subestación de potencia".
Mexicano.

MORENO QUINTERO, ERIK

M. en I. investigación de operaciones. "Problemas de apareamiento".
Mexicano.

NARRO RAMIREZ, ANA ELENA

M. en I. investigación de operaciones. "Problemas lineales duales en redes de flujo".
Mexicana.

PALACIO PEREZ, ARTURO

Doctor en I. mecánica teórica y aplicada. "Dinámica de pozos geotérmicos".
Mexicano.

PEÑA SANTANA, PATRICIA GUILLERMINA

M. en I. hidráulica. "Obras hidráulicas en México. Abastecimiento de agua potable hasta el porfiriato".
Mexicana.

OLAYA BENITEZ, JESUS E.

M. en I. petrolera. "Programa computarizado para optimizar el peso sobre la barrera, velocidad de rotación e hidráulica para minimizar los costos de perforación".
Colombiano.

VERA BADILLO, FERNANDO

M. en I. estructuras. "Análisis no lineal. Un enfoque por el método del elemento finito". Mexicano.

NOVIEMBRE**AYALA SUERO, HECTOR ALEJANDRO**

M. en I. aprovechamientos hidráulicos. "Análisis crítico de la programación dinámica utilizada para definir políticas de operación de plantas hidroeléctricas". Mexicano.

CAMPOS ARANDA, DANIEL FRANCISCO

Doctor en I. aprovechamientos hidráulicos. "Modelo de precipitación de un escurrimiento de eventos". Mexicano.

DIAZ HENAO, CLARA CONSUELO

M. en I. estructuras. "Evaluación del diseño de la respuesta sísmica analítica de estructura a base de loza plana aligerada". Colombiana.

DIAZ DE LEON FERNANDEZ DE CASTRO, FELIPE

Especialización I. construcción. "Análisis comparativo de vigas pretensadas". Mexicano.

HERNANDEZ DELGADO, CESAR ULISES

M. en I. estructuras. "Efectos de la variación de la carga viva en las fuerzas cortantes sísmicas que actúan sobre un edificio". Mexicano.

SANCHEZ HUERTA, ALEJANDRO

M. en I. hidráulica. "Análisis teórico experimental de las presiones causadas por separación de columna líquida". Mexicano.

VILLARRAGA HERRERA, MANUEL ROBERTO

M. en I. mecánica de suelos. "Respuesta aleatoria tridimensional de presas de tierra". Colombiano.

DICIEMBRE**BERUMEN CAMPOS, SERGIO**

M. en I. petrolera. "Análisis del comportamiento de yacimientos de gas que producen en condiciones de presión constante". Mexicano.

FRAUSTO SOLIS, ARMANDO

M. en I. potencia. "Inteligencia artificial aplicada al control de sistemas eléctricos". Mexicano.

HERNANDEZ ALARCON, LUIS ALFREDO

M. en I. energética. "Aprovechamientos energéticos del bagazo de caña en la industria azucarera". Colombiano.

RAMIREZ PIMENTEL, ARNULFO

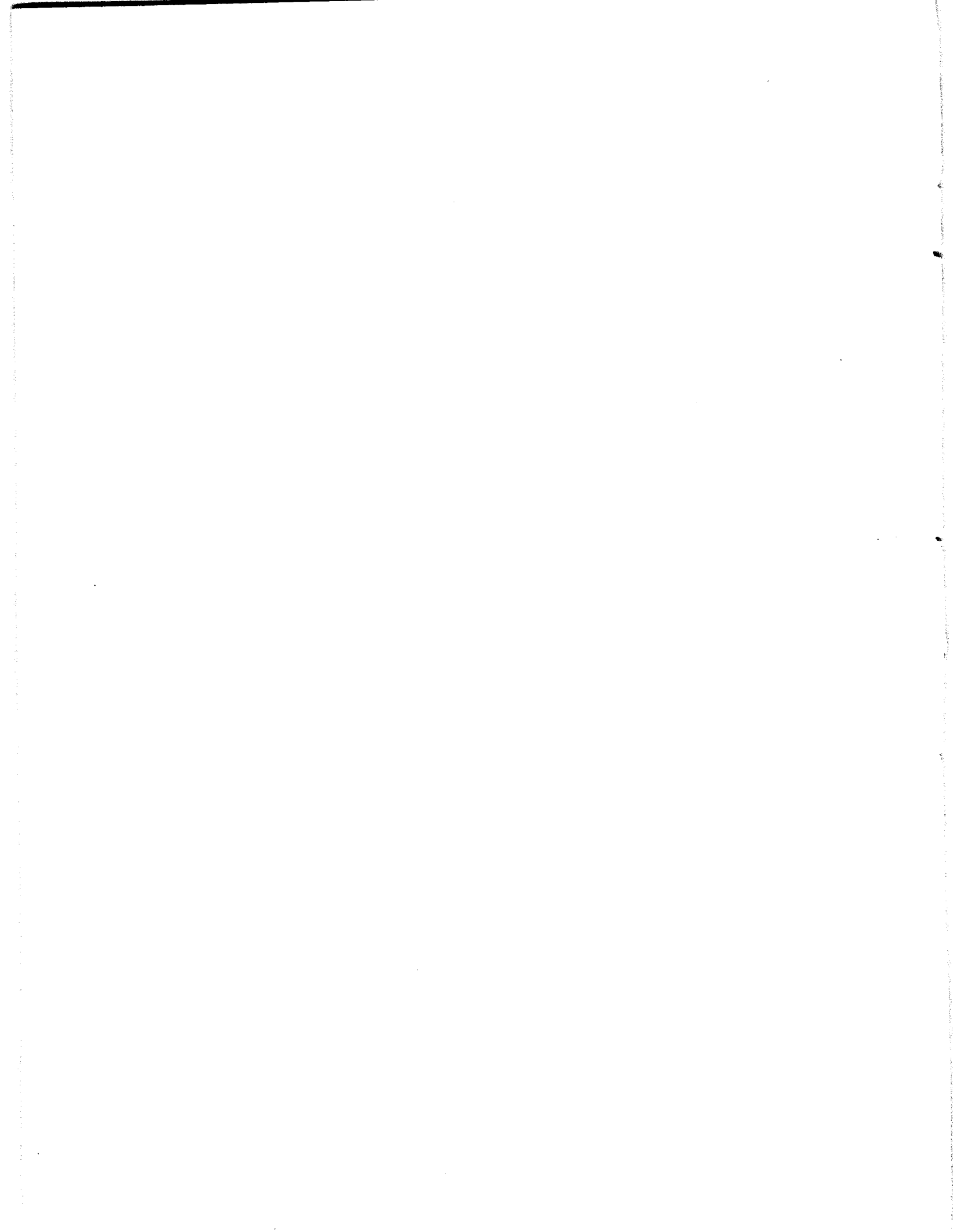
M. en I. petrolera. "Análisis del flujo de fluidos a través de disparos". Mexicano.

GARCIA CABANA, MABEL

M. en I. mecánica de suelos. "Comportamiento dinámico de arcillas

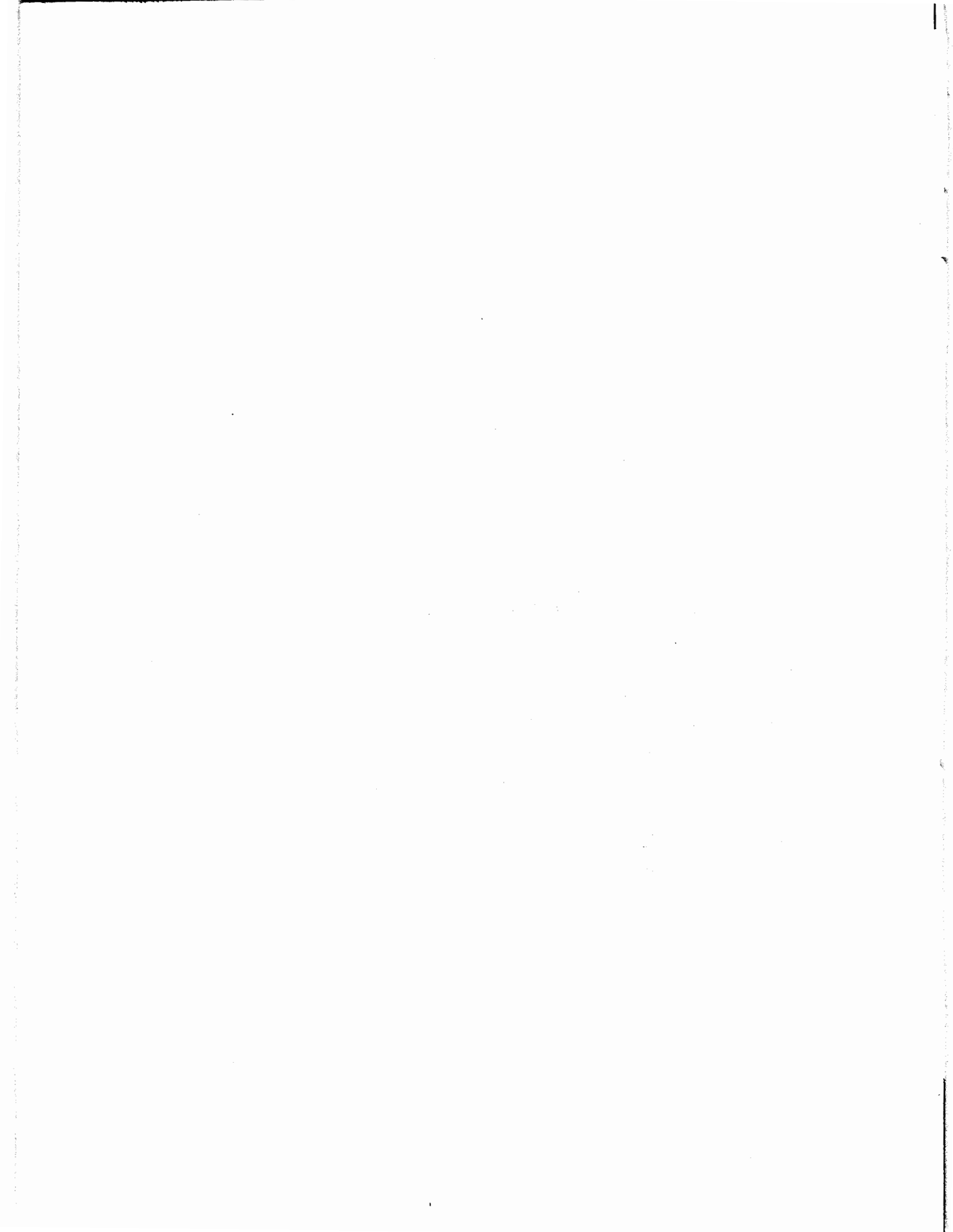
preconsolidadas".

Colombiana.



I N D I C E

Presentación	9
Introducción	11
La División de Estudios de Posgrado de la Facultad de Ingeniería	13
Estructura Académica	14
Departamento de Ingeniería Civil	17
Sección de Ambiental	19
Sección de Hidráulica	21
Artículos reproducidos	23
Sección de Construcción, Estructuras y Mecánica de Suelos	49
Artículos reproducidos	53
Sección de Sistemas	99
Artículo reproducido	101
Departamento de Ingeniería Electromecánica	107
Artículos reproducidos	115
Departamento de Ingeniería de Recursos del Subsuelo	139
Artículo reproducido	143
Departamento de Matemáticas	155
Alumnos Graduados	159



Esta obra se editó en Impresora Ideal, Fragonard 44,
México 03910, D.F., y se terminó el dia 30 de mayo de
1988. Edición a cargo de Marie Puga y Elsa Martínez B.



F/DEPFI/MISC/0005/EJ.4



717692